AD-A149 292 SHIELDED ENCLOSURES FOR EXPERIMENTAL STUDIES OF SHIELDING TOPOLOGY(U) DIKEWOOD ALBUQUERQUE NM F C YANG ET AL. NOV 84 DC-FR-1026.610-1B AFWL-TR-84-11 1/1

UNCLASSIFIED F29601-82-C-0027 F/G 20/14 NL

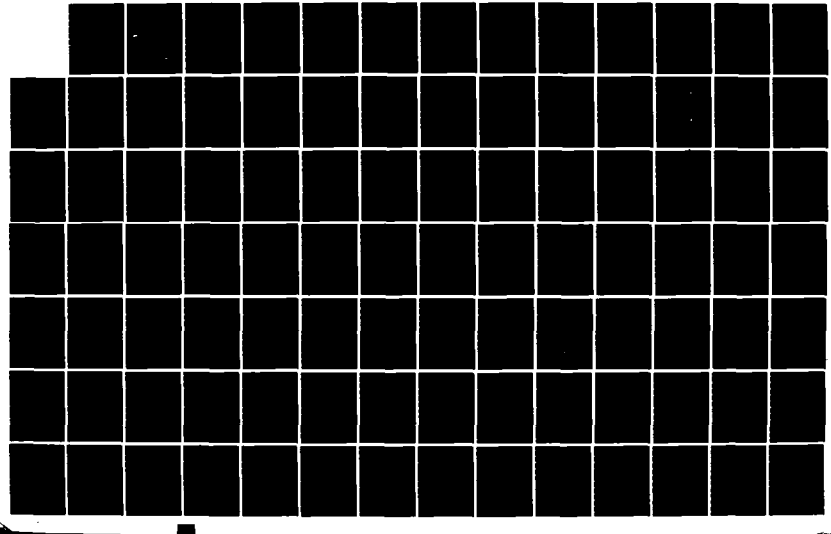

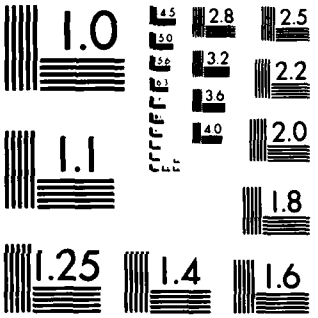

AFWL-TR-
84-11

SHIELDED ENCLOSURES FOR EXPERIMENTAL STUDIES OF SHIELDING TOPOLOGY

F.C. Yang, et al.

Dikewood, Div of Kaman Sciences Corp
1613 University Boulevard, NE
Albuquerque, NM 87102

November 1984

Final Report

AIR FORCE WEAPONS LABORATORY
Air Force Systems Command
Kirtland Air Force Base, NM 87117

This final report was prepared by the Dikewood, Division of Kaman Sciences Corporation, Albuquerque, New Mexico, under Contract F29601-82-C-0027, Job Order 37630131 with the Air Force Weapons Laboratory, Kirtland Air Force Base, New Mexico. Lieutenant Dennis J. Andersh (NTAA) was the Laboratory Project Officer-in-Charge.

When Government drawings, specifications, or other data are used for any purpose other than in connection with a definitely Government-related procurement, the United States Government incurs no responsibility or any obligation whatsoever. The fact that the Government may have formulated or in any way supplied the said drawings, specifications, or other data, is not to be regarded by implication, or otherwise in any manner construed, as licensing the holder, or any other person or corporation; or conveying any rights or permission to manufacture, use, or sell any patented invention that may in any way be related thereto.

This report has been authored by a contractor of the United States Government. Accordingly, the United States Government retains a nonexclusive, royalty-free license to publish or reproduce the material contained herein, or allow others to do so, for the United States Government purposes.

This report has been reviewed by the Public Affairs Office and is releasable to the National Technical Information Services (NTIS). At NTIS, it will be available to the general public, including foreign nations.

If your address has changed, if you wish to be removed from our mailing list, or if your organization no longer employs the addressee, please notify AFWL/NTAA, Kirtland AFB, NM 87117 to help us maintain a current mailing list.

This technical report has been reviewed and is approved for publication.

Dennis J Andersh

DENNIS J. ANDERSH
Lieutenant, USAF
Project Officer

FOR THE COMMANDER

David W Garrison

DAVID W. GARRISON
Lt Colonel, USAF
Chief, Applications Branch

Roger S Case

ROGER S. CASE, JR
Lt Colonel, USAF
Chief, Aircraft & Missiles Division

DO NOT RETURN COPIES OF THIS REPORT UNLESS CONTRACTUAL OBLIGATIONS OR NOTICE ON A SPECIFIC DOCUMENT REQUIRES THAT IT BE RETURNED.

UNCLASSIFIED

SECURITY CLASSIFICATION OF THIS PAGE

AD-A149292

REPORT DOCUMENTATION PAGE

1a. REPORT SECURITY CLASSIFICATION Unclassified	1b. RESTRICTIVE MARKINGS
2a. SECURITY CLASSIFICATION AUTHORITY	3. DISTRIBUTION/AVAILABILITY OF REPORT Approved for public release; distribution unlimited.
2b. DECLASSIFICATION/DOWNGRADING SCHEDULE	
4. PERFORMING ORGANIZATION REPORT NUMBER(S) DC-FR-1026.610-1B	5. MONITORING ORGANIZATION REPORT NUMBER(S) AFWL-TR-84-11
6a. NAME OF PERFORMING ORGANIZATION Dikewood, Division of Kaman Sciences Corp 6b. OFFICE SYMBOL (If applicable)	7a. NAME OF MONITORING ORGANIZATION Air Force Weapons Laboratory
6c. ADDRESS (City, State and ZIP Code) 1613 University Boulevard, NE Albuquerque, NM 87102	7b. ADDRESS (City, State and ZIP Code) Kirtland Air Force Base, NM 87117
8a. NAME OF FUNDING/SPONSORING ORGANIZATION 8b. OFFICE SYMBOL (If applicable)	9. PROCUREMENT INSTRUMENT IDENTIFICATION NUMBER F29601-82-C-0027
8c. ADDRESS (City, State and ZIP Code)	10. SOURCE OF FUNDING NOS. PROGRAM ELEMENT NO. 64711F; PROJECT NO. 3763; TASK NO. 01; WORK UNIT NO. 31
11. TITLE (Include Security Classification) SHIELDED ENCLOSURES FOR EXPERIMENTAL STUDIES OF SHIELDING TOPOLOGY (U)	
12. PERSONAL AUTHOR(S) Yang, F. C.; Lee, K. S. H. and Kokorowski, S. A.*; Baum, C. E.**; Hamm, J.; Graf, W. and Vance, E. F.+	
13a. TYPE OF REPORT Final Report 13b. TIME COVERED FROM Jun 82 TO Nov 83	14. DATE OF REPORT (Yr., Mo., Day) 1984 November 15. PAGE COUNT 100
16. SUPPLEMENTARY NOTATION *Dikewood, Division of Kaman Sciences Corporation **Air Force Weapons Laboratory +SRI International	
17. COSATI CODES FIELD / GROUP / SUB. GR.	18. SUBJECT TERMS (Continue on reverse if necessary and identify by block number) Aperture Penetration, Electromagnetic Topology, EMP Lightning, Line Penetration, Qualification Test, Scattering Supermatrix, Shielded Enclosure, Shielding Performance (over)

19. ABSTRACT (Continue on reverse if necessary and identify by block number)

The report discusses the effort to provide shielded enclosures for EMP experimental studies of shielding topology. Section I discusses the theoretical modeling for which scattering matrices of subshields and their norms are used to relate the internal signals to the electromagnetic source environment. Both the line and aperture penetrations are included in the scattering matrix formulation. Experimental and analytical methods are proposed for estimating parameters of the scattering matrices. It is pointed out in the discussion that these methods can, in turn, be employed to analyze the overall shielding performance and to synthesize the subshield requirements of a system. The discussion in Section I includes an illustrative example.

Section II describes experiments to characterize and quantify the shielding performance of a rectangular metal enclosure containing various line and aperture penetrations. Experimental techniques and procedures are given for obtaining certain parameters involved (over)

20. DISTRIBUTION/AVAILABILITY OF ABSTRACT UNCLASSIFIED/UNLIMITED ☐ SAME AS RPT. ☐ DTIC USERS ☒	21. ABSTRACT SECURITY CLASSIFICATION Unclassified
22a. NAME OF RESPONSIBLE INDIVIDUAL Lt D. J. Andersh	22b. TELEPHONE NUMBER (Include Area Code) (505) 844-0326 22c. OFFICE SYMBOL NTAA

DD FORM 1473, 83 APR EDITION OF 1 JAN 73 IS OBSOLETE.

UNCLASSIFIED

SECURITY CLASSIFICATION OF THIS PAGE

18. SUBJECT TERMS (Continued)

Vector and Matrix Norms

19. ABSTRACT (Continued)

in the theoretical model for bounding the shielding performance of an enclosure. Techniques for evaluation of the accuracy of the theoretical calculation and its comparison to measured data are also discussed.

Section III describes specifications that were developed to construct two shielded enclosures, one with a single layer topology and one with a double layer topology. Details are given on the mechanical design of the two enclosures, and on the design of various replaceable panels that can be used to test the accuracy of the theoretical model.

Section IV describes the experimental results of the shielding performance of the two enclosures constructed by SRI International. The test was conducted for frequencies ranging from 1 kHz to 1 GHz. The results show that the enclosures provided at least 80 dB attenuation, whereas the gasket faces of the boxes gave at least 74 dB attenuation.

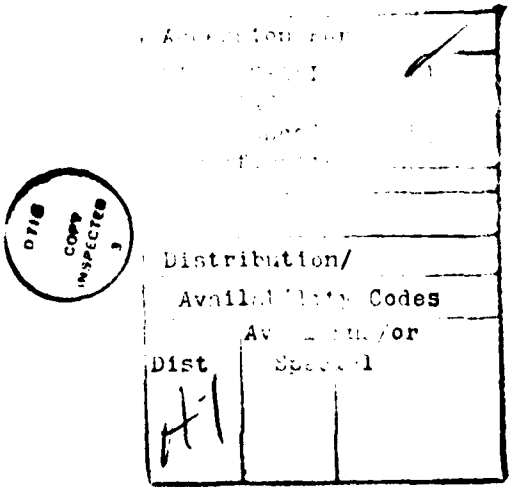

CONTENTS

CONTENTS (Continued)

CONTENTS (Concluded)

I. SPECIFICATIONS OF ENCLOSURES SHIELDING PERFORMANCE

1. INTRODUCTION

It is an extremely complicated problem to analyze the overall shielding performance or to synthesize the shielding allocation requirement for an aeronautical system to protect against electromagnetic interferences, such as those of nuclear electromagnetic pulse (NEMP) and lightning. One approach to analyze and synthesize such a problem has been developed in Reference 1 using the concept of electromagnetic topology and an interaction sequence diagram, which eventually evolves into a supermatrix equation. Under certain practical assumptions, this supermatrix equation can be approximately solved, and the internal signals and their upper bounds are found to be related to the external electromagnetic environment and the shielding properties of shields. That is to say, with this approach the complicated problem is reduced to evaluating a set of environment and shield variables.

However, there are questions that remain to be answered regarding the approach. The electromagnetic penetration through a shield can be categorized as either a line or an aperture penetration (the diffusion penetration is less important for an aeronautical system with metallic surface and will not be included in this discussion). When the interaction sequence diagram is constructed, all of the line and aperture penetration paths are modeled as "edges" with associated combined voltage waves (Ref. 1). While the combined voltage waves can be easily defined along a line penetration path, there is no clear way to incorporate the field quantities along the aperture penetration path in the combined voltage formulation. One purpose of this report is to resolve this difficulty.

In order to use the above approach for shielding analysis and synthesis purposes, the environment and shield variables have to be calculated or measured in a way according to their definitions described by this approach. Unfortunately, most of the existing military standards for measuring the shielding performance do not satisfy these definitions. For example, each shielding variable in the approach is defined to be nearly independent of adjacent shields, whereas the shielding effectiveness measured according to MIL-STD-285 (Refs. 2 and 3) varies a lot with the structure inside the

shield. Another purpose of this report is, thus, to establish certain rules for the preparation of future military standards to measure the shielding performance of an enclosure.

Section I-2 summarizes the approach of Reference 1 and gives a method of resolving difficulties in characterizing the aperture penetration. Section I-3 presents an illustrative example. Section I-4 explains how the shield environment variables can be experimentally determined. Section I-5 demonstrates how the results in Sections I-2 through I-4 can be used in the shielding design procedure for hardening an aeronautical system. Section I-6 gives conclusions and recommendations for future developments to bring the supermatrix-norm approach to maturity.

2. BASIC CONSIDERATION

Aeronautic systems have many electronic components which are connected by wires or cables, exposed to electromagnetic interferences (EMIs) either arriving from the outside electromagnetic pulse (EMP), lightning, or are system-generated EMP (SGEMP) or EMI. These interferences may damage or upset the circuit components. The vulnerability to these interferences may be reduced by reducing the electromagnetic coupling to the connecting wires, limiting the propagation of the interferences to the components, and/or, or course, increasing the components' damage or upset threshold. These protection schemes can be implemented with hardening fixes on surfaces separating one layer (or sublayer) from the other. This subsection defines parameters (or variables) characterizing the shielding surfaces and discusses the relationship of these parameters to the overall shielding performance.

a. General discussion--Reference 1 gave a supermatrix equation for calculating the signal responses inside an aeronautical system due to an electromagnetic interference. The first step in deriving the supermatrix equation is to construct a topological diagram for the electronic system (Fig. 1) and then to draw a corresponding interaction sequence diagram (Fig. 2). The interaction paths in the diagram include all the important penetration paths through apertures and along conducting wires. The vertices and edges of the interaction sequence diagram are similar to the junctions and tubes of a transmission-line network (Ref. 4).

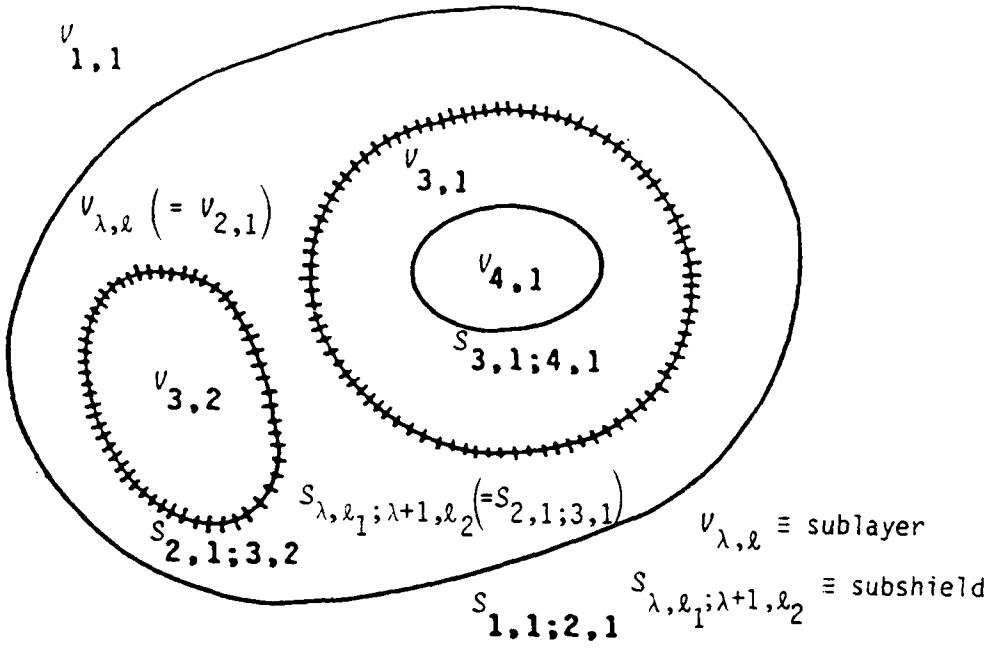

Figure 1. Electronic system topological diagram.

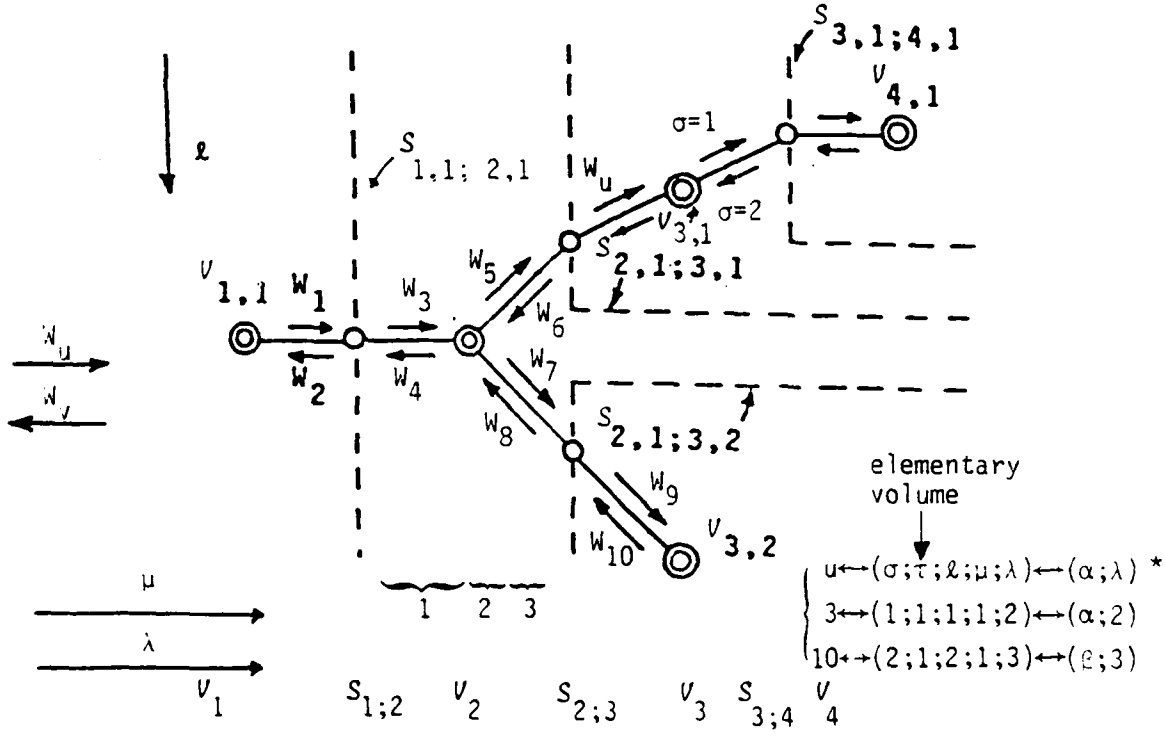

Figure 2. Interaction sequence diagram for Figure 1.

*See Figure 3 for more partition examples and the glossary for definition of the indices.

Thus, a supermatrix equation can be obtained which is similar to the transmission-line network equation that was obtained in Reference 4. That is, Equation 1 (with the tubes shrinking to zero length),

$$[((1_{n,m})_{u,v})-((\tilde{S}_{n,m})_{u,v})] \odot ((\tilde{V}_n)_u)$$

$$\equiv((\tilde{I}_{n,m})_{u,v}) \odot ((\tilde{V}_n)_u)$$

$$=((\tilde{S}_{n,m})_{u,v}) \odot ((\tilde{V}_{s_n})_u) \equiv ((\tilde{E}_n)_u) \tag{1}$$

where u and v, which can be further partitioned to correspond to the levels of the hierarchical topology (Ref. 1), are indices for the waves (W_u, W_v) on the edge (or tube) of the interaction sequence diagram (each edge has two waves propagating in opposite directions); n, m are indices for the individual wire or penetration path inside the edges; ~ is to indicate complex frequency-domain quantities; and • means generalized dot multiplication as defined by Equation 3.4 of Reference 1. The symbols are defined in the glossary. A short description concerning how Equation 1 is derived is given in Appendix A. Also,

$(1_{n,m})_{u,v}) \equiv$ identity supermatrix

$(\tilde{I}_{n,m})_{u,v}) \equiv$ interaction supermatrix

$$\equiv((1_{n,m})_{u,v}) - ((\tilde{S}_{n,m})_{u,v}) \tag{2}$$

$(\tilde{S}_{n,m})_{u,v}) \equiv$ scattering supermatrix with $(\tilde{S}_{n,m})_{u,v}$ which scatters W_v wave into W_u wave

$(\tilde{E}_n)_u) \equiv$ source supervector

$(\tilde{V}_n)_u \equiv$ combined voltage vector of wave W_u

$$= (\tilde{V}_n^{(+)})_u + (\tilde{Z}_{c_{n,m}})_u \cdot (\tilde{I}_n^{(+)})_u \tag{3}$$

$(\tilde{V}_{s_n})_u$ ≡ combined voltage source vector for W_u

$$\equiv (\tilde{V}^{(+)}_{s_n})_u + (\tilde{Z}_{c_{n,m}})_u \cdot (\tilde{I}^{(+)}_{s_n})_u$$

$(\tilde{Z}_{c_{n,m}})_u$ ≡ normalization impedance matrix for W_u

$(\tilde{V}^{(+)}_n)_u$, $(\tilde{I}^{(+)}_n)_u$ ≡ true voltage and current vectors on the surface containing W_u with "+" indicating the current is positive in the propagating direction of W_u (Fig. 3)

$(\tilde{V}^{(+)}_{s_n})_u$, $(\tilde{I}^{(+)}_{s_n})_u$ ≡ voltage source vector and current source vectors for W_u, with + indicating that the voltage is positive when it increases with the propagating direction of W_u and the current is positive when it flows into the edge (Fig. 3) (4)

After solving for $((\tilde{V}_n)_u)$ from Equation 1, the true voltage and current can be obtained from the two combined propagating voltages waves.

To carry out the above calculation for a complex system is tedious and time-consuming. A more important practical approach is to introduce reasonable assumptions and approximations so that the equations can be simplified and the signal upper bounds inside the system can be estimated. Reference 1 uses the good shielding approximation.

b. Good shielding approximation and signal upper bounds--Based on the structure of the identity and scattering supermatrices, the interaction supermatrix is block tridiagonal at the layer level of partition. That is, with indices λ, η for layers and $u \sim \alpha,\lambda$, $v \sim \beta,\eta$.

$$(\tilde{I}_{n,m})_{u,v} \equiv ((\tilde{I}_{n,m})_{\alpha,\beta})_{\lambda,\eta} = ((0_{n,m})_{\alpha,\beta})_{\lambda,\eta}, \text{ for } |\lambda-\eta| \geq 2, \quad (5)$$

When the combined voltage source vector $((\tilde{V}_{s_n})_\alpha)_\lambda$ is nonzero only in the outermost layer ($\lambda = 1$), Equation 1 can be solved using the good shielding

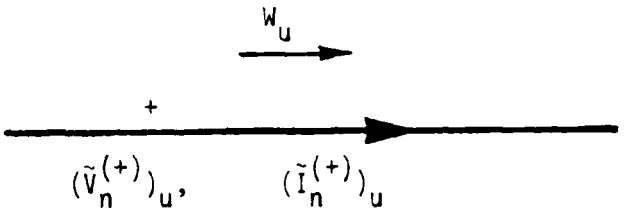

$$(\tilde{V}_n)_u = (\tilde{V}_n^{(+)})_u + (\tilde{Z}_{c_{n,m}})_u \cdot (\tilde{I}_n^{(+)})_u$$

(a) Combined voltage

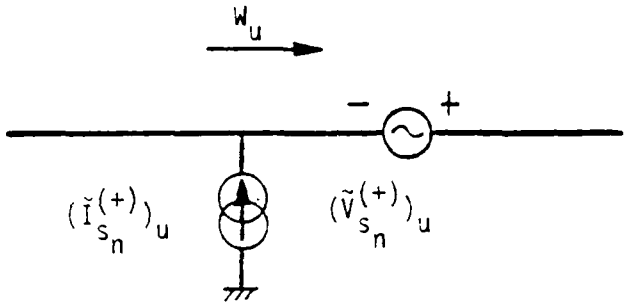

$$(\tilde{V}_{s_n})_u = (\tilde{V}_{s_n}^{(+)})_u + (\tilde{Z}_{c_{n,m}})_u \cdot (\tilde{I}_{s_n}^{(+)})_u$$

(b) Combined source voltage

Figure 3. Sign conventions for the real voltages and currents used in the definitions of (a) the combined voltage and (b) the combined source voltage.

approximation. The good shielding approximation is imposed by assuming that the off-diagonal blocks of the interaction supermatrix are small in the norm sense (for a description of the norm concept, see Refs. 5 and 6) compared to those of diagonal blocks. Physically, the good shielding approximation thus uses the assumption that the combined voltages of an outer layer are not influenced by those of its inner layers. The solution is, with the step-by-step procedure working from the bottom of the supermatrix equation,

$$((\tilde{V}_n)_\alpha)_\lambda \simeq (-1)((\tilde{I}_{n,m})_{\alpha,\beta})^{-1}_{\lambda,\lambda} \odot ((\tilde{I}_{n,m})_{\alpha,\beta})_{\lambda,\lambda-1} \odot$$

$$\odot ((\tilde{V}_n)_\alpha)_{\lambda-1}$$

$$\simeq (-1)^2((\tilde{I}_{n,m})_{\alpha,\beta})^{-1}_{\lambda,\lambda} \odot ((\tilde{I}_{n,m})_{\alpha,\beta})_{\lambda,\lambda-1} \odot$$

$$\odot ((\tilde{I}_{n,m})_{\alpha,\beta})^{-1}_{\lambda-1,\ \lambda-1} \odot ((\tilde{I}_{n,m})_{\alpha,\beta})_{\lambda-1,\ \lambda-2} \odot$$

$$\odot ((\tilde{V}_n)_\alpha)_{\lambda-2}$$

$$\simeq \text{----------}$$

$$\text{----------}$$

$$\simeq (-1)^{\lambda-1}((\tilde{I}_{n,m})_{\alpha,\beta})^{-1}_{\lambda,\lambda} \odot ((\tilde{I}_{n,m})_{\alpha,\beta})_{\lambda,\ \lambda-1} \odot \text{--------} \odot$$

$$\odot ((\tilde{I}_{n,m})_{\alpha,\beta})^{-1}_{2,2} \odot ((\tilde{I}_{n,m})_{\alpha,\beta})_{2,1} \odot$$

$$\odot ((\tilde{V}_n)_\alpha)_1$$

$$\simeq (-1)^{\lambda-1}((\tilde{I}_{n,m})_{\alpha,\beta})^{-1}_{\lambda,\lambda} \odot ((\tilde{I}_{n,m})_{\alpha,\beta})_{\lambda,\ \lambda-1} \odot \text{-------} \odot$$

$$\odot ((\tilde{I}_{n,m})_{\alpha,\beta})^{-1}_{2,2} \odot ((\tilde{I}_{n,m})_{\alpha,\beta})_{2,1} \odot$$

$$\odot ((\tilde{I}_{n,m})_{\alpha,\beta})^{-1}_{1,1} \odot ((\tilde{S}_{n,m})_{\alpha,\beta})_{1,1} \odot ((\tilde{V}_{s_n})_\alpha)_1 \qquad (6)$$

When the source vector is nonzero in an inner layer or in more than one layer, the complete solution can still be obtained using the Equation 6 solution by applying superpositions and topological inversions (Ref. 7).

When there are decoupled sublayers within a layer the above approximate result can be carried one step further. In this case, all that is needed is to include interaction matrices associated with the paths connected between the interested sublayers in Equation 6 (Ref. 1).

The signal upper bounds can be calculated from Equation 6 by using the norm concepts as follows:

$$\| ((\tilde{V}_n)_\alpha)_\lambda \| \leq \left\{ \prod_{\lambda'=0}^{\lambda-2} \| ((\tilde{I}_{n,m})_{\alpha,\beta})^{-1}_{\lambda-\lambda',\lambda-\lambda'} \| \; \| ((\tilde{I}_{n,m})_{\alpha,\beta})_{\lambda-\lambda',\lambda-\lambda'-1} \| \right\}$$

$$\| ((\tilde{I}_{n,m})_{\alpha,\beta})^{-1}_{1,1} \| \quad \| ((\tilde{S}_{n,m})_{\alpha,\beta})_{1,1} \| \quad \| ((\tilde{V}_{s_n})_\alpha)_1 \| \qquad (7)$$

Various vectors and their induced natural matrix norms can be used, depending on what the quantity of interest is. For example, if the current or voltage upper bound on an individual wire is desired, the maximum norm (Hölder norm with $p \to \infty$) should be used; if the maximum energy transferred to a volume is desired, the Euclidean norm ($p = 2$) (see the last formula of Eq. 8) should be used. If the quantity is intended for assessing a black box by comparing with a "black box failure norm," then the 1-norm ($\| \|_1$) should be used (Ref. 8). For the maximum ($\| \|_\infty$) and Euclidean ($\| \|_2$) norms, only the 2-norms for the terms on the right-hand side of Equation 7 need to be considered because $\|((\tilde{V}_n)_\alpha)_\lambda\|_\infty \leq \|((\tilde{V}_n)_\alpha)_\lambda\|_2$, unless the maximum norms give a tighter upper bound and are easier to calculate.

The properties of matrix and vector norms can be found in References 5 and 6. Some useful properties for the following discussion are

$$\| ((1_{n,m})-(A_{n,m}))^{-1} \| \leq \begin{cases} \{1-\| (A_{n,m}) \|\}^{-1}, & \text{if } \|(A_{n,m})\| \leq 1 \\ \| (A_{n,m})^{-1} \| \{1-\| (A_{n,m})^{-1} \|\}^{-1}, & \text{if } \| (A_{n,m})^{-1} \| < 1 \end{cases}$$

$$\|(A_{n,m})\|_\infty = \max_n \sum_m A_{n,m}$$

$$\|(A_{n,m})\|_2 = [\rho\{(A_{n,m})^\dagger \cdot (A_{n,m})\}]^{1/2}$$

$$\|(V_n)\|_p = \left\{\sum_n |V_n|^p\right\}^{1/p}$$

$$= \max_n \{|V_n|\}, \text{ for } p \to \infty \tag{8}$$

where "†" represents the conjugate transpose and $\rho\{\}$ means the spectral radius. Certain norm relations derived from the above equation, which are particularly useful for the scattering supermatrix considerations, can be found in Reference 9.

Having derived Equations 6 and 7, the influence of each block matrix on the signal response can be quantitatively considered. The diagonal block matrices (the inverse matrices) contain the information on the reflection coefficients of the shields. The off-diagonal block matrices bear the signatures of the transmission coefficients of the shields and are the main quantitites to reduce internal signals. Since the off-diagonal block matrices are essentially constructed from the transmission coefficients of various ports of entry (POEs), the first step is to evaluate the various POE transmission coefficients. The evaluation of the transmission (reflection) coefficient for a line POE is straightforward. The evaluation of an aperture POE's transmission coefficients requires further consideration.

c. Scattering matrix for aperture penetration--One way to bypass the difficulty of evaluating the scattering matrix elements associated with aperture penetrations is to neglect the less important field-to-field interaction. In doing this, all the edges in the interaction sequence diagram, except those belonging to the outermost layer, are the conducting wires. The more important field-to-wire (which will be considered only for the outermost shield) and wire-to-wire interactions through an aperture can be taken into account by introducing additional sources on the wires in the inner layer. The effect of these additional sources can be shown to be equivalent to the introduction of appropriate scattering (transmission) matrices. To elaborate this point further consider the two interaction mechanisms separately.

(1) Wire-to-wire interaction through aperture--First, consider Figure 4 in which the subshield has an aperture in it and the wires interact through the aperture. To calculate the aperture transmission coefficient, consider Figure 5, the equivalent circuit of Figure 4 for the inner wire when the inner wire has only the outgoing wave.

From Figure 5:

$$\tilde{S}_{\beta,\alpha;\lambda+1,\lambda} = \frac{\tilde{V}^{(+)}_{\beta\,;\,\lambda+1} + \tilde{Z}_{C_{\beta;\lambda+1}}\,\tilde{I}^{(+)}_{\beta\,;\,\lambda+1}}{\tilde{V}^{(+)}_{\alpha\,;\,\lambda} + \tilde{Z}_{C_{\alpha;\lambda}}\,\tilde{I}^{(+)}_{\alpha\,;\,\lambda}}$$

$$= \frac{2\,\tilde{Z}_{C_{\beta;\lambda+1}}}{\tilde{Z}_{C_{\beta;\lambda+1}} + \tilde{Z}_{L_{\beta;\lambda+1}}} \quad \frac{\tilde{V}^{(+)}_{s_{\lambda+1}} + \tilde{Z}_{L_{\beta;\lambda+1}}\,\tilde{I}^{(+)}_{s_{\lambda+1}}}{\tilde{V}^{(+)}_{\alpha\,;\,\lambda} + \tilde{Z}_{C_{\alpha;\lambda}}\,\tilde{I}^{(+)}_{\alpha;\lambda}}$$

$$= \frac{2\,\tilde{Z}_{C_{\beta;\lambda+1}}}{\tilde{Z}_{C_{\beta;\lambda+1}} + \tilde{Z}_{L_{\beta;\lambda+1}}} \quad \frac{\tilde{Z}_{C_{\alpha;\lambda}}}{\tilde{Z}_{L_{\alpha;\lambda}} + \tilde{Z}_{C_{\alpha;\lambda}}} \quad \frac{\tilde{V}^{(+)}_{s_{\lambda+1}}}{\tilde{Z}_{C_{\alpha;\lambda}}\,\tilde{I}^{(+)}_{\alpha;\lambda}}$$

$$+ \frac{2\,\tilde{Z}_{L_{\beta;\lambda+1}}}{\tilde{Z}_{C_{\beta;\lambda+1}} + \tilde{Z}_{L_{\beta;\lambda+1}}} \quad \frac{\tilde{Z}_{L_{\alpha;\lambda}}}{\tilde{Z}_{L_{\alpha;\lambda}} + \tilde{Z}_{C_{\alpha;\lambda}}} \quad \frac{\tilde{Z}_{C_{\beta;\lambda+1}}\,\tilde{I}^{(+)}_{s_{\lambda+1}}}{\tilde{V}^{(+)}_{\alpha;\lambda}} \qquad (9)$$

The quantity of interest for the upper bound transmission coefficient is

$$|\tilde{S}_{\beta,\alpha;\lambda+1,\lambda}| \leq \max\left\{|2\,\tilde{v}_{s_{\lambda+1,\lambda}}|;|2\,\tilde{i}_{s_{\lambda+1,\lambda}}|\right\} \qquad (10)$$

after using the conditions that $\tilde{Z}_{C_{\beta;\lambda+1}}$ and $\tilde{Z}_{C_{\alpha;\lambda}}$ have small imaginary parts, and that

$$\tilde{v}_{s_{\lambda+1,\lambda}} = \tilde{V}^{(+)}_{s_{\lambda+1}} - \tilde{Z}_{C_{\alpha;\lambda}}\,\tilde{I}^{(+)}_{\alpha;\lambda}\,; \quad \tilde{i}_{s_{\lambda+1,\lambda}} = \left(\tilde{Z}_{C_{\beta;\lambda+1}}\,\tilde{I}^{(+)}_{s_{\lambda+1}}\right) / \tilde{V}^{(+)}_{\alpha;\lambda} \qquad (11)$$

The wire-to-wire aperture interaction can essentially be treated as the line penetration by using Equations 10 and 11. When the wires are not

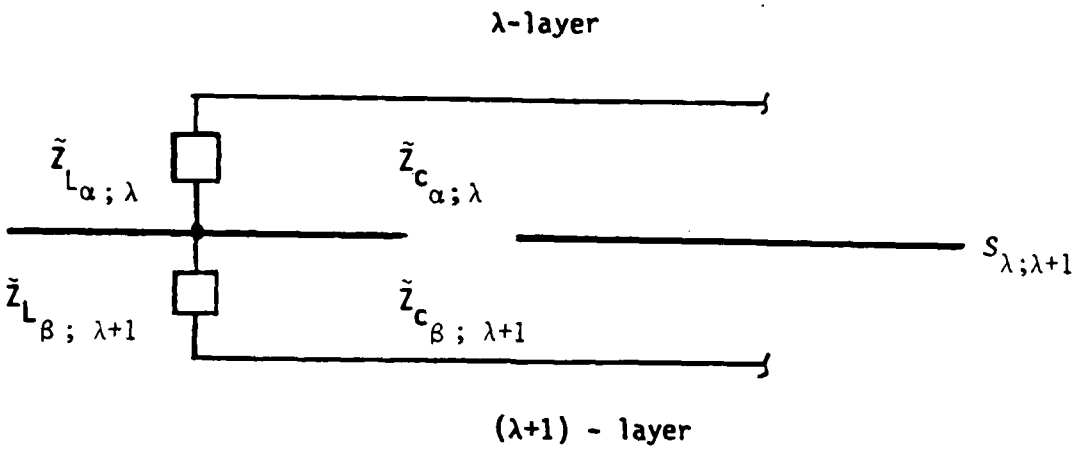

Note: The indices n,m have been omitted, because only one wire in each layer is assumed.

Figure 4. Schematic circuit of wires interacting through an aperture.

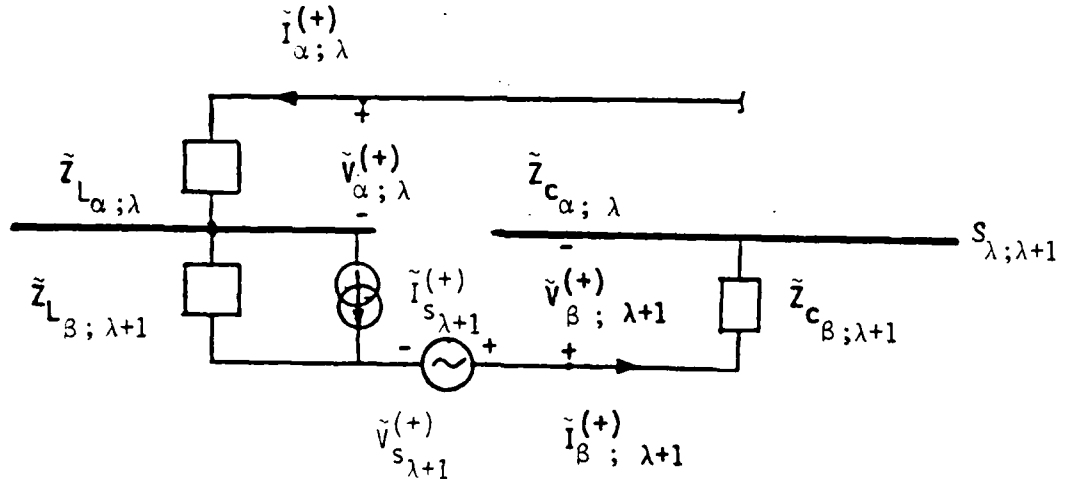

$$\tilde{V}^{(+)}_{s_{\lambda+1}} = \tilde{v}_{s_{\lambda+1},\lambda} \qquad \tilde{Z}_{C_{\alpha;\lambda}} \tilde{I}^{(+)}_{\alpha;\lambda} = s\,\tilde{\Phi}_m$$

$$\tilde{Z}_{C_{\beta;\lambda+1}} \tilde{I}^{(+)}_{s_{\lambda+1}} = \tilde{i}_{s_{\lambda+1},\lambda} \tilde{V}^{(+)}_{\alpha;\lambda} \quad (\text{where } \tilde{I}^{(+)}_{s_{\lambda+1}} = s\,\tilde{\Phi}_e)$$

$\tilde{\Phi}_m$ = magnetic flux linking wire

$\tilde{\Phi}_e$ = electric charge deposited on wire

Figure 5. Equivalent circuit schematic of Figure 4 for the inner wire when the inner wire allows only outgoing waves.

involved in the real line penetration, Equations 10 and 11 give the estimate of the transmission coefficient for the wire-to-wire interaction. In the case that the wires interact through more than one aperture and also through the real line penetration, all penetration effects should be combined. The transmission coefficient upper bound for this case is

$$|\tilde{S}_{\beta,\alpha;\lambda+1,\lambda}| \leq |\tilde{S}^{(L)}_{\beta,\alpha;\lambda+1,\lambda}| + \sum_i \max \left\{ 2|\tilde{v}^{(i)}_{s_{\lambda+1,\lambda}}|;\ 2|\tilde{i}^{(i)}_{s_{\lambda+1,\lambda}}| \right\} \qquad (12)$$

where the superscript (L) indicates that the quantity is for the line penetration and (i) is the index for the apertures. As for the reflection coefficients in the subshield scattering matrix under the good shielding approximation and the condition that the wires are outside the exclusion regions, their values should not be changed appreciably by the aperture. An exclusion region is designated for good shielding practice and wires are not allowed to reside in it. The upper-bound estimate obtained using Equation 12 can be used to obtain the appropriate scattering matrix and its norm when more than one wire on either and/or both sides of the shield are involved in the interaction process.

The transmission coefficient derived by Equation 12 is used for a wave definition so that the magnitude (or norm) of the combined voltage of the incoming wave in the outer layer is not smaller than that of the outgoing wave. This is further clarified in Appendix B where an alternative definition of the transmission matrix is given.

(2) Field-to-wire interaction through aperture--To treat the field-to-wire interaction through an aperture, consider the geometry shown in Figure 6. In this figure, there is an aperture in shield $S_{1;2}$. The field in the outer layer (V_1) will induce equivalent sources on the internal wire (Fig. 7). The effect of the equivalent sources can, in turn, be expressed in terms of an appropriate transmission coefficient.

In order to fit into the general interaction supermatrix formulation, the transmission coefficient has to be calculated as the ratio of the combined voltages of the internal outgoing wave to the external incoming wave. The combined voltage for the external electric and magnetic fields is yet to be defined. For an electrically small aperture, the electric and magnetic field

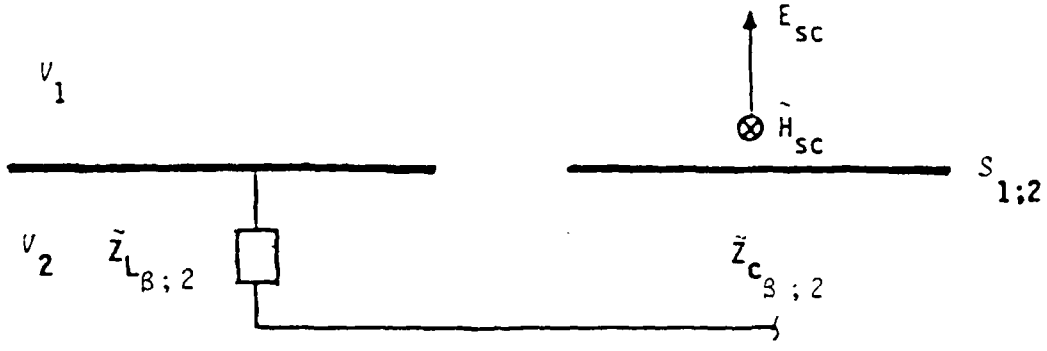

Note: The indices n,m have been omitted because there is only one wire in Λ_2.

Figure 6. Schematic of a field interacting with a wire through an aperture.

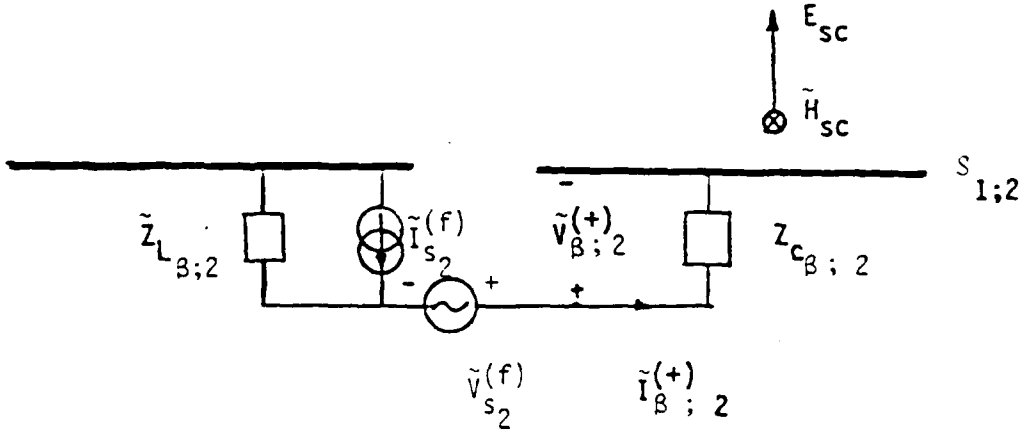

$$\tilde{V}^{(f)}_{s_2} = \tilde{v}^{(f)}_{s_{2,1}}[aZ_o \tilde{H}_{sc}] = s\,\tilde{\Phi}^{(f)}_m$$

$$\tilde{Z}_{C_{\beta;2}} \tilde{I}^{(f)}_{s_2} = \tilde{i}^{(f)}_{s_{2,1}}[a\tilde{E}_{sc}] \text{ (where } \tilde{I}^{(f)}_{s_2} = s\,\tilde{\Phi}^{(f)}_e)$$

$\tilde{E}_{sc}$, $\tilde{H}_{sc}$ = short-circuited electric, magnetic fields when the aperture is covered with conductor

$\tilde{\Phi}^{(f)}_m$ = magnetic flux linking wire due to $\tilde{H}_{sc}$

$\tilde{\Phi}^{(f)}_e$ = electric charge depoisited on wire due to $\tilde{E}_{sc}$

Figure 7. Equivalent circuit of Figure 6 for the inner wire when the inner wire allows only outgoing waves.

interactions with an internal wire are independent of each other. Although the choice of a normalization impedance for the combined voltage definition is artificial in this case, the natural choice is the free space wave impedance, $Z_o = \sqrt{\mu_o/\varepsilon_o} \approx 120\ \pi \approx 377\ \Omega$. With the normalization impedance of Z_o and the introduction of a length normalization factor "a", an imaginary wire can be created for the electric and magnetic fields. The wire configuration is shown in Figure 8. This is analogous to a plane wave incident at an angle. A possible alternative is given in Figure 9. This, on the other hand, simulates a plane wave propagating parallel to the surface. Both configurations give a combined voltage of $a[\tilde{E}_{sc} + Z_o\tilde{H}_{sc}]$ for the incoming waves at the shield, and

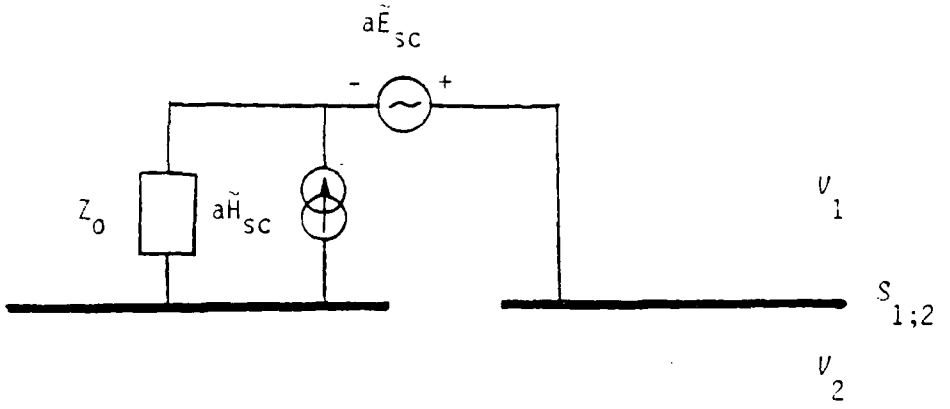

Figure 8. Example of imaginary wire configuration for the electric and magnetic fields.

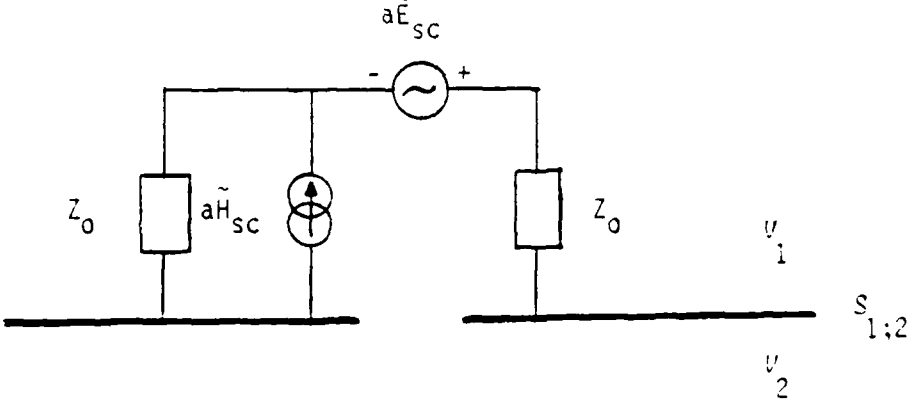

Figure 9. Example of an alternate imaginary wire configuration for the electric and magnetic fields.

give the same internal signal responses. This imaginary wire can further be assumed to be noninteracting with other external wires. The effect of the interaction between the field and other external wires is taken care of by introducing appropriate sources on other external wires.

From Figure 7 and the combined voltage definition in Figure 3a, the transmission coefficient for the field-to-wire aperture interaction can be estimated as follows (take $\lambda = 1$):

$$\tilde{S}_{\beta,\alpha;2,1} = \frac{\tilde{V}^{(+)}_{\beta\,;\,2} + \tilde{Z}_{C_{\beta;\,2}}\,\tilde{I}^{(+)}_{\beta;2}}{a\left[\tilde{E}_{sc} + Z_o\,\tilde{H}_{sc}\right]}$$

$$= \frac{2\,\tilde{Z}_{C_{\beta;2}}}{\tilde{Z}_{C_{\beta;2}} + \tilde{Z}_{L_{\beta;2}}} \quad \frac{\tilde{V}^{(f)}_{s_2} + \tilde{Z}_{L_{\beta;2}}\,\tilde{I}^{(f)}_{s_2}}{a\left[\tilde{E}_{sc} + Z_o\,\tilde{H}_{sc}\right]}$$

$$= \frac{2\,\tilde{Z}_{C_{\beta;2}}}{\tilde{Z}_{C_{\beta;2}} + \tilde{Z}_{L_{\beta;2}}} \quad \frac{a\,Z_o\,\tilde{H}_{sc}}{a\left[\tilde{E}_{sc} + Z_o\tilde{H}_{sc}\right]} \quad \frac{\tilde{V}^{(f)}_{s_2}}{a\,Z_o\tilde{H}_{sc}}$$

$$+ \frac{2\,\tilde{Z}_{L_{\beta;2}}}{\tilde{Z}_{C_{\beta;2}} + \tilde{Z}_{L_{\beta;2}}} \quad \frac{a\,\tilde{E}_{sc}}{a\left[\tilde{E}_{sc} + Z_o\tilde{H}_{sc}\right]} \quad \frac{\tilde{Z}_{C_{\beta;2}}\,\tilde{I}^{(f)}_{s_2}}{a\,\tilde{E}_{sc}} \qquad (13)$$

Here, the index α has been assigned for the incoming wave on the imaginary field wire, and the superscript (f) for quantities coresponding to field interaction. To proceed further in the estimate of the transmission coefficient upper bound, $\tilde{E}_{sc}$ and $\tilde{H}_{sc}$ are taken so that

$$\frac{|\,a\,Z_o\,\tilde{H}_{sc}\,|}{|\,a\left[\tilde{E}_{sc} + Z_o\,\tilde{H}_{sc}\right]\,|} \leq 1; \quad \frac{|\,a\,\tilde{E}_{sc}\,|}{|\,a\left[\tilde{E}_{sc} + Z_o\,\tilde{H}_{sc}\right]\,|} \leq 1 \qquad (14)$$

These conditions are not required if the scattering matrix is defined by using both $a[\tilde{E}_{sc} + Z_o\tilde{H}_{sc}]$ and $a[\tilde{E}_{sc} - Z_o\tilde{H}_{sc}]$ for the external combined voltages, as described in Appendix B. This then gives

$$|\tilde{S}_{\beta,\alpha;2,1}| \leq \max\{2|\tilde{v}^{(f)}_{s_{2,1}}|;\ 2|\tilde{i}^{(f)}_{s_{2,1}}|\} \tag{15}$$

where

$$\tilde{v}^{(f)}_{s_{2,1}} = \tilde{V}^{(f)}_{s_2} / [a\, Z_o\, \tilde{H}_{sc}]$$

$$\tilde{i}^{(f)}_{s_{2,1}} = \tilde{Z}_{c_{\beta;2}}\, \tilde{I}^{(f)}_{s_2} / [a\, \tilde{E}_{sc}] \tag{16}$$

Equation 15 can give a transmission coefficient upper bound for the field-to-wire aperture interaction when the wires are placed immediately outside the exclusion regions. Again, for $|\tilde{i}^{(f)}_s|$ the upper bound depends on the size of the internal wire. A maximum upper bound can be obtained by using a bowl instead of a wire for the internal circuit. Equation 15 can be used for calculating the scattering matrix and its norm when there is more than one wire and more than one aperture involved in the interaction process. In the case that the internal wire goes in both directions away from the aperture, the single wire should be treated as two wires, similar to that given in Appendix B where an alternative transmission coefficient definition for the aperture penetration is given.

d. Source vectors--It is appropriate at this point to discuss the configuration for the outermost layer, especially the source vectors. For field penetration through an aperture, the circuits for the imaginary wire are given in Figures 8 and 9. Similar circuits can also be obtained for a wire exposed to a source environment. The exposed wire acts as an antenna on which voltages and/or currents can be induced. The effect of the antenna on the connected shield and internal wires can be represented by either a Thevenin or Norton equivalent circuit (Fig. 10). With the introduction of an appropriate normalization impedance, the circuit can be easily incorporated into the supermatrix formulation for estimation of the associated source vectors and scattering matrix elements.

The circuit elements in the equivalent circuits of Figure 10 can be analytically or experimentally determined. Their values will depend on the source environment and the wire structure. The techniques for their determination and the results for certain special antenna structures can be found in several books and papers (for example, Ref. 10).

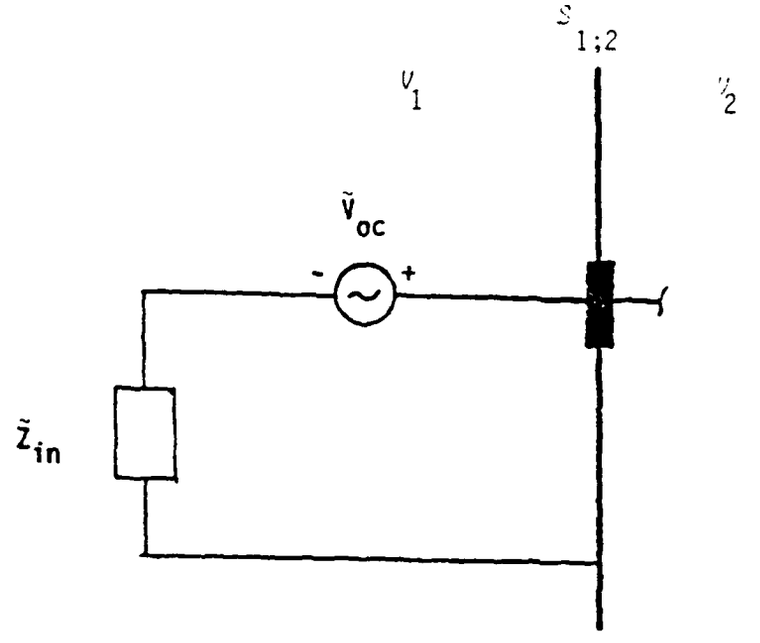

(a) Thevenin equivalent circuit

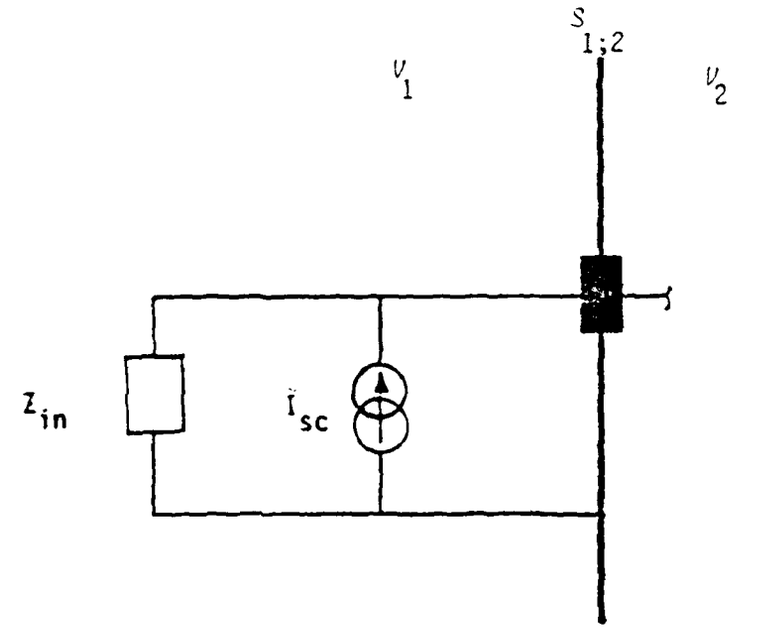

(b) Norton equivalent circuit

Figure 10. Equivalent circuits for an external wire exposed to an electromagnetic source.

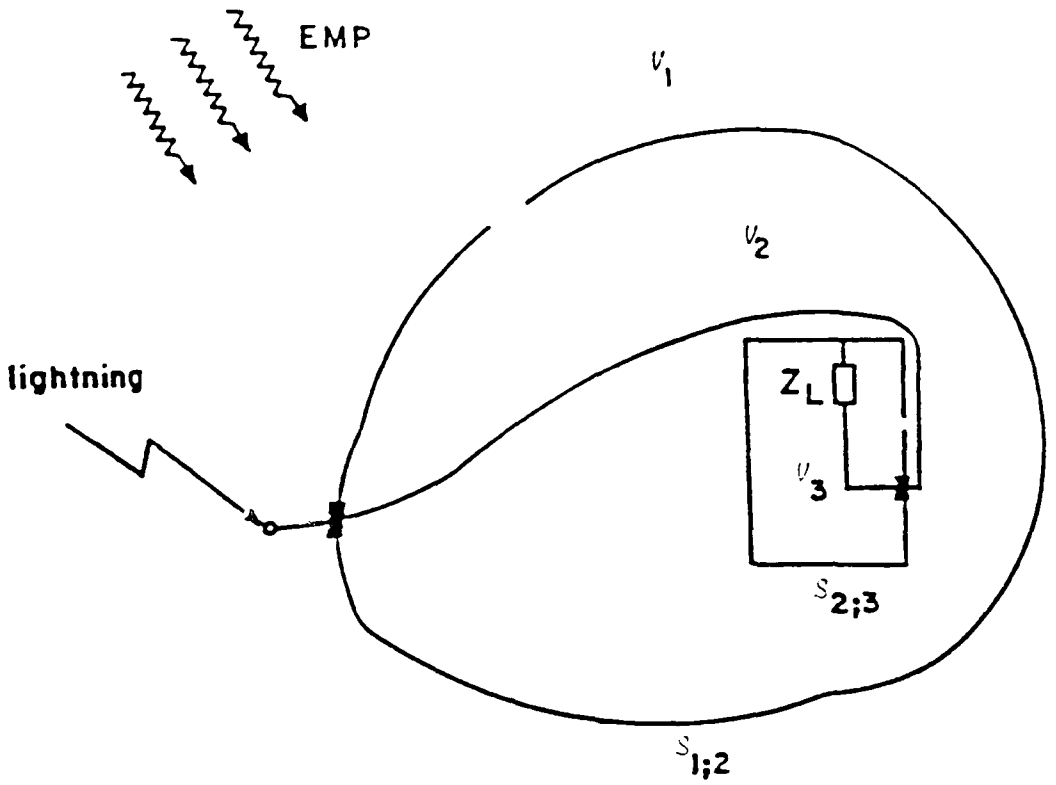

Figure 11. Illustrative example topological diagram.

3. AN ILLUSTRATIVE EXAMPLE

The illustrative example given in this subsection demonstrates how the basic ideas described in Section I-2 can be used. The topological diagram of the example is shown in Figure 11. This example has a relative shielding order of 2 (Ref. 7) and is therefore relatively simple. Nevertheless, the demonstration can be easily extended to a more complicated system. The exterior layer (V_1) in the example corresponds to the location of various important electromagnetic interference sources, such as EMP, lightning, etc. The innermost layer (V_3) contains sensitive and critical electronics. Of course, the innermost layer can also include strong interference sources (such as transmitting equipment) and equipment carrying signals that are not intended to be detected in the exterior layer. In this case, a topological inversion can be applied to transform the innermost layer to the exterior and vice versa, so that a similar topological diagram can be obtained. For this reason, only the case with an electromagnetic interference source in the exterior layer need be discussed.

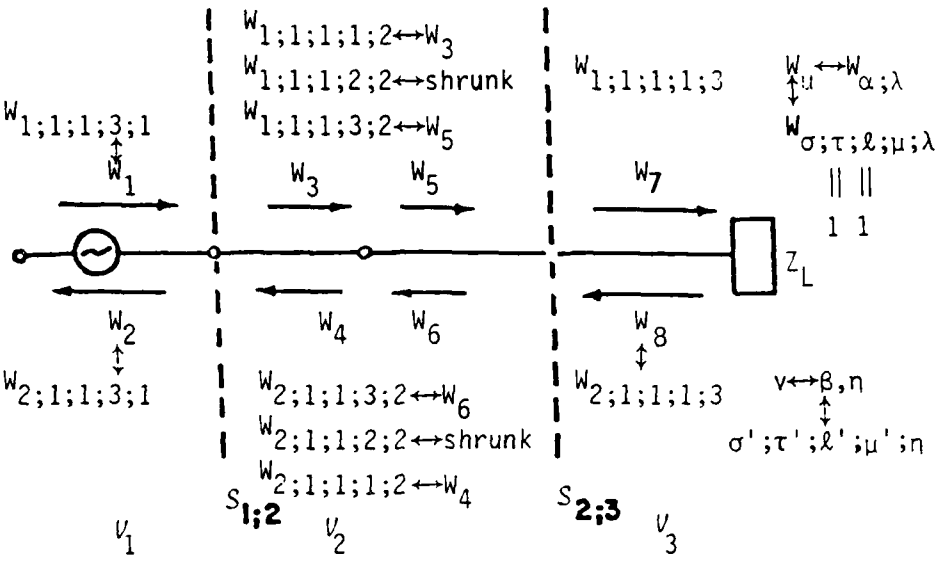

Figure 12. Corresponding interaction sequence diagram for illustrative topological diagram example shown in Figure 11.

a. General solution--Figure 11 shows that both shields allow aperture and line penetrations. The locations of the penetration points (Fig. 11) show that the aperture penetrations are important only through field-wire interaction for the outer shield and through wire-to-wire interaction for the inner shield. A corresponding interaction sequence diagram is given in Figure 12 which shows that there are either one or two tubes in each layer and two combined voltage waves propagating on each tube. Except for the outermost tube which includes two wires, one real wire and one imaginary wire to represent the external electric and magnetic field penetration, each tube has only one wire. Using the sign convention, symbol definitions, and Equation 1 gives Equation 17.

$$\left(\left(\left(\tilde{I}_{n,m}\right)_{\alpha,\beta}\right)_{\lambda,\eta}\right) \odot \left(\left(\left(\tilde{V}_n\right)_{\alpha}\right)_{\lambda}\right) = \left(\left(\left(\tilde{E}_n\right)_{\alpha}\right)_{\lambda}\right) \tag{17}$$

where

$$\left(\left(\left(\tilde{I}_{n,m}\right)_{\alpha,\beta}\right)_{\lambda,\eta}\right) \equiv \left(\left(\left(I_{n,m}\right)_{\alpha,\beta}\right)_{\lambda,\eta}\right) - \left(\left(\left(\tilde{S}_{n,m}\right)_{\alpha,\beta}\right)_{\lambda,\eta}\right)$$

$$\equiv \begin{pmatrix} \left(\left(\tilde{I}_{n,m}\right)_{\alpha,\beta}\right)_{1,1} & \left(\left(\tilde{I}_{n,m}\right)_{\alpha,\beta}\right)_{1,2} & \left(\left(\tilde{I}_{n,m}\right)_{\alpha,\beta}\right)_{1,3} \\ \left(\left(\tilde{I}_{n,m}\right)_{\alpha,\beta}\right)_{2,1} & \left(\left(\tilde{I}_{n,m}\right)_{\alpha,\beta}\right)_{2,2} & \left(\left(\tilde{I}_{n,m}\right)_{\alpha,\beta}\right)_{1,3} \\ \left(\left(\tilde{I}_{n,m}\right)_{\alpha,\beta}\right)_{3,1} & \left(\left(\tilde{I}_{n,m}\right)_{\alpha,\beta}\right)_{3,2} & \left(\left(\tilde{I}_{n,m}\right)_{\alpha,\beta}\right)_{3,3} \end{pmatrix}$$

$$= \left(\begin{array}{cccc|cccc|cc} 1 & 0 & -[\tilde{S}_{11}]_{1,2} & 0 & 0 & 0 & 0 & 0 & 0 & 0 \\ 0 & 1 & 0 & -[\tilde{S}_{22}]_{1,2} & 0 & 0 & 0 & 0 & 0 & 0 \\ -[\tilde{S}_{11}]_{2,1} & 0 & 1 & 0 & 0 & -[\tilde{S}_1]_{2,4} & 0 & 0 & 0 & 0 \\ 0 & -[\tilde{S}_{22}]_{2,1} & 0 & 1 & 0 & -[\tilde{S}_2]_{2,4} & 0 & 0 & 0 & 0 \\ \hline -[\tilde{S}_1]_{3,1} & -[\tilde{S}_2]_{3,1} & 0 & 0 & 1 & -\tilde{S}_{3,4} & 0 & 0 & 0 & 0 \\ 0 & 0 & 0 & 0 & 0 & 1 & 0 & -1 & 0 & 0 \\ 0 & 0 & 0 & 0 & -1 & 0 & 1 & 0 & 0 & 0 \\ 0 & 0 & 0 & 0 & 0 & 0 & -\tilde{S}_{6,5} & 1 & 0 & -\tilde{S}_{6,8} \\ \hline 0 & 0 & 0 & 0 & 0 & 0 & -\tilde{S}_{7,5} & 0 & 1 & -\tilde{S}_{7,8} \\ 0 & 0 & 0 & 0 & 0 & 0 & 0 & 0 & -\tilde{S}_{8,7} & 1 \end{array}\right)$$

$$\underbrace{\underbrace{m=1 \quad m=2}_{v=1} \quad \underbrace{m=1 \quad m=2}_{v=2}}_{\sigma'=1 \qquad \sigma'=2} \quad \underbrace{\underbrace{v=3 \quad v=4}_{\sigma'=1 \quad \sigma'=2} \quad \underbrace{v=5 \quad v=6}_{\sigma'=1 \quad \sigma'=2}}_{\mu'=1 \qquad \mu'=3} \quad \underbrace{\underbrace{v=7 \quad v=8}_{\sigma'=1 \quad \sigma'=2}}_{\mu'=1}$$

$$\underbrace{\qquad\qquad\qquad\qquad}_{\mu'=3,\ell'=1,\tau'=1} \qquad\qquad \underbrace{\qquad\qquad\qquad\qquad}_{\ell'=1,\tau'=1} \qquad\qquad \underbrace{\qquad\qquad}_{\ell'=1,\tau'=1}$$

$$\eta=1 \qquad\qquad \eta=2 \qquad\qquad \eta=3 \qquad\qquad (18)$$

where $\alpha,\beta \leftrightarrow \sigma,\sigma';\ \tau,\tau';\ell,\ell';\mu,\mu'$

$$\left(\left(\left(\tilde{V}_n\right)_\alpha\right)_\lambda\right) \equiv \begin{pmatrix} \left(\left(\tilde{V}_n\right)_\alpha\right)_1 \\ \left(\left(\tilde{V}_n\right)_\alpha\right)_2 \\ \left(\left(\tilde{V}_n\right)_\alpha\right)_3 \end{pmatrix} = \begin{pmatrix} [\tilde{V}_1]_1 \\ [\tilde{V}_2]_1 \\ [\tilde{V}_1]_2 \\ [\tilde{V}_2]_2 \\ \text{-----} \\ \tilde{V}_3 \\ \tilde{V}_4 \\ \tilde{V}_5 \\ \tilde{V}_6 \\ \text{-----} \\ \tilde{V}_7 \\ \tilde{V}_8 \end{pmatrix}$$

$$\left(\left(\left(\tilde{E}_n\right)_\alpha\right)_\lambda\right) \equiv \left(\left(\left(\tilde{S}_{n,m}\right)_{\alpha,\beta}\right)_{\lambda,n}\right) \odot \left(\left(\left(\tilde{V}_{s_n}\right)_\alpha\right)_\lambda\right) \tag{19}$$

or

$$\begin{pmatrix} \left(\left(\tilde{E}_n\right)_\alpha\right)_1 \\ \left(\left(\tilde{E}_n\right)_\alpha\right)_2 \\ \left(\left(\tilde{E}_n\right)_\alpha\right)_3 \end{pmatrix} \equiv \left(\left(\left(\tilde{S}_{n,m}\right)_{\alpha,\beta}\right)_{\lambda,n}\right) \odot \begin{pmatrix} \left(\left(\tilde{V}_{s_n}\right)_\alpha\right)_1 \\ \left(\left(\tilde{V}_{s_n}\right)_\alpha\right)_2 \\ \left(\left(\tilde{V}_{s_n}\right)_\alpha\right)_3 \end{pmatrix} \tag{20}$$

and

$$(V_{s_n})_\alpha)_1 = \begin{pmatrix} \begin{pmatrix} [\tilde{V}_{s_1}]_1 \\ [\tilde{V}_{s_2}]_1 \end{pmatrix} \\ \hline \begin{pmatrix} [\tilde{V}_{s_1}]_2 \\ [\tilde{V}_{s_2}]_2 \end{pmatrix} \end{pmatrix}$$

$$((V_{s_n})_\alpha)_2 = \begin{pmatrix} 0 \\ 0 \\ 0 \\ 0 \end{pmatrix}$$

$$((\tilde{V}_{s_n})_\alpha)_3 = \begin{pmatrix} 0 \\ 0 \end{pmatrix} \qquad (21)$$

where, in order to have the simple representations of Equations 18, 19, and 20, the n,m indices (inside the square brackets) are used only for the wires in the outermost layer, and the indices outside the square brackets and those unbracketed variables are referred to the waves, i.e., in

$$[\tilde{A}_x]_*,\ [\tilde{A}_{x,x}]_{*,*},\ [\tilde{A}_x]_{*,*},\ \tilde{A}_{*,*},\ \tilde{A}_*$$

$x,*,$ are respectively referred to the wire index (n or m) in the outermost layer and the wave index (u or v). The corresponding partitioned indices according to the levels of the hierarchical topology are given in Figure 12. Here, the zero-tube-length assumption has been used, and hence the layer propagation matrices are identity matrices. For a tighter bound estimate, suitable delay and/or decay factors should be included in the above formulation.

b. Good shielding approximation and signal upper bound--After imposing the good shielding assumption, the approximate solution to Equation 17 is explicitly given by

$$((\tilde{V}_n)_\alpha)_3 = ((\tilde{I}_{n,m})_{\alpha,\beta})^{-1}_{3,3} \odot ((\tilde{I}_{n,m})_{\alpha,\beta})_{3,2} \odot ((\tilde{I}_{n,m})_{\alpha,\beta})^{-1}_{2,2}$$

$$\odot ((\tilde{I}_{n,m})_{\alpha,\beta})_{2,1} \odot ((\tilde{I}_{n,m})_{\alpha,\beta})^{-1}_{1,1} \odot ((\tilde{S}_{n,m})_{\alpha,\beta})_{1,1} \odot ((\tilde{V}_{s_n})_\alpha)_1 \quad (22)$$

from which the norm relationship suitable for bounding the internal signal is

$$\| ((\tilde{V}_n)_\alpha)_3 \| \leq \| ((\tilde{I}_{n,m})_{\alpha,\beta})^{-1}_{3,3} \| \, \| ((\tilde{I}_{n,m})_{\alpha,\beta})_{3,2} \| \, \| ((\tilde{I}_{n,m})_{\alpha,\beta})^{-1}_{2,2} \|$$

$$\| ((\tilde{I}_{n,m})_{\alpha,\beta})_{2,1} \| \, \| ((\tilde{I}_{n,m})_{\alpha,\beta})^{-1}_{1,1} \| \, \| ((\tilde{S}_{n,m})_{\alpha,\beta})_{1,1} \| \, \| ((\tilde{V}_{s_n})_\alpha)_1 \| \quad (23)$$

As mentioned in Section I-2, there are various methods to obtain bounds for the norms in Equation 23. The most straightforward method is to consider the 2-norms for the terms on the right-hand side of Equation 23. From this consideration,

$$\| ((\tilde{V}_n)_\alpha)_3 \|_\infty \leq \| ((\tilde{V}_n)_\alpha)_3 \|_2 \leq \frac{\| ((\tilde{S}_{n,m})_{\alpha,\beta})_{3,2} \|_2}{1 - \| ((S_{n,m})_{\alpha,\beta})_{3,3} \|_2} \, \frac{\| ((\tilde{S}_{n,m})_{\alpha,\beta})_{2,1} \|_2}{1 - \| ((\tilde{S}_{n,m})_{\alpha,\beta})_{2,2} \|_2}$$

$$\frac{\| ((\tilde{S}_{n,m})_{\alpha,\beta})_{1,1} \|_2}{1 - \| ((\tilde{S}_{n,m})_{\alpha,\beta})_{1,1} \|_2} \cdot \| ((\tilde{V}_{s_n})_\alpha)_1 \|_2 \quad (24)$$

Equation 24 was obtained by using $(\tilde{T}) = (1) - (\tilde{S})$, $\|(\tilde{S})_{\lambda,\lambda}\|_2 < 1$, and $\|((1_{n,m}) - (A_{n,m}))^{-1}\|$ as given in Equation 8. The expression, $\|(\tilde{S})_{\lambda,\lambda}\|_2 < 1$, is true under certain restrictive conditions, such as when $(Z_c)_\lambda$ is a diagonal matrix with equal positive real elements, and is a consequence of the conservation of energy (Refs. 5 and 9). More general conditions will be worked out in the future.

With the interaction (scattering) supermatrix given in Equation 18, Equation 24 becomes

$$\max\{|\tilde{V}_5|;|\tilde{V}_6|\} \le \sqrt{|\tilde{V}_5|^2 + |\tilde{V}_6|^2} \le \frac{|\tilde{S}_{5,3}|}{1-\max\{|\tilde{S}_{5,6}|;|\tilde{S}_{6,5}|\}} \cdot$$

$$\cdot \frac{\sqrt{|[\tilde{S}_1]_{3,1}|^2 + |[\tilde{S}_2]_{3,1}|^2}}{1-\max\{|\tilde{S}_{3,4}|;|\tilde{S}_{4,3}|\}} \cdot$$

$$\cdot \frac{\max\{|[\tilde{S}_{11}]_{1,2}|;|[\tilde{S}_{22}]_{1,2}|;|[\tilde{S}_{11}]_{2,1}|;|[\tilde{S}_{22}]_{2,1}|\}}{1-\max\{|[\tilde{S}_{11}]_{1,2}|;|[\tilde{S}_{22}]_{1,2}|;|[\tilde{S}_{11}]_{2,1}|;|[\tilde{S}_{22}]_{2,1}|\}} \cdot \| ((\tilde{V}_{s_n})_u)_1 \|_2 \quad (25)$$

The upper bound given in Equation 25 becomes infinity when any one of the reflection coefficients (i.e., those with $|u-v| = 1$) equals ± 1. For this situation, alternative bounding procedures should be employed on $\|(\tilde{I}_{n,m})_{\alpha,\beta})_{\lambda,\lambda}^{-1}\|$ in Equation 23. One such procedure is to first perform the matrix inversion before bounding the norm. For the example considered here, this procedure gives

$$\max\{|\tilde{V}_7|;|\tilde{V}_8|\} \le \sqrt{|\tilde{V}_7|^2 + |\tilde{V}_8|^2} \le \frac{2\sqrt{2}|\tilde{S}_{7,5}|}{1-|\tilde{S}_{7,8}|\ |\tilde{S}_{8,7}|} \quad \frac{8\sqrt{|[\tilde{S}_1]_{3,1}|^2 + |[\tilde{S}_2]_{3,1}|^2}}{1-|\tilde{S}_{3,4}|\ |\tilde{S}_{6,5}|}$$

$$\times \frac{4}{1-\max\{|[\tilde{S}_{11}]_{1,2}\ [\tilde{S}_{11}]_{2,1}|;|[\tilde{S}_{22}]_{1,2}\ \ [\tilde{S}_{22}]_{2,1}|\}} \quad \| ((\tilde{V}_{s_n})_\alpha)_1 \|_2 \quad (26)$$

In obtaining Equation 26, the following relation has also been used (Ref. 9)

$$\| (A_{n,m}) \|_2 \le \sqrt{N}\ \| (A_{n,m}) \|_\infty \quad (27)$$

where N is the number of columns of the square matrix $(A_{n,m})$.

Equation 26 clearly shows that the most effective approach to reduce the internal signal upper bound is to decrease the transmission coefficients $|[\tilde{S}_1]_{3,1}|$, $|[\tilde{S}_2]_{3,1}|$, and $|\tilde{S}_{7,5}|$. These transmission coefficients and the other reflection coefficients have all been defined in Subsection 2. More specifically,

$|\tilde{S}_{7,5}|$ ≡ transmission coefficient at $S_{2;3}$ due to both wire-to-wire aperture penetration and line penetration ($|\tilde{S}^{(L)}_{7,5}|$)

$$|\tilde{S}_{7,5}| \leq |\tilde{S}^{(L)}_{7,5}| + \max\left\{2|\tilde{v}_{s_{3,2}}|;\ 2|\tilde{i}_{s_{3,2}}|\right\} \tag{28}$$

$|[\tilde{S}_1]_{3,1}|$, $|[\tilde{S}_2]_{3,1}|$ ≡ transmission coefficients at $S_{1;2}$ due to field-to-wire aperture and line penetrations, and

$$\sqrt{|[\tilde{S}_1]_{3,1}|^2 + |[\tilde{S}_2]_{3,1}|^2} \leq \sqrt{|[\tilde{S}^{(L)}_2]_{3,1}|^2 + \max\left\{4|v^{(f)}_{s_{2,1}}|^2;\ 4|\tilde{i}^{(f)}_{s_{2,1}}|^2\right\}} \tag{29}$$

Here, the subscripts of $\tilde{v}_s$, $\tilde{i}_s$, $\tilde{v}^{(f)}_s$ and $\tilde{i}^{(f)}_s$ refer to layers (Eqs. 10 and 13).

$|[\tilde{S}_{11}]_{1,2}|$, $|[\tilde{S}_{22}]_{1,2}|$ ≡ reflection coefficients at the termination junction in V_1 (see Figs. 8, 9, and 10) for the imaginary and real wires, respectively.

$|[\tilde{S}_{11}]_{2,1}|$, $|[\tilde{S}_{22}]_{2,1}|$ ≡ reflection coefficients at $S_{1;2}$ for the wires (one real wire and one imaginary wire) in V_1.

$|\tilde{S}_{3,4}|$, $|\tilde{S}_{6,5}|$ ≡ reflection coefficients at $S_{1;2}$ and $S_{2;3}$, respectively, for the wire in V_2.

$|\tilde{S}_{-,8}|$, $|\tilde{S}_{8,7}|$ ≡ reflection coefficients at $S_{2;3}$ and the termination junction for the wire in V_3.

Experimental methods leading to the determination of these shielding coefficients are discussed in Section I-4.

For the discussion of the source vector in Equations 25 and 26, the wire arrangement in Figures 5a and 6b will be used. Thus,

$$\| ((\tilde{V}_{s_n})_\alpha)_1 \|_2 = \left\| \begin{pmatrix} a[\tilde{E}_{sc} + Z_o \tilde{H}_{sc}] \\ \tilde{Z}_c \tilde{I}_{sc} \end{pmatrix} \right\|_2$$

$$\left\| \begin{pmatrix} a[-\tilde{E}_{sc} + Z_o \tilde{H}_{sc}] \\ \tilde{Z}_c \tilde{I}_{sc} \end{pmatrix} \right\|_2$$

$$\leq \sqrt{2}\{a^2[|\tilde{E}_{sc}| + Z_o|\tilde{H}_{sc}|]^2 + |\tilde{Z}_c \tilde{I}_{sc}|^2\}^{1/2} \tag{30}$$

where Z_c is the normalization impedance for the real wire and

$$[\tilde{S}_{11}]_{2,1} = -1, \quad [\tilde{S}_{11}]_{1,2} = 0 \tag{31}$$

for the imaginary wire.

4. DETERMINATION OF INTERACTION (SCATTERING) SUPERMATRIX ELEMENTS FOR LINE AND APERTURE PENETRATIONS

Sections I-2 and I-3 concluded that an internal signal upper bound can be estimated once the scattering matrices of the shields, the termination junctions, and the source environment are known. Methods for determining the scattering matrix elements are discussed in this section.

a. Scattering matrix for line penetration--The scattering matrix for the line penetrations through a shield is defined through the combined voltages via (see Eq. 2 and Fig. 13)

$$\begin{pmatrix} ((\tilde{V}_n^{(+)})_\alpha)_\lambda - ((\tilde{Z}_{c_{n,m}})_\alpha)_\lambda \cdot ((\tilde{I}_n^{(+)})_\alpha)_\lambda \\ ((\tilde{V}_n^{(+)})_\beta)_{\lambda+1} + ((\tilde{Z}_{c_{n,m}})_\beta)_{\lambda+1} ((\tilde{I}_n^{(+)})_\beta)_{\lambda+1} \end{pmatrix} \equiv$$

$$\begin{pmatrix} ((\tilde{S}_{n,m})_{\alpha',\alpha})_{\lambda,\lambda} ((\tilde{S}_{n,m})_{\alpha',\beta'})_{\lambda,\lambda+1} \\ ((\tilde{S}_{n,m})_{\beta,\alpha})_{\lambda+1,\lambda} ((\tilde{S}_{n,m})_{\beta,\beta'})_{\lambda+1,\lambda+1} \end{pmatrix} \odot \begin{pmatrix} ((\tilde{V}_n^{(+)})_\alpha)_\lambda + ((\tilde{Z}_{c_{n,m}})_\alpha)_\lambda \cdot ((\tilde{I}_n^{(+)})_\alpha)_\lambda \\ ((\tilde{V}_n^{(+)})_\beta)_{\lambda+1} - ((\tilde{Z}_{c_{n,m}})_\beta)_{\lambda+1} ((\tilde{I}_n^{(+)})_\beta)_{\lambda+1} \end{pmatrix}$$

(32)

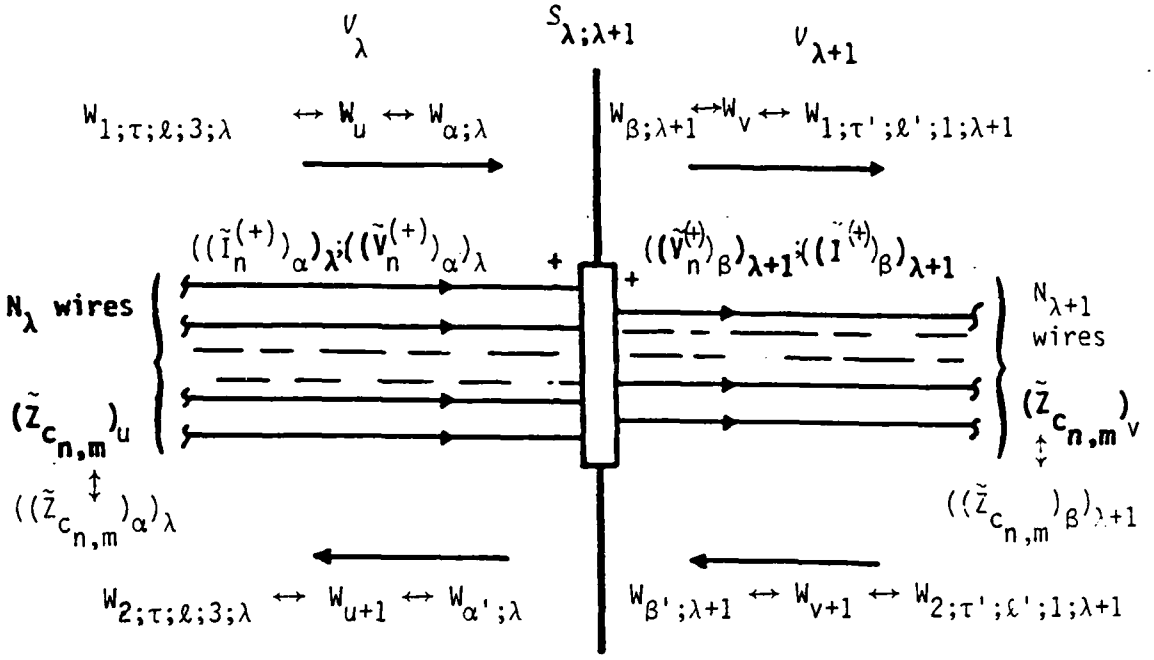

Figure 13. Schematic of wire bundle penetrating a shield.

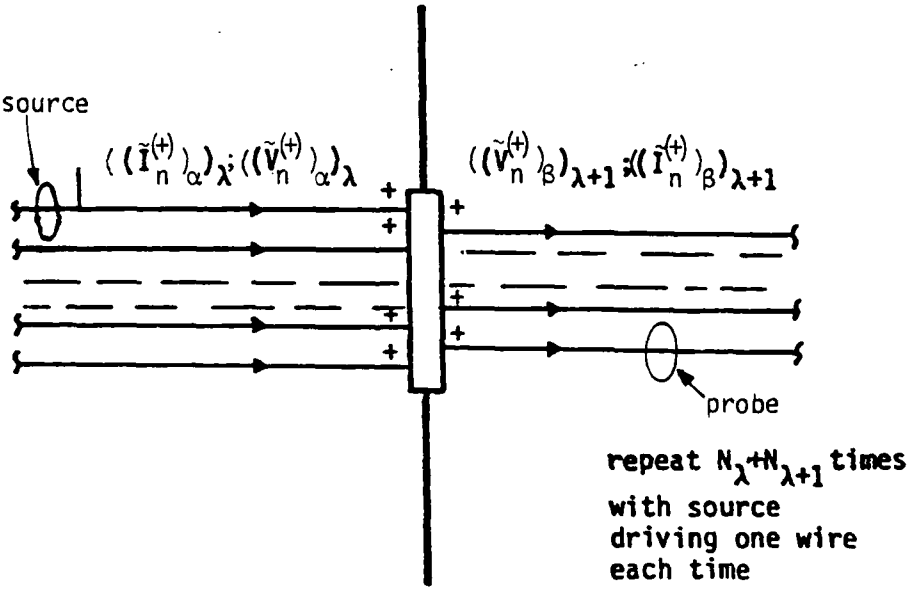

Figure 14. Experimental setup to estimate scattering matrix associated with wire bundle penetrating through a shield.

where

$$\begin{pmatrix} ((\tilde{S}_{n,m})_{\alpha',\alpha})_{\lambda,\lambda} & ((\tilde{S}_{n,m})_{\alpha',\beta'})_{\lambda,\lambda+1} \\ ((\tilde{S}_{n,m})_{\beta,\alpha})_{\lambda+1,\lambda} & ((\tilde{S}_{n,m})_{\beta,\beta'})_{\lambda+1,\lambda+1} \end{pmatrix} \equiv \begin{pmatrix} (\tilde{S}_{n,m})_{u+1,u} & (\tilde{S}_{n,m})_{u+1,v+1} \\ (\tilde{S}_{n,m})_{v,u} & (\tilde{S}_{n,m})_{v,v+1} \end{pmatrix} \quad (33)$$

if the wave indices (Figs. 13 and 14) are used.

The definition of the combined voltages clearly requires that the characteristic impedance matrix ($\tilde{Z}_{c_{n,m}}$) of the wires be known. For a multiwire case, the determination of ($\tilde{Z}_{c_{n,m}}$) might be difficult, if not impossible. However, at this moment, the assumption that ($\tilde{Z}_{c_{n,m}}$) is known will be made.

Equation 32 shows that there are $(N_\lambda + N_{\lambda+1})^2$ scattering matrix coefficients to be determined if there are N_λ and $N_{\lambda+1}$ wires, respectively. If certain voltage and/or current sources are applied to the wire systems and voltage and current responses are measured on all the wires, then the $(N_\lambda + N_{\lambda+1})$ equations can be obtained for the scattering matrix coefficients. That is to say, in order to completely determine the scattering matrix $(N_\lambda + N_{\lambda+1})$ such tests need to be performed independently. One way to accomplish this is to apply the source to one wire for each test (Fig. 14). The number of independent experiments can be reduced, with certain a priori knowledge about the shields. For example, if the shield is symmetric and satisfies reciprocity, the required experiments can be cut by one-half.

In the case where there is only one wire on each side, Equation 32 takes the following form (Fig. 13)

$$\begin{pmatrix} \tilde{V}^{(+)}_{\alpha\,;\,\lambda} - \tilde{Z}_{c_{\alpha\,;\,\lambda}} & \tilde{I}^{(+)}_{\alpha\,;\,\lambda} \\ \tilde{V}^{(+)}_{\beta\,;\,\lambda+1} + \tilde{Z}_{c_{\beta\,;\,\lambda+1}} & \tilde{I}^{(+)}_{\beta\,;\,\lambda+1} \end{pmatrix} \equiv$$

$$\begin{pmatrix} \tilde{S}_{\alpha',\alpha\,;\,\lambda,\lambda} & \tilde{S}_{\alpha',\beta';\lambda,\lambda+1} \\ \tilde{S}_{\beta,\alpha;\lambda+1,\lambda} & \tilde{S}_{\beta,\beta';\lambda+1,\lambda+1} \end{pmatrix} \cdot \begin{pmatrix} \tilde{V}^{(+)}_{\alpha\,;\,\lambda} + \tilde{Z}_{c_{\alpha\,;\,\lambda}} & \tilde{I}^{(+)}_{\alpha\,;\,\lambda} \\ \tilde{V}^{(+)}_{\beta\,;\,\lambda+1} - \tilde{Z}_{c_{\beta\,;\,\lambda+1}} & \tilde{I}^{(+)}_{\beta\,;\,\lambda+1} \end{pmatrix} \quad (34)$$

where

$$\begin{pmatrix} \tilde{S}_{\alpha',\alpha;\lambda,\lambda} & \tilde{S}_{\alpha',\beta';\lambda,\lambda+1} \\ \tilde{S}_{\beta,\alpha;\lambda+1,\lambda} & \tilde{S}_{\beta,\beta';\lambda+1,\lambda+1} \end{pmatrix} \equiv \begin{pmatrix} \tilde{S}_{u+1,u} & \tilde{S}_{u+1,v+1} \\ \tilde{S}_{v,u} & \tilde{S}_{v,v+1} \end{pmatrix} \tag{35}$$

if the wave indices are used. The scattering matrix can be determined from the experiments shown in Figure 15 and solving some linear algebraic equations. In the case that the wires can be disconnected, the process of solving the linear equations can be avoided by performing a somewhat different experiment. Such experiments are shown in Figure 16. The experiment in Figure 16 results immediately in

$$\tilde{S}_{u+1,u} = \tilde{S}_{\alpha',\alpha;\lambda,\lambda} = \left. \frac{\tilde{V}^{(+)}_{\alpha\,;\,\lambda} - \tilde{Z}_{c_{\alpha\,;\,\lambda}} \tilde{I}^{(+)}_{\alpha\,;\,\lambda}}{\tilde{V}^{(+)}_{\alpha\,;\,\lambda} + \tilde{Z}_{c_{\alpha\,;\,\lambda}} \tilde{I}^{(+)}_{\alpha\,;\,\lambda}} \right|_{\tilde{V}^{(+)}_{\beta\,;\,\lambda+1} - \tilde{Z}_{c_{\beta;\lambda+1}} \tilde{I}^{(+)}_{\beta\,;\,\lambda+1} = 0}$$

$$\tilde{S}_{v,u} = \tilde{S}_{\beta,\alpha;\lambda+1,\lambda} = \left. \frac{\tilde{V}^{(+)}_{\beta\,;\,\lambda+1} + \tilde{Z}_{c_{\beta\,;\,\lambda+1}} \tilde{I}^{(+)}_{\beta\,;\,\lambda+1}}{\tilde{V}^{(+)}_{\alpha\,;\,\lambda} + \tilde{Z}_{c_{\alpha\,;\,\lambda}} \tilde{I}^{(+)}_{\alpha\,;\,\lambda}} \right|_{\tilde{V}^{(+)}_{\beta\,;\,\lambda+1} - \tilde{Z}_{c_{\beta\,;\,\lambda+1}} \tilde{I}^{(+)}_{\beta\,;\,\lambda+1} = 0} \tag{36}$$

while the experiment in Figure 3c results in

$$\tilde{S}_{u+1,v+1} = \tilde{S}_{\alpha',\beta';\lambda,\lambda+1} = \left. \frac{\tilde{V}^{(+)}_{\alpha\,;\,\lambda} - \tilde{Z}_{c_{\alpha\,;\,\lambda}} \tilde{I}^{(+)}_{\alpha\,;\,\lambda}}{\tilde{V}^{(+)}_{\beta\,;\,\lambda+1} - \tilde{Z}_{c_{\beta;\lambda+1}} \tilde{I}^{(+)}_{\beta\,;\,\lambda+1}} \right|_{\tilde{V}^{(+)}_{\alpha\,;\,\lambda} + \tilde{Z}_{c_{\alpha;\lambda}} \tilde{I}^{(+)}_{\alpha;\,\lambda} = 0}$$

$$\tilde{S}_{v,v+1} = \tilde{S}_{\beta,\beta';\lambda+1,\lambda+1} = \left. \frac{\tilde{V}^{(+)}_{\beta\,;\,\lambda+1} + \tilde{Z}_{c_{\beta;\lambda+1}} \tilde{I}^{(+)}_{\beta\,;\,\lambda+1}}{\tilde{V}^{(+)}_{\beta\,;\,\lambda+1} - \tilde{Z}_{c_{\beta;\lambda+1}} \tilde{I}^{(+)}_{\beta\,;\,\lambda+1}} \right|_{\tilde{V}^{(+)}_{\alpha\,;\,\lambda} + \tilde{Z}_{c_{\alpha;\lambda}} \tilde{I}^{(+)}_{\alpha\,;\,\lambda} = 0} \tag{37}$$

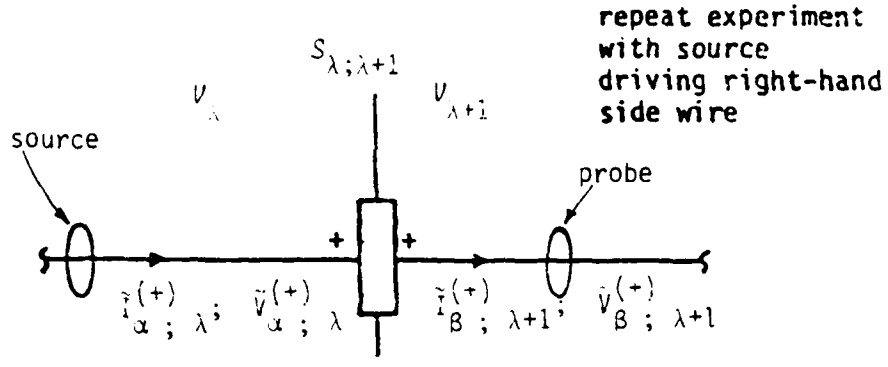

Note: The indices n,m have been omitted because only one wire in each layer is assumed.

Figure 15. Schematic of experimental setup for estimating the scattering matrix for the single wire line penetration.

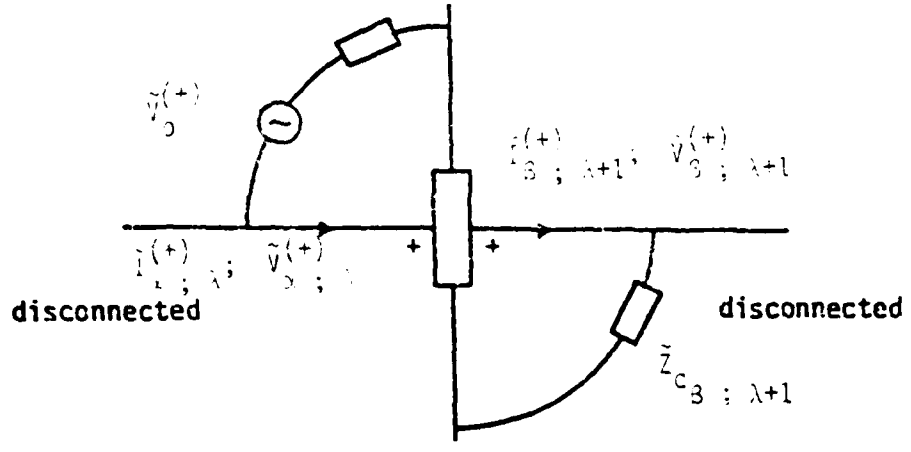

Figure 16. An alternative experimental setup for estimating the scattering matrix for single wire line penetration with wires disconnected.

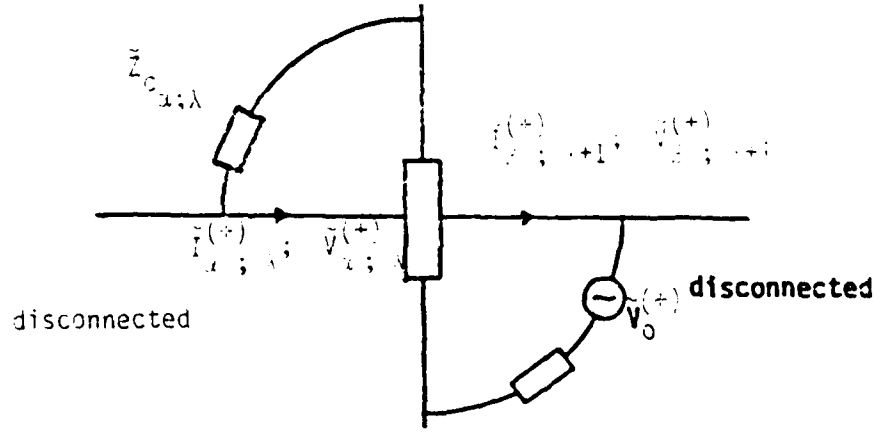

Figure 17. Another disconnected wire alternative experimental setup for estimating the scattering matrix for single wire line penetration.

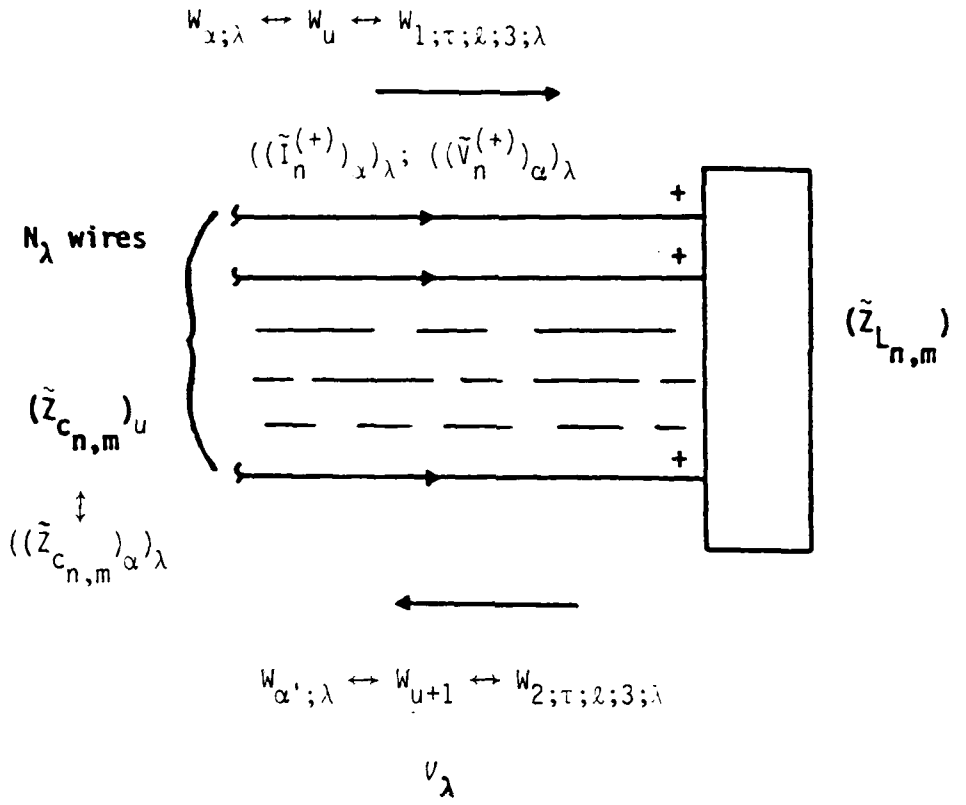

Figure 18. Terminating junction schematic.

The experimental setups in Figures 16 and 17 can also be extended to multiwire cases.

b. Scattering (reflection) matrix for termination junction--A termination junction can be considered as a shield which does not allow signal penetration into the next layer. The discussion in Section I-4a is thus applicable to a junction. This case simply gives [instead of Eq. 32 (see Fig. 18)]

$$((\tilde{V}_n^{(+)})_\alpha)_\lambda - ((\tilde{Z}_{c_{n,m}})_\alpha)_\lambda \cdot ((\tilde{I}_n^{(+)})_\alpha)_\lambda$$

$$\equiv ((\tilde{S}_{n,m})_{\alpha',\alpha})_{\lambda,\lambda} \cdot \left[((\tilde{V}_n^{(+)})_\alpha)_\lambda + ((\tilde{Z}_{c_{n,m}})_\alpha)_\lambda \cdot ((\tilde{I}_n^{(+)})_\alpha)_\lambda \right] \qquad (38)$$

where $((\tilde{S}_{n,m})_{\alpha',\alpha})_{\lambda,\lambda} \equiv (\tilde{S}_{n,m})_{u+1,u}$ if the wave indices are used. The reflection matrix can be determined by performing experiments similar to those shown in Figures 13 through 17, but with the wires in the $(\lambda+1)$ layer discarded.

When the loading impedance is known, this reflection matrix can also be calculated analytically by

$$(\tilde{S}_{n,m})_{u+1,u} \equiv ((\tilde{S}_{n,m})_{\alpha',\alpha})_{\lambda,\lambda}$$

$$= \left[(\tilde{Z}_{L_{n,m}}) + ((\tilde{Z}_{C_{n,m}})_{\alpha\lambda})\right]^{-1} \cdot \left[(\tilde{Z}_{L_{n,m}}) - ((\tilde{Z}_{C_{n,m}})_{\alpha\lambda})\right] \qquad (39)$$

Equation 39 is particularly useful for estimating the reflection matrix elements associated with small antennas at the outermost layer where the input impedances $(\tilde{Z}_{L_{n,m}})$ of the antennas are known.

c. Scattering matrix for wire-to-wire aperture penetrations--When the shield of Figure 13 has apertures, the scattering supermatrix derived for the line penetration has to be modified. Section I-2 showed that only the off-diagonal blocks (namely, the transmission matrices) need modification. For upper-bound estimates, only two experimental setups are needed for each aperture to determine the maximum of $|\tilde{V}^{(+)}_{s_{\lambda+1}}/\tilde{I}^{(+)}_{\alpha;\lambda}|$ and $|\tilde{I}^{(+)}_{s_{\lambda+1}}/\tilde{V}^{(+)}_{\alpha;\lambda}|$ (see Eq. 10). The results can then be used for all the scattering matrix elements associated with wires interacting through an aperture.

The experiments shown in Figure 19 can be performed by using wires not associated with the system, thereby avoiding the necessity of shorting and/or disconnecting the wires in the system. The experiments are also arranged with the wires immediately outside the exclusion regions to obtain the maximum allowable interaction. The exclusion regions should be at least one maximum aperture linear dimension away from the aperture. The effect of the aperture on the current and voltage on the excitation wire can then be neglected.

Using the experimental results thus obtained, the upper bounds of the scattering matrix elements can be calculated by Equation 10.

The quantities $|\tilde{V}^{(+)}_{s_{\lambda+1}}/\tilde{I}^{(+)}_{\alpha;\lambda}|$ and $|\tilde{I}^{(+)}_{s_{\lambda+1}}/\tilde{V}^{(+)}_{\alpha;\lambda}|$ can also be analytically estimated, provided that the maximum electric (α_e) and magnetic (α_m)

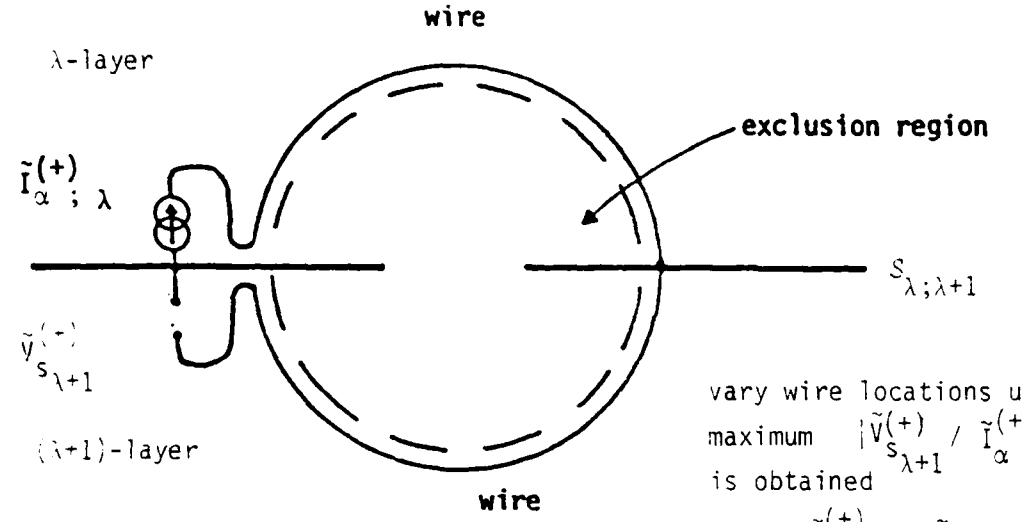

Note: The indices n,m have been omitted, because only one wire in each layer is assumed.

(a) Magnetic field penetration.

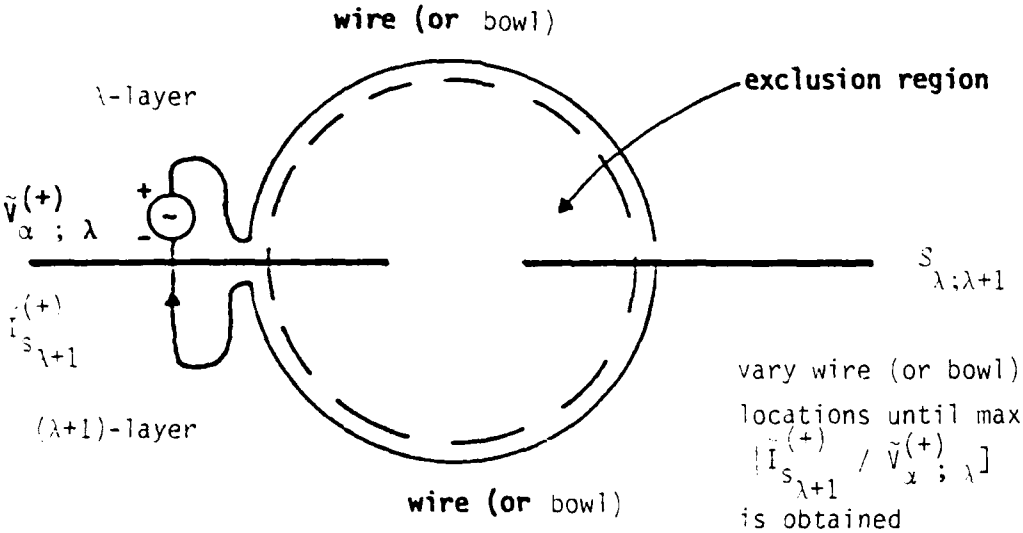

(b) Electric field penetration.

Figure 19. Experimental setups for estimating the scattering matrix elements associated with the wires involved in the wire-to-wire aperture penetrations.

polarizabilities are known. In Figure 19, if the exclusion regions are hemispheres (with radius R of the exclusion region > maximum linear aperture dimension), these quantities are approximately (Ref. 10)

$$|\tilde{I}^{(+)}_{s_{\lambda+1}} / \tilde{V}^{(+)}_{\alpha}; \lambda| \simeq \left| \frac{2s\varepsilon_o}{R^2} \quad \frac{\alpha_e}{\ell n[2R/r_o]} \right|$$

$$|\tilde{V}^{(+)}_{s_{\lambda+1}} / \tilde{I}^{(+)}_{\alpha}; \lambda| \simeq \left| \frac{s\mu_o}{2\pi R^2} \quad \alpha_m \right| \tag{40}$$

where r_o is the radius of the wire in the $(\lambda+1)$-layer in the experimental setup and should be greater than those of the wires in the actual system involved in the aperture interaction process. An alternative analytical estimate can also be obtained based on the maximum electric and magnetic fluxes penetrating an aperture. The estimate is given by

$$|\tilde{I}^{(+)}_{s_{\lambda+1}} / \tilde{V}^{(+)}_{\alpha}; \lambda| \simeq |s\ \varepsilon_o\ A/R|$$

$$|\tilde{V}^{(+)}_{s_{\lambda+1}} / \tilde{I}^{(+)}_{\alpha}; \lambda| \simeq |s\mu_o\ A_m/[2R]| \tag{41}$$

where A is the area of the aperture and A_m is the maximum magnetic flux ($\tilde{\Phi}_m$) penetration factor defined via $A_m = \tilde{\Phi}_m/(\mu_o \tilde{H}_{sc})$ for a circular aperture with radius = R/2, $A_m = R^2/4$). The first equation in Equation 41 can be used as the approximate result for the case when bowls are used in the electric field interaction experiment.

d. Scattering matrix for field-to-wire aperture penetrations--Section I-2 showed that the field-to-wire interaction through an aperture (which is important only in the outermost shield) can be treated by introducing an additional imaginary wire in the outer layer. Additional scattering matrix elements must be included because of the introduction of this wire. The upper bound of the additional scattering matrix elements can be estimated by Equation 13.

Equation 13 is similar to Equation 10. Therefore, most arguments raised in Section I-4c are applicable here. The experiment setups shown in Figure 20

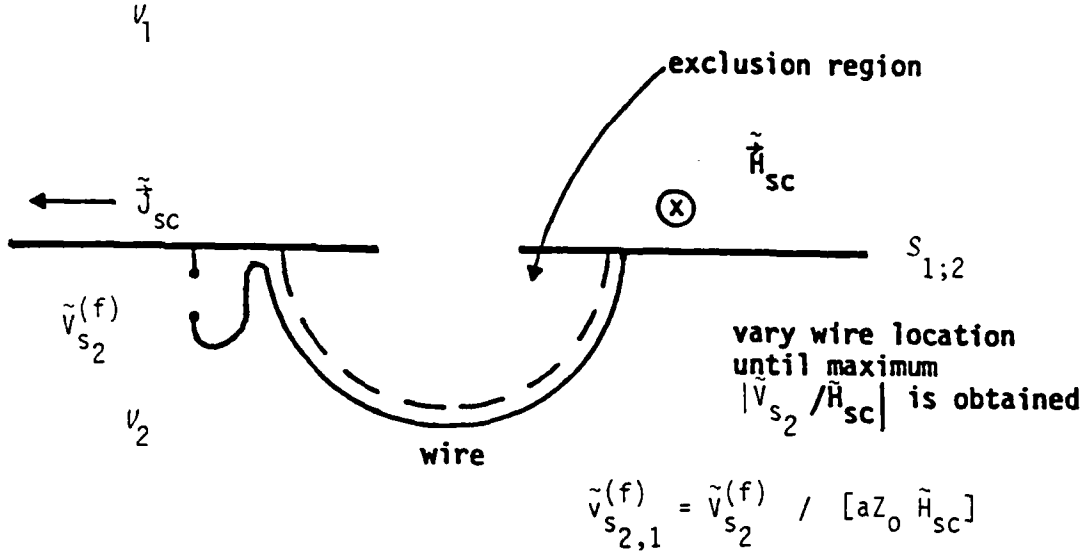

Note: The indices n,m have been omitted because there is only one wire in V_2.

(a) Magnetic field penetration.

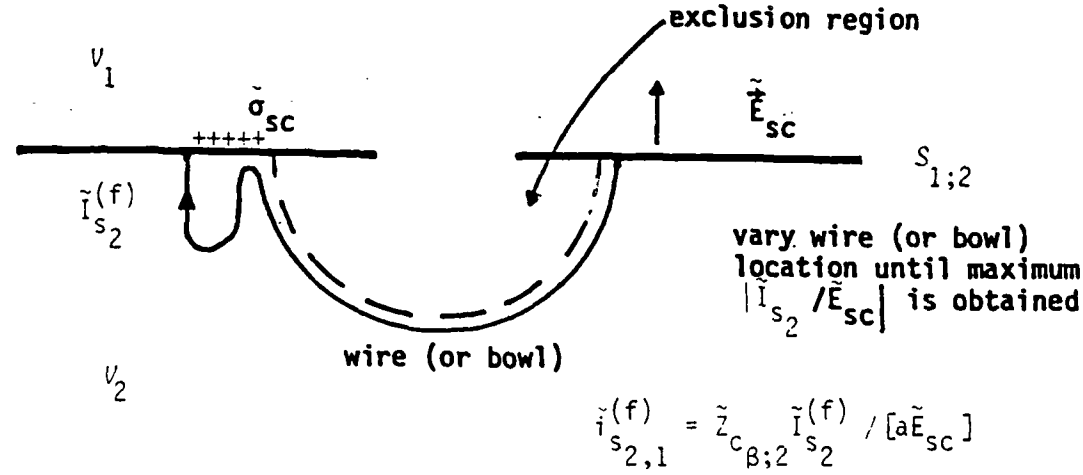

(b) Electric field penetration.

Figure 20. Experimental setups for estimating the scattering matrix elements associated with the wires involved in the field-to-wire field aperture penetrations.

can be used for determining the upper-bound estimates of $|\tilde{S}_{\beta,\alpha;2,1}|$ in Equation 13. The sources required in the experiments are uniform electric and/or magnetic fields near the aperture when the aperture is covered with conductor. This can be accomplished by performing the experiments in a special finite intermediate nuclear EMP simulator (FINES) (see Ref. 11).

Formulas similar to Equations 40 and 41 can be obtained for this type of interaction as, with a = R,

$$\left| [\tilde{I}_s^{(f)}]_2 \;/\; [R\,\tilde{E}_{sc}] \right| \simeq \left| \frac{2\ s\varepsilon_o\alpha_e}{R^2 \ell n[2R/r_o]} \right|$$

$$\left| V_{s_2}^{(f)} \;/\; [R\ Z_o\tilde{H}_{sc}] \right| \simeq \left| \frac{s\mu_o\alpha_m}{Z_o\pi R^2} \right| \tag{42}$$

and

$$\left| \tilde{I}_{s_2}^{(f)} \;/\; [R\,\tilde{E}_{sc}] \right| \simeq |s\ \varepsilon_o\ A/R|$$

$$\left| \tilde{V}_{s_2}^{(f)} \;/\; [R\,Z_o\tilde{H}_{sc}] \right| \simeq |s\ \mu_o\ A_m \;/\; [R\,Z_o]| \tag{43}$$

The discussions in Sections I-4c and I-4d neglected possible resonances of the cavity formed by two adjacent shields (i.e., shield-to-shield interactions for the field are neglected). One way to include the resonance effect is to perform the experiments with both shields present.

5. USE OF EXPERIMENTAL RESULT IN SHIELD DESIGN PROCEDURES

Having related the signal responses to the electromagnetic sources in terms of norms of shield scattering matrices and having established methods to estimate these norms, the process can then be used to analyze and synthesize (or design) shields in a system. Only the design (or synthesis) aspect is addressed here.

There are two kinds of system shielding designs that may be encountered. One is for a system still on the drawing board, and the other is for an

existing system requiring shielding improvement (i.e., hardening). The existing system might not allow the freedom of changing the layer configuration and, therefore, the only possibility of hardening the system may be to alter the shield characteristics by implementing hardening fixes at the shields. This section addresses how the results obtained in previous sections can be used in the shielding design for an existing system. The discussion will also be useful in the shielding design of a new system.

a. General procedure--A shielding design procedure was laid down in Reference 1. The procedure is duplicated in Steps 1 through 9 with minor modifications and additions.

(1) Consider some elementary topology defined to at least sublayer level (e.g., Fig. 1).

(2) Identify the sources in each sublayer corresponding to electromagnetic environments of interest.

(3) Identify the allowable maximum signal levels in each sublayer of concern associated with each electromagnetic environment.

(4) Identify the paths, P_n, associated with each pair of source sublayers (Step 2) and response sublayer (Step 3) of concern.

(5) Allocate shielding along each P_n path so that the sources (Step 2) produce no more response than allowed in sublayers (Step 3).

(6) Partition the shielding along each P_n path among the corresponding subshields encountered on the P_n path. This gives maximum allowable values to the norms of each corresponding subshield transmission and reflection matrix.

(7) For each subshield, consider all P_n paths that pass through it. Choose the transmission and reflection matrix norms to be the least values for all P_n in Step 6.

(8) Perform experiments to select subshield hardening approaches satisfying the transmission and reflection matrix norm requirements established in Step 7.

(9) Write specifications for subshield hardening requirements.

b. Example--To demonstrate how to use the shielding design procedure duplicated in the previous subsection, consider the example discussed in Subsection I-3. For simplicity, each subshield in the example is assumed to have only one line and one aperture penetration. The relationship between the sources and responses is then given in Equation 26. The shielding design procedure proceeds as follows [see corresponding step number under General Procedure (Subsection I-5a)].

(1) The topological and interaction sequence diagrams are shown in Figures 11 and 12.

(2) The sources (EMP, lightning, etc.) exist only in V_1, and are assumed not to be greater than 10^4 V,i.e.,

$$\| ((\tilde{V}_{s_n})_\alpha)_1 \|_2 \leq \sqrt{2} \left\{ a^2 \left[|\tilde{E}_{sc}| + Z_o |\tilde{H}_{sc}| \right]^2 + |\tilde{Z}_c \tilde{I}_{sc}|^2 \right\}^{\frac{1}{2}}$$

$$\leq 10^4 \ (V) \tag{44}$$

(3) The signal responses of concern are in V_3. The maximum allowable combined voltage is assumed to be 100 mV, i.e.,

$$\left\| \begin{pmatrix} \tilde{V}_7 \\ \tilde{V}_3 \end{pmatrix} \right\| \leq 100 \ (mV) \tag{45}$$

(4) There is only one path (each shield along the path has two penetrations).

(5) From Steps 2 and 3 of the general procedure, the shields along the path must reduce the signal levels by at least 5 orders of magnitude ($10^4 \rightarrow 10^{-1}$, 100 dB).

(6) There are various ways to satisfy the overall shielding requirement established in Step 5 of the general procedure. Take $|[\tilde{S}_{ss}]_{1,2}| = 0.5$ in Equation 26 which is determined mainly by the structure of the external protruding wire (or antenna), and

$|\tilde{S}_{8,7}| < 1$ which is determined by the loading impedance. Then, one possible way to satisfy the overall shielding requirement is to have

$$|[\tilde{S}_{22}]_{2,1}| < 1$$

$$|\tilde{S}_{3,4}| \approx |\tilde{S}_{6,5}| \approx |\tilde{S}_{7,8}| \leq 0.9$$

$$|\tilde{S}_{7,5}| - |\tilde{S}_{7,5}^{(L)}| + \max\left\{2|\tilde{v}_{s_{3,2}}|;\ 2|\tilde{i}_{s_{3,2}}|\right\} \leq 2 \times 10^{-5}$$

$$\sqrt{|[\tilde{S}_1]_{3,1}|^2 + |[\tilde{S}_2]_{3,1}|^2}$$

$$\leq \sqrt{|[\tilde{S}_2^{(L)}]_{3,1}|^2 + \max\left\{4|\tilde{v}_{s_{2,1}}^{(f)}|^2;\ 4|\tilde{i}_{s_{2,1}}^{(f)}|^2\right\}} \leq 10^{-4} \qquad (46)$$

It should be emphasized that except for $\tilde{v}_s$, $\tilde{i}_s$, $\tilde{v}_s^{(f)}$, and $\tilde{i}_s^{(f)}$, where indices are referred to layers, all the outermost indices for the variables are referred to as waves. If it turns out this set of values is difficult to achieve with available hardening fixes, other sets of values may work.

(7) Step 7 of the general procedure should be skipped since there is only one path.

(8) Perform experiments with various hardening fixes (such as filters, arrestors along the wires, and wire meshes at the aperture) to select the ones satisfying the requirements established in Step 6 of the general procedure.

(9) Write specifications for the proven hardening approach.

6. CONCLUSIONS/RECOMMENDATIONS

It is concluded that the bounding methodology presented here suffers from several restrictive features and thus leaves grounds for improvement. This leads to the following recommendations for future developments.

a. Optimization of normalization impedances--The normalization impedances are required in the definition of the combined voltages which in turn are the basic quantities in the discussion. For the internal wires, the natural quantities to use for the normalization impedances are their characteristic impedances. These characteristic impedances indicate how the wires interact among themselves. Determination of the characteristic impedances for a complicated system could be nearly impossible. On the other hand, for the external wires in V_1, the use of the normalization impedances to construct the combined voltages is completely artificial. If too large or too small a normalization impedance is used, the norm will give an inaccurate conclusion (for example, if $\tilde{Z}_c$ is infinitely large for the source vector of Eq. 30, then the source vector information for the field coupling through the aperture will be lost).

For these reasons, one inevitable question would be: "What are the optimal normalization impedances that should be used to make the bounding methodology simple and accurate?" For an order-of-magnitude estimate, the use of a diagonal normalization matrix with the diagonal elements in the order of 100 Ω could be a reasonable choice. However, its validity or the choice of other values so that a tighter bound can be obtained requires further consideration.

b. Optimization of length parameter in characterization of field aperture penetration--Section I-2 showed that the length parameter "a" is required in defining combined voltages for the field-to-wire interactions through an aperture. This length parameter is artificial. In the case where there is only aperture interaction through the outermost shield, the use of an arbitrary "a" should be acceptable. On the other hand, in the case where the shield allows both line and aperture penetrations, an inadequate "a" value might give an inaccurate emphasis on the aperture penetration. A reasonable value for this length parameter might be the linear dimension of the aperture. This conjecture requires further consideration.

c. Shield-shield interaction--The zero tube-length approximation was used to simplify the scattering matrix formulation. By doing so, the shield-shield (or subshield-subshield) interaction and the propagation behavior between shields are excluded from the formulation. The exclusion might result in

loose upper bound estimates and inaccurate resonance phenomena. The formulation to include the shield-shield interaction and the propagation behavior between shields requires further consideration.

d. Diffusion penetration--When the part of a shield that allows for diffusion penetration covers only an electrically small region, the diffusion penetration can be treated as an aperture penetration. When the region is electrically large, an alternative approach needs to be sought.

e. Time-domain consideration--The signal bounding has been discussed in the complex frequency domain, or for continuous-wave (CW) signals. For a transient electromagnetic interference such as EMP or lightning, the time-domain consideration is also needed. In principle, it can be obtained from the frequency-domain consideration. For example, in the time-domain the matrices in Equations 6 and 7 resulting from the good shielding approximation will become convolution operators. For a more general case, there may be even nonlinear time-domain operators.

II. EXPERIMENTS CHARACTERIZING THE SHIELDING PERFORMANCE OF ENCLOSURES

1. INTRODUCTION

This section documents the results of the second phase of an effort intended to achieve a quantitative characterization of the shielding performance of a metal enclosure.

The first phase of this effort (covered in Section I) resulted in a theoretical analysis which models the interaction between the electronics inside such an enclosure and an electromagnetic excitation source outside it. This second phase identifies experiments designed to test the accuracy of the model and to furnish a measure of the shielding performance of a metal enclosure. Two rectangular aluminum boxes (4 ft by 5 ft by 6 ft) with replaceable panels have been constructed for this purpose.

Section I describes the quantities that must be measured to determine the scattering matrix elements needed in the theoretical model. Experiments are suggested in Sections II-2 and II-3 to measure these quantities for various POE configurations. A number of commonly encountered line penetrations are described in Section II-2, while various aperture penetrations are discussed in Section II-3. After characterizing the various individual POEs identified in these sections using the techniques covered in Section I, the shielding performance of an entire enclosure can be addressed. This is done in Section II-4, where an experimental procedure is described for characterizing the shielding performance of the experimental enclosure for various configurations of POEs and different arrangements of cables/electronics contained within it. Section II-4 also identifies theoretical calculations that need to be performed to compare the theoretical predictions to the measured data.

2. LINE PENETRATIONS

a. Purpose--The experiments described in this section are designed to permit measurement of appropriate parameters discussed in Section I. They also permit a quantitative assessment of the relative protection afforded by the various treatments commonly applied to line penetrations. The list of experiments given in the next subsection includes the most important penetrations found in practice; it can be extended as new treatments become available.

The purpose of the experiments is to test the penetration treatments at a generic level. Thus, no attempt is made to simulate an actual system. The complexity of an actual system, either ground-based or airborne, would tend to obscure the fundamental parameters that are of interest in the formal description discussed in Section I.

b. Scope--The experiments include the following:

- Setup of penetration panel for each procedure described in the following subsection
- Setup of instrumentation
- Performance of actual test required and recording of data
- Preliminary evaluation of data, modification of setup if deemed appropriate, and repeat of experiment
- Reduction and evaluation of final data in light of matrix parameters described in Section I

c. Experimental procedure--All of the experiments can be performed as described in Section I (e.g., see Figs. 15, 16, and 17). However, it is of considerable interest also to measure transfer function quantities in a more traditional manner for comparison to the more theoretical approach discussed in Section I. These quantities are indicated in the figures that follow.

(1) Groundable line penetrations--The preferred treatment for a groundable line penetration is a peripheral bond to the barrier surface. This ideal cannot always to achieved. It is, therefore, desirable to evaluate the following treatments:

- Solid rod and pipe (e.g., circular waveguide penetration) bonded to the barrier surface in the following ways
  - Peripheral weld
  - Pigtail clamp
  - No treatment

(2) Insulated line penetrations--These are the most difficult to evaluate in a generic sense because no two systems are alike. Two families of insulated penetrations can be distinguished: single wire and multiple wire. An example of a single wire penetration is a power line; an example of a multiple wire is a cable bundle with many signal conductors interfacing with an equipment unit. Experiments in this category will, therefore, evaluate

- Single line penetration treated with a filter
- Multiple cable bundle treated with a multiple-filter pin connector
- Zinc-oxide multipin connectors (when available)

(3) Other line penetrations--A common problem for missiles carried aboard aircraft is the umbilical connector. After release from the aircraft, the pins in this connector represent a penetration of the missile skin, unless the connector contains a deadface mechanism. The penetration does not fall into either of the categories mentioned in Sections II-2c(1) and II-2c(2) because the penetration ends right at the barrier surface. It is difficult to design an experiment that would test an umbilical connector in a generic way. Therefore, no experiments with such connectors are planned at the present time.

(4) Quantities to be measured--Figure 21 illustrates the solid rod and pipe experiments. The excitation in these experiments is envisioned to be a CW source. However, measurements could also be made in the time-domain with a pulsed power source.

Figure 22 shows the dielectric and resistive insertion devices, while Figure 23 shows one example of a pigtail terminaton. There are many different ways that pigtails can be used in practice, and it will be impossible to simulate all of them. It is suggested that two different lengths of external pigtails be used, and one internally terminated pigtail.

Figure 24 illustrates the power line filter and Figure 25 shows the multiple-filter pin connector. For both of these, CW excitation is preferred, since this permits a direct determination of the transfer function. However, it may also be desirable to test a combination of a power line filter and a surge arrestor, in which case a pulsed excitation is necessary (to fire the surge arrestor).

(5) Analysis of measured quantities--The quantities measured in the experiments will permit a detailed description of a line penetration with its associated treatment. The description will be both in terms of traditional transfer quantities and in terms of the transmission and reflection coefficients appropriate for the interaction supermatrix. The data will also permit an explicit quantification of penetration treatments. This should lead to standard ways for specifying and testing line penetration treatments.

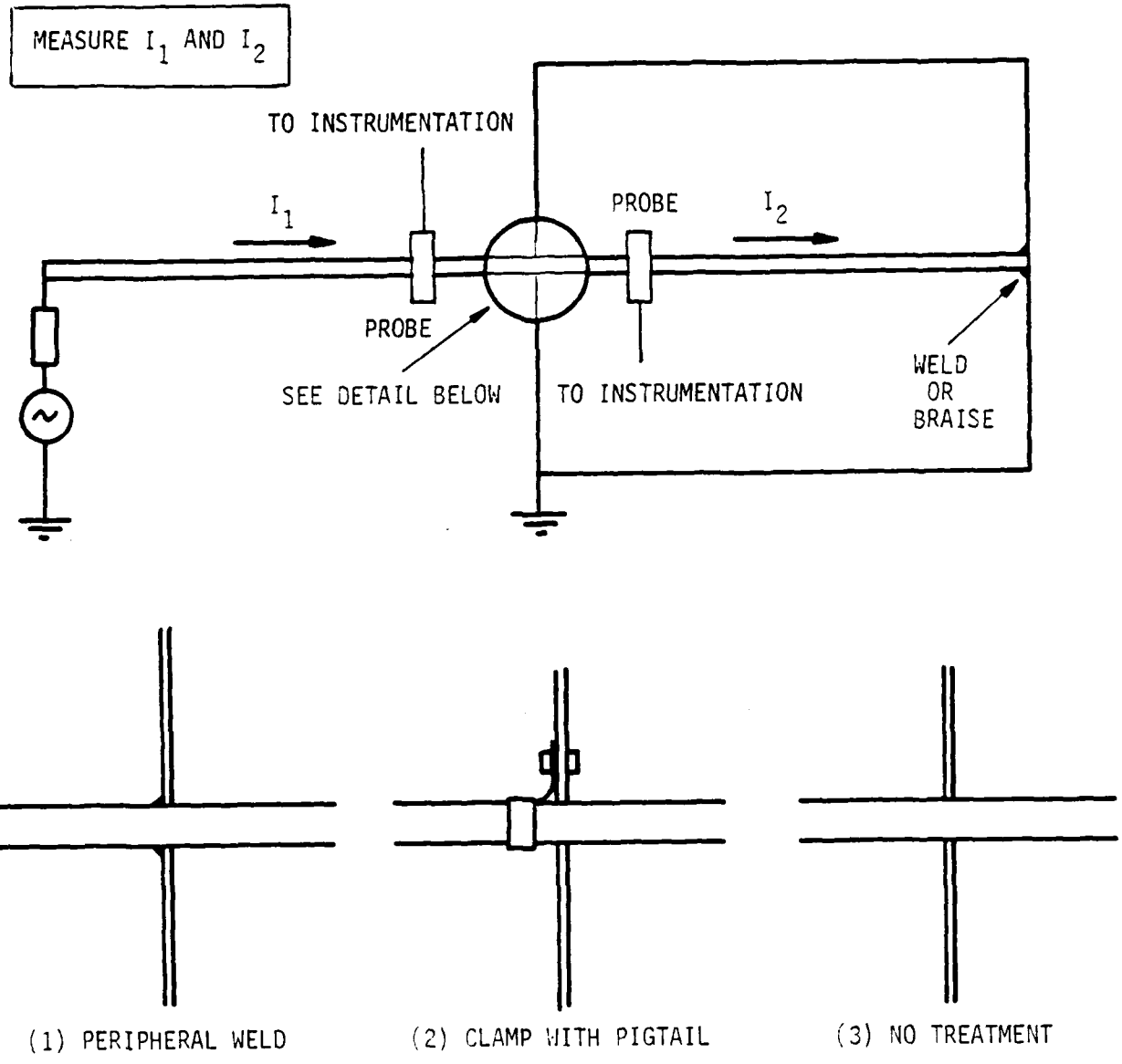

Figure 21. Solid rod or pipe penetration. For (2) and (3), no attempt is made to achieve a good bond where the pipe penetrates the wall.

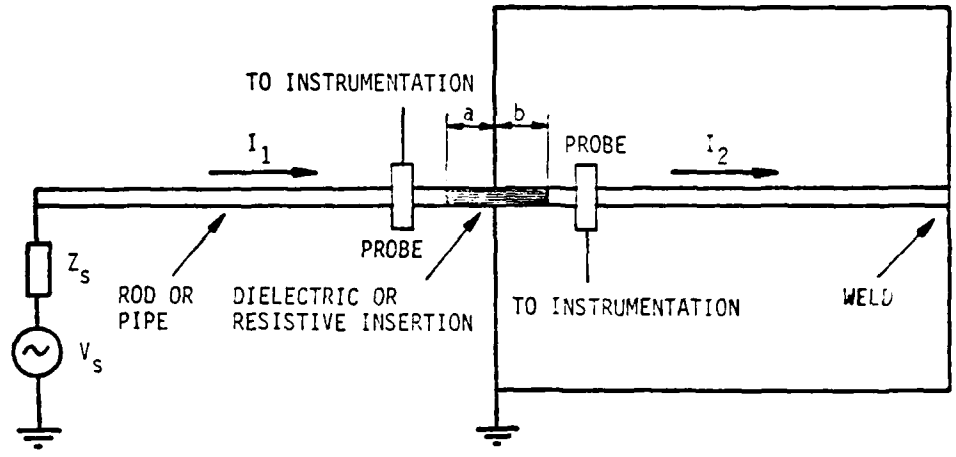

Measure I_1 and I_2 for various lengths of insertion device.

Figure 22. Dielectric insertion device.

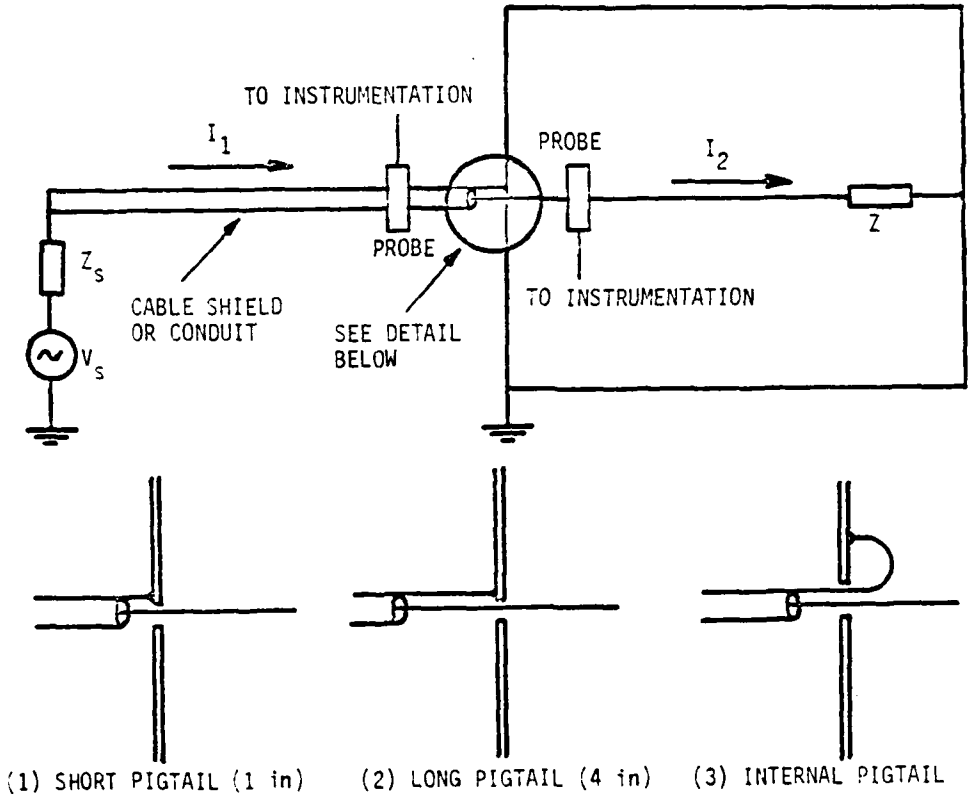

Measure I_1 and I_2 with Z = 0, 100 kΩ, and characteristic impedance of coax for each case.

Figure 23. Pigtail terminations.

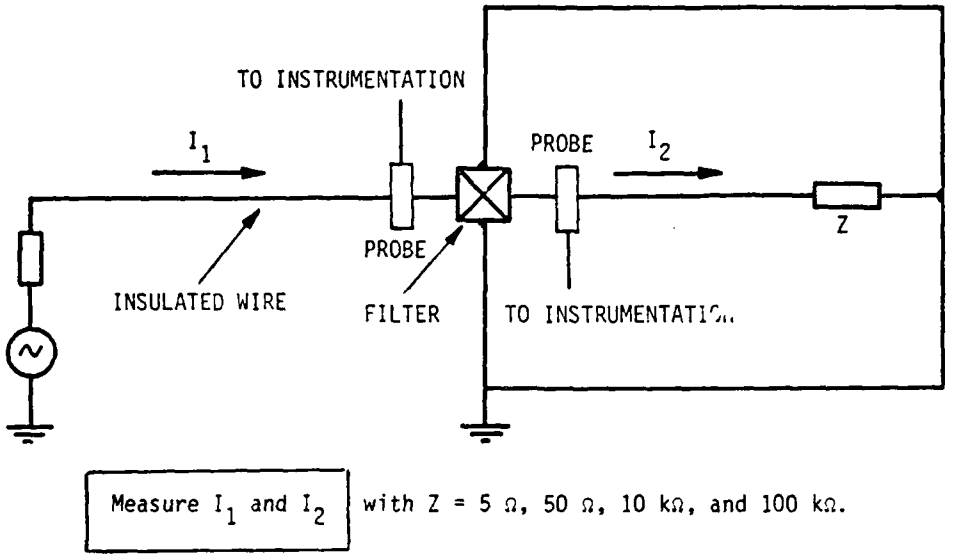

Figure 24. Insulated wire penetration with power line filter.

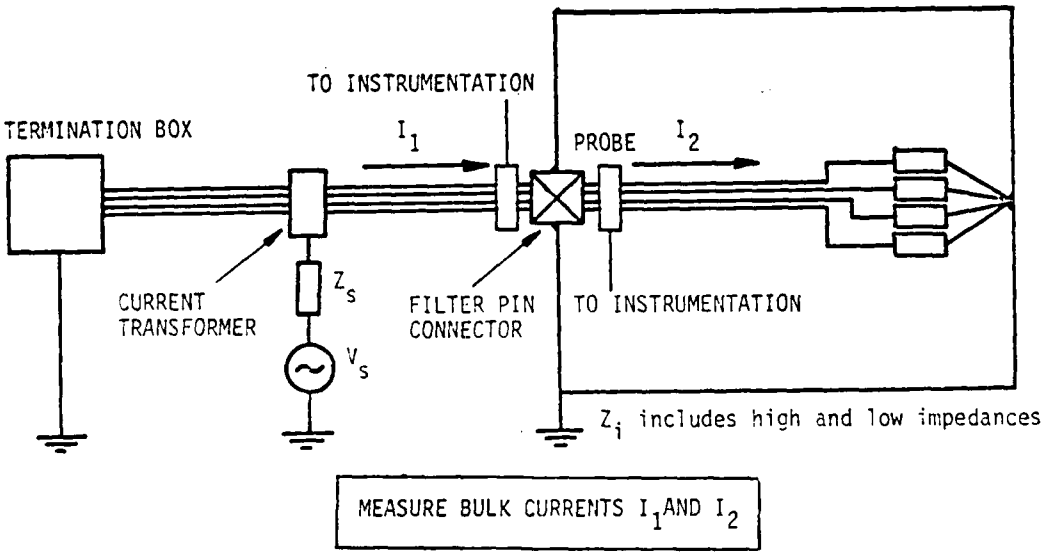

Figure 25. Multiwire bundle with filter pin connector.

Furthermore, the data (and the experiments) will permit an assessment of the appropriateness of the interaction supermatrix description for actual systems. The supermatrix approach is very attractive from a theoretical point of view; however, it is not yet clear how the complex mathematical formalism can be applied to the specification of practical quantities. The data obtained in these experiments will provide answers to these questions.

d. Instrumentation requirements--The sensors and instrumentation necessary for these experiments are listed below. The mention of manufacturer's names has been avoided; many different brands of these instruments are readily available.

(1) Sensors--The following probes are necessary for these experiments:

- Current probes: standard clip-on or snap-on probes with a bandwidth of at least 14 kHz to 500 MHz. It may be necessary to use different probes for the lowest and highest frequencies of interest. (Probes that can be used up to 1 GHz are readily available, but they cannot be used for very low frequencies.)

(2) Instrumentation--The following instruments can be used in these experiments:

- High-speed oscilloscopes for time-domain measurements.
- A network analyzer for CW measurements, with a range of at least 0.5 to 500 MHz. A wider bandwidth is desirable but may not be readily available.
- A spectrum analyzer or other radio frequency (RF) receiver for frequency bands that are not covered by the network analyer. This will also extend the dynamic range for single frequency measurements.

3. APERTURE PENETRATIONS

a. Purpose--The analysis in Section I shows that only two measurements (short-circuit current and open-circuit voltage) are required to determine upper bounds on the scattering matrix elements appropriate for aperture coupling. Two separate coupling configurations are considered: wire-to-wire and field-to-wire coupling through ar aperture. The measurements described in this section will allow an investigation of these matrix elements as they apply to apertures of various size and shape, apertures in the form of seams and joints, and various types of loaded apertures. Figures 19 and 20 describe

the measurement configurations. The diameter of the exclusion region is assumed to be larger than the largest linear dimension of the aperture under test.

Other measurements are described which are related to the framework of Section I but which either violate the conditions of that framework or add complexity to it. For example, the measurements in Section I require an exclusion volume to be maintained at the aperture. While adherence to an exclusion volume is certainly a good design practice, it is often impossible to implement (e.g., aircraft wiring which is routed near windows or along the fuselage wall). These added measurements are made with conductors located in the exclusion volume and must be understood in a bounding sense in order to be useful. While the bounds developed from these measurements may not be directly relatable to the vector norms described in Section I, they must be investigated as an alternative for use in situations where a proper exclusion volume cannot be established or maintained.

b. Scope--The experiments described in this section include unloaded apertures of the following shapes: circles, squares, and long, narrow rectangles. The largest dimension of any of these apertures will be less than 20 cm to insure that the exclusion volume is large enough to satisfy theoretical requirements, yet small enough to be unaffected by the aperture panel mounting hardware inside the enclosure. Apertures of various size will be used (e.g., circular apertures of 18, 12, and 6 cm diameter).

Measurements will also be made for apertures which are loaded (i.e., covered) in various ways. This includes mesh screen with bonded and unbonded intersections, waveguide-beyond-cutoff devices of various length and with varying cross-sectional complexity (e.g., single cylindrical tube, array of tubes, honeycomb panels), and panels constructed of composite materials. The composite materials used are restricted to those which have a significant amount of conducting material, primarily graphite epoxy. If the composite material is anisotropic (i.e., if the measurement is sensitive to the orientation of the composite panel), then several orientations will be used in order to insure that the maximum coupling configuration has been investigated. The experiments must also investigate the properties of different methods of bonding the composite panel to the edges of the aperture.

Coupling parameters for apertures in the form of seams or joints will also be measured but the gasketted hatch associated with the aperture panel may affect the measurement. The measurements will be most appropriate for test joints which are much more leaky than the double row of gaskets used on the aperture panel.

c. Experimental procedure--The experiment consists of four basic test activities: test preparation, preliminary measurements, aperture coupling measurements, and data analysis. Each of these activities is necessary to fulfill the objectives of the work.

(1) Test preparation activities--The preparation activities required for this experiment are the following:

- Choice of test parameters, which includes the sources, the test volume, and the location of sensors
- Pretest prediction of test results using the chosen test configurations
- Choice of sensors, probes, and instrumentation
- Development of procedures for data gathering, recording, and processing

While the analysis in Section I requires that the experiments be performed in the frequency domain, it is recommended that both swept frequency CW sources and pulsed sources be used in these experiments. Since one of the implied objectives of this effort is the establishment of new standard test techniques for enclosures, both time-domain and frequency-domain test sources must be considered at this stage of the development. An additional impetus for using both types of sources is the fact that frequency-domain and time-domain data yield different insights regarding coupling, which will be of value to the analyst. A theoretical basis for understanding aperture coupling in the time domain is discussed in Reference 12.

The basic test configurations are defined in Figures 19 and 20. The wire-to-wire coupling experiment may be able to be performed in a laboratory environment with minimal interference from extraneous conductors in the laboratory. The field-to-wire experiments may require a separate isolated test volume such as the Air Force Weapons Laboratory (AFWL) Characterization of Antennas and Test for Entry Simulator (ACHATES), described in Reference 13, which provides a source environment which is not influenced by extraneous

conductors. In the absence of an ACHATES environment, a configuration similar to that of Figure 26 can be considered. A small transmission line (either parallel plate or rhombic) can be erected over the illuminated face of the enclosure. Reference 14 discusses the properties of these types of environments. It should be noted that, while the laboratory environments of Figure 26 may not be directly relatable to all types of plane wave excitation in free space, the short-circuit surface fields at the closed aperture ($\vec{H}_{sc}$ and $\vec{E}_{sc}$) can be measured and can be used in the formulations of Section I and Reference 12.

The short-circuit surface fields at the aperture location are dependent upon the properties of the incident field (e.g., angles of incidences and polarization), upon the physical parameters (size, shape, orientation) of the conducting surface on which the aperture is located, and upon the geometric parameters characterizing nearby conducting objects (such as structural metal in the laboratory). As a result, it is not possible to reproduce exactly the environment of EMP in a laboratory configuration like that shown in Figure 26. In spite of this limitation, the configuration in the figures does permit several important objectives of the measurement program to be achieved--namely, the evaluation of the effectiveness of aperture treatments and the verification of the theoretical models of Section I and Reference 12.

The sensors and instrumentation must be chosen to be compatible with the source amplitudes and with the desired range of frequencies. Procedures for gathering, recording, and processing the data must be established so that the data base can be accessed easily and used intelligently. It is recommended that, as a minimum, Polaroid photographs of the frequency-domain and time-domain data be obtained, at least in this first series of experiments. These photographs are valuable for trouble-shooting and they provide instant access to the measured data. The use of transient digitizers and computer tape storage may also be desired for these experiments, but this may not allow instant access to the data.

It is recommended that pretest activities include the prediction of the test results to the extent possible. While these predictions are not a requirement for performing the experiments, the exercise will be extremely valuable for the analysis of the data and will aid in the selection of probes and other elements of the instrumentation system (e.g., amplifiers and attenuators).

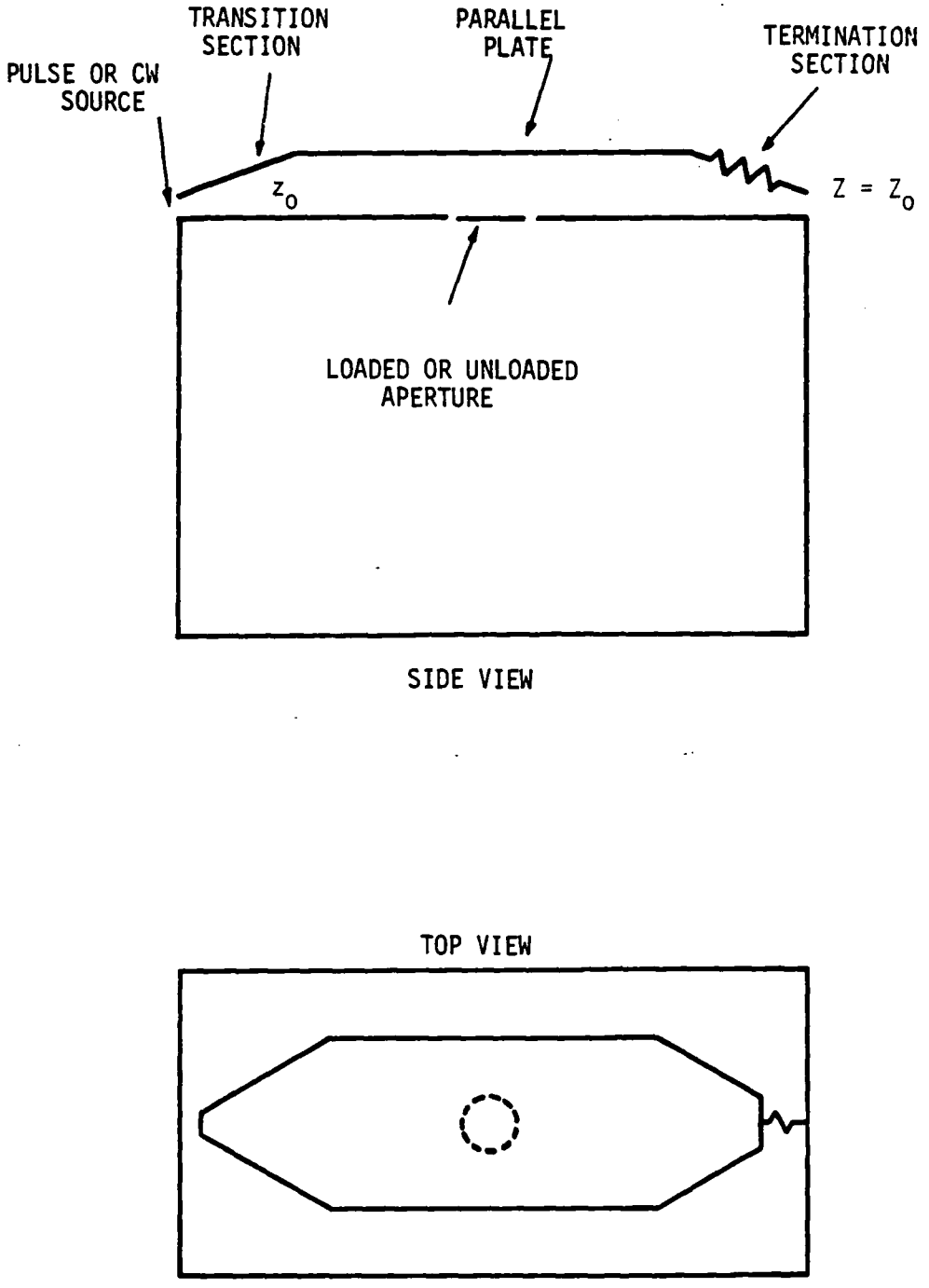

Figure 26. Alternative to ACHATES for field-to-wire coupling environment.

(2) Preliminary measurements--Before obtaining measurements with the various loaded and unloaded apertures, the test personnel should make the following preliminary measurements:

- Field mapping of the empty test environment for the field-to-wire coupling experiments, including measurement of the surface fields and their time-derivatives at the center of the aperture locations with the aperture closed (i.e., shorted).
- Internal measurements with the aperture shorted as specified in Figures 19 and 20.

(3) Aperture coupling measurements--The wire-to-wire and bowl-to-bowl aperture coupling measurements should be made as described in Figure 19. The diameter of the exclusion region volume should be at least as large as the largest dimension of the aperture being tested. The problem of determining the size of the exclusion volume has not been solved exactly, but recent analyses have provided guidelines for addressing this question (Refs. 15 and 16). The exclusion volume is required so that the aperture polarizabilities implied by the measurements are dependent only upon the parameters of the aperture and not upon interactions between the aperture and the wiring inside. The analysis of Reference 14 indicated the quantitative effects of these interactions on the equivalent aperture polarizabilities.

Measurements should also be made with the sensing circuits located inside the original exclusion volume, as shown in Figure 27. While this configuration does not satisfy the conditions of the analysis in Section I (where the sensing circuits are assumed to be located far enough away from the aperture so that mutual interactions are negligible), the measurements described in Figure 27 will allow the development of upper bound predictions for many realistic situations in which an adequate exclusion volume cannot be applied.

The field-to-wire and field-to-bowl aperture coupling measurements should be made as described in Figure 20. Measurements should also be made with smaller exclusion volumes, as shown in the examples of Figure 28.

These measurements should be made for unloaded apertures of various sizes and shapes, as discussed earlier, and for a variety of loaded apertures (e.g., wire mesh, waveguide-beyond-cutoff, and composite panel loading). Aperture panels containing seams and joints should also be tested, subject to the condition that the test seams and joints leak more than the aperture panel

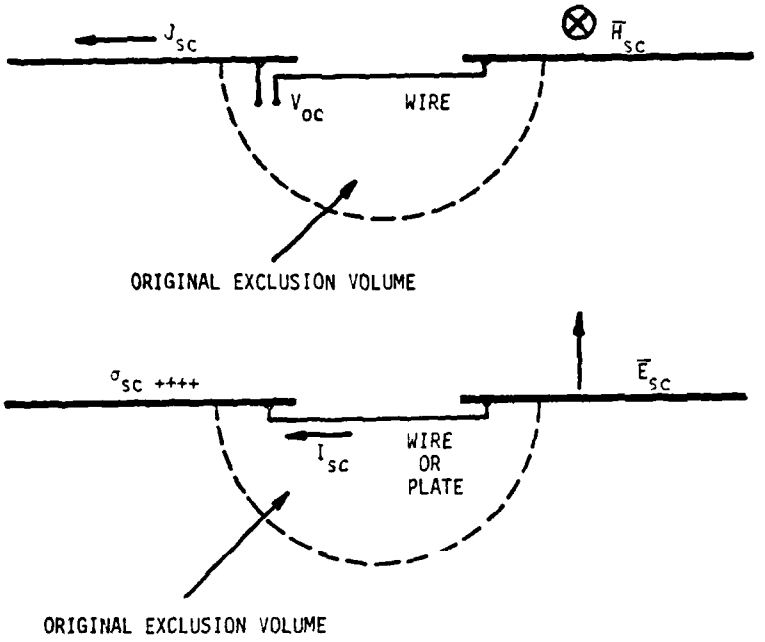

Figure 27. Alternative measurement configuration for use when original exclusion volume cannot be maintained (field-to-wire coupling).

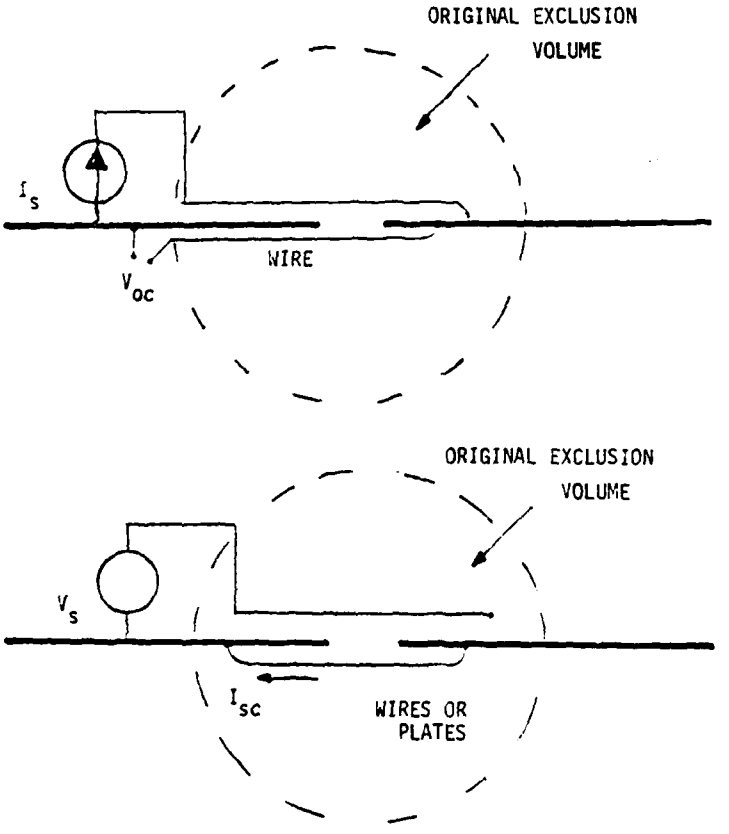

Figure 28. Alternative measurement configuration for use when original exclusion volume cannot be maintained (wire-to-wire coupling).

gaskets. An alternative method for evaluating seams and joints is to use sensing circuits which measure only local seam leakage. An example of this type of measurement is the use of small leak detectors (or seam-sniffers) located very close to the test seams but relatively far from the gasketted seams along the periphery of the aperture panel. The measurements will not necessarily allow a rigorous quantitative description of the test seam, but they do permit a comparison between the test seam leakage and the leakage through the aperture panel seams.

(4) Data analysis--Equations 41 through 43 should be used in the analysis of the measured data for unloaded apertures. The ratios defined on the left-hand side of these equations should be compared to the approximations given on the right-hand sides. Measurements on apertures loaded with wire mesh should be compared to the expressions developed in Reference 17. These comparisons should be made for each type of exclusion volume used in the experiments.

d. Instrumentation requirements--The sensors and instrumentation described in Section II-2d should also be used for the aperture coupling experiments. These experiments will require additional surface field probes equivalent to those described below:

- Wideband B-dot sensors
- Wideband D-dot sensors equivalent to EG&G models HSD-3(R), HSD-S3(R), or ACD-S1(R)
- Integrators with time constants of the order of 1 μs
- Video amplifier equivalent to EG&G Model AVA-100

4. EXPERIMENTAL CHARACTERIZATION OF A SHIELDED ENCLOSURE

a. Purpose--The purpose of the experiment described in this section is:

- To characterize the electromagnetic shielding performance of a simple enclosure
- To evaluate the relative effectiveness of alternate hardening methods for POEs
- To verify the predictions of the theoretical model developed in Section I
- To determine the sensitivity of the theoretical predictions to variations in normalization impedance and normalization length as defined in Section I.

The theoretical upper bound of the combined voltage* which may be induced anywhere within a shielded enclosure will be calculated for various configurations and combinatons of aperture and line penetrations into a shielded volume as described in Sections II-2 and II-3. This theoretical value will then be checked by comparing it to measured values of combined voltage in order to verify that is indeed an upper bound, and to check the tightness or relative magnitude of the bound compared to the actual value. In addition, since the normalization impedance and the normalization length (see Sec. I for definitions) are not well-defined quantities for most aperture and conductor arrangements, the values assigned to these parameters will be varied to determine the sensitivity of the theoretical prediction to their variations.

b. Scope--This experiment will consist of the electromagnetic excitation of two prototype metal enclosures (a double walled and a single walled), and measurement of the combined voltage at selected locations within these enclosures. The excitations will include CW electromagnetic field illumination in appropriate simulators, such as AFWL Los Alamos electromagnetic pulse calibration and simulation (ALECS) facility, and CW direct drive near POEs as illustrated schematically in Figure 29. Each enclosure will be placed in various orientations within the simulator to ensure maximum penetration into the interior volume. During direct drive excitation both the aperture and line penetrations may be driven, either simultaneously or in sequence, using portable radiators such as FINES near the apertures and using current and/or voltage sources to drive line penetration.

c. Procedure--The combined voltage at various positions within an experimental enclosure will be measured while it is being externally excited by field illumination and/or direct drive at the POEs. Various combinations of internal electronic configurations inside the enclosure will be tested. This will include different types of electronics to act as load impedances (i.e., Z_L in Fig. 30), a variety of internal cable routes, and a variety of load positions within the enclosure. Combined voltage measurements will be taken for all these conditions to determine the range of values for a given set of

*The combined voltage is V + ZI, where V, I, and Z are the voltage, current, and normalization impedance, respectively.

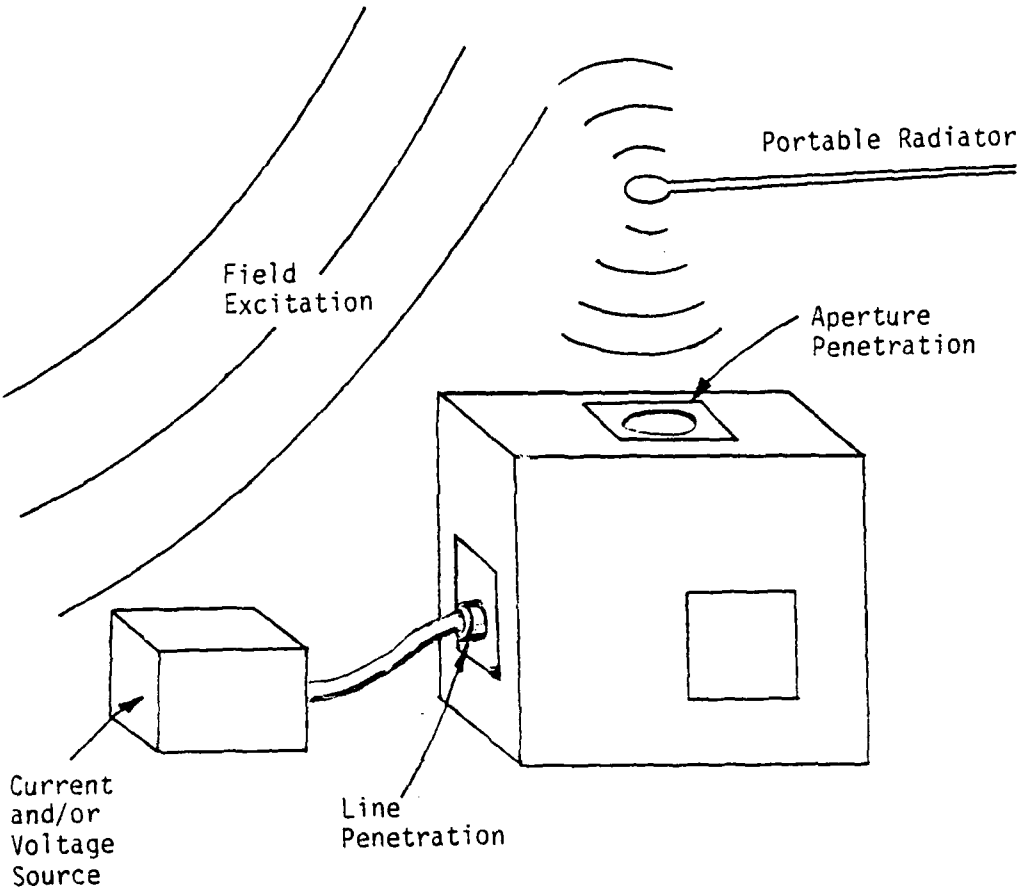

Figure 29. Different types of electromagnetic excitations.

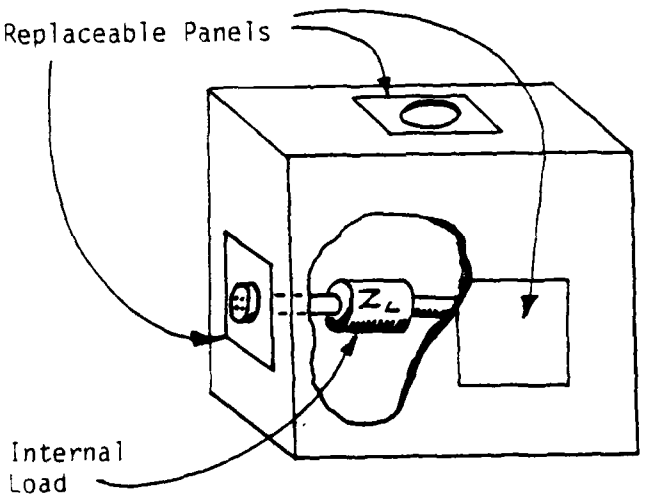

Figure 30. Test variables. Panels may be replaced to alter the types of aperture and line penetrations tested. The internal load may also be replaced and relocated.

excitations. These measured values can then be compared to the calculated values (described in Section II-4d) to corroborate the theoretical analysis and/or suggest possible improvements. This procedure for measuring the combined voltage will be repeated for various combinations of POEs. Three replaceable panels (Fig. 30) allow different types of aperture and line penetrations to be installed on the experimental enclosure. This permits a large variety of different types and arrangements of line and aperture penetrations to be tested. Some of the different possibilities are:

(1) Aperture penetrations

- Different sizes and shapes (e.g., circle, square, rectangle)
- Seams and narrow slots
- Apertures in graphite composite material
- Different aperture orientations
- Apertures with different treatments (e.g., wire mesh, conducting film)

(2) Line penetrations

- Shielded/unshielded conductors
- Coaxial cables with different grounding schemes
- Hollow tubes
- Different conductors and/or penetration geometries
- Power lines and signal lines
- Treated/untreated penetrations (e.g., using filters, dielectric insertion devices, waveguides below cutoff with/without fiber optics, etc.)

A value for the upper bound of the combined voltage will be calculated and then compared to the measured data for each different POE configuration and prescribed excitation condition. The shielding performance of the enclosure for many different configurations will thus be determined and the usefulness of the theoretical model will be evaluated. In addition, by performing these measurements using different hardening schemes for the POEs, the relative effectiveness of each scheme can be determined. Similar data will be gathered using both the double-walled and the single-walled enclosures. The data will then be compared so that all similarities and differences may be identified. Comparisons will also be made between data taken using different excitation schemes (e.g., direct drive, free field, etc.).

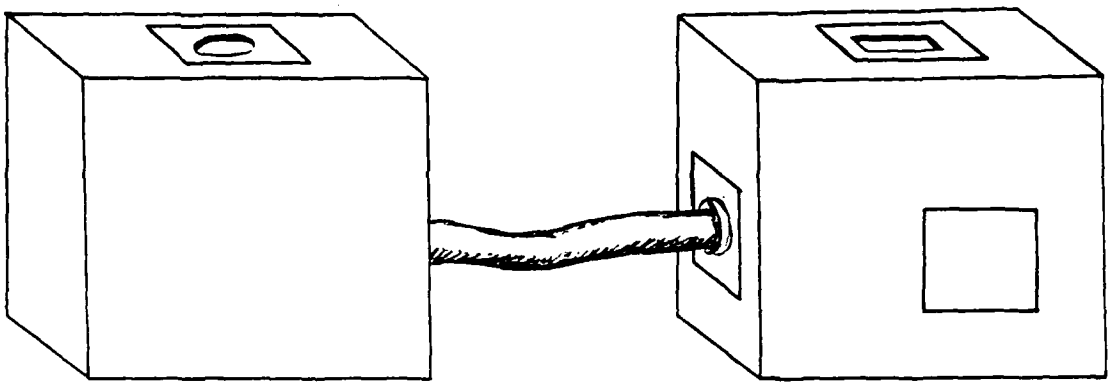

Figure 31. Two enclosure configurations.

Another class of enclosure configurations which will be tested and evaluated consists of the two experimental enclosures connected together via a shielded cable to form one continuous shielded volume, as shown in Figure 31. This is a commonly encountered interconnect arrangement which can be found in many electronic systems. The experimental procedure in this case is the same as that described above for a single enclosure, except that in this case there are many more combinations and permutations of POEs, and a larger variety of internal rearrangements of electronic components which can be tested.

d. Discussion--The BLT* equation which relates the combined voltage vector, $\tilde{V}_s$, is given in Section I as

$$(\mathbb{1} - \mathbb{S}) \odot \mathbb{V} = \mathbb{S} \odot \mathbb{V}$$

where $\mathbb{1}$ is the identity matrix, and $\mathbb{S}$ is the scattering matrix at the shield surfaces. Using the good shielding approximation an upper bound can be calculated for the combined voltage inside the enclosure following the procedure described in Section I. However, to do so the scattering matrix elements and the source terms must first be determined. The former can be obtained

*This acronym is formed from the first letters of the surnames of the originators of this particular equation, namely, Drs. Baum, Liu, and Tesche.

experimentally by the procedure described in Section I for the various POE arrangements of Sections II-2 and II-3, while the latter can be determined from measurements of the short-circuit currents and open-circuit voltages at line penetrations, and from measurements of short-circuit electric and magnetic fields at apertures. For the relatively simple topology of a single enclosure, the actual value of combined voltage for any given internal electronic configurations and prescribed excitation can also be calculated. This can be done rigorously and also by using the good shielding approximation, thus providing a theoretical test of the good shielding approximation as well as a tightness measure for the upper bound calculation using the norm concept. The utility of these calculations can then be evaluated by comparison to the measured values of combined voltage.

In order to perform these calculations, certain values must be arbitrarily assigned to the normalization impedance and the normalization length described in Section I. These parameters can only be specified adequately enough for measurement in highly idealized cases and therefore generally cannot be measured. Consequently the assigned values will be varied in the calculations performed in order to determine the sensitivity of the combined voltage, as well as its upper bound, to this variation.

e. Instrumentation requirements--The instrumentation described in Sections II-2 and II-3 may also be used for the measurements described above. No new equipment will be required.

5. CONCLUSIONS

The experiments described in Section II are designed to provide certain parameters involved in a theoretical model that was developed for analysis of the shielding performance of an enclosure. Experimental techniques and procedures are given. No difficulties in performing these experiments are foreseen. No conclusions can be drawn at this time about the experiments, but it is expected that the results of the experiments will be useful in studying the shielding performance of an enclosure.

III. SPECIFICATIONS FOR SHIELDED ENCLOSURES

1. INTRODUCTION

This section documents the results of the third phase of an effort to characterize quantitatively the shielding performance of a metal enclosure.

The first-phase effort was a theoretical analysis that modeled the interaction between the electronics inside such an enclosure and an electromagnetic excitation (Ref. 18). In the second phase, experiments were identified for testing the accuracy of the model and furnishing a measure of the shielding performance of the enclosure (Ref. 18). In the third phase, specifications for such a shielded enclosure were developed. Two enclosures have been constructed, one with a single-layer topology and the other with a double-layer topology. This section gives details on the specification and construction of these enclosures.

2. GENERAL SPECIFICATION OF ENCLOSURE

a. Dimensions--The outside dimensions of the two enclosures are 4 ft wide, 6 ft long, and 5 ft high. Each has three plain sides and three sides with removable panels, approximately 2 ft by 2 ft. A perspective view of the enclosure is shown in Figure 32. Three generic panels are shown; the hidden sides are continuous sheet metal. Panel A is an aperture panel, B is an access panel, and C is a connector panel. Details of these panels are given in Section II-3. The panels are arranged as indicated in the figure: A is centered on the top, B is off center towards the bottom and towards the connectors panel, and C is centered from side to side, but as close to the bottom of the enclosure as possible (which is about 4 in from the bottom of the panel).

b. Materials--Three materials were considered for the construction: aluminum, stainless steel, and galvanized steel. The contract required optimizing durability, weight, and cost, while maximizing shielding effectiveness. Differences in the shielding effectiveness between the three materials are negligible in the sense that they all provide well in excess of 120 dB of attenuation from 10 kHz to 100 MHz for the material thickness needed for mechanical strength (see below).

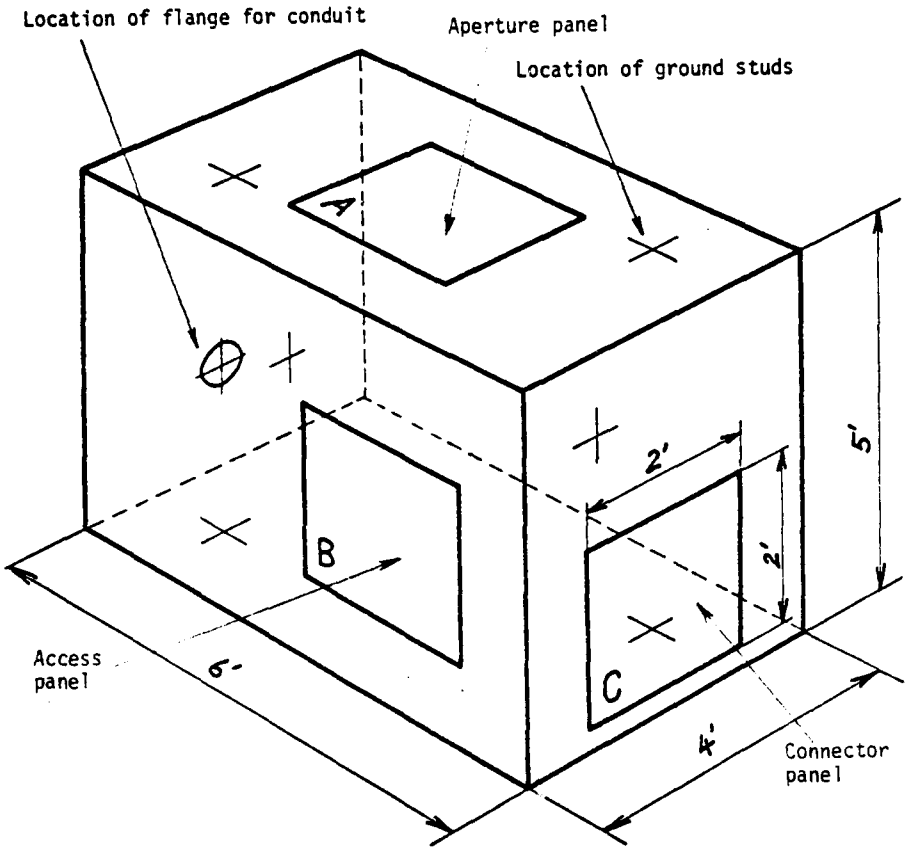

Figure 32. General view of shielded enclosure; all panels are interchangeable.

Aluminum was chosen to be the optimum material for the construction of the enclosures. It is easy to weld, light weight, durable, reasonably corrosion resistant, and has high conductivity. Stainless steel would have been easy to weld, and would be more corrosion resistant, but it would have lower conductivity than aluminum and would be heavier. Galvanized steel would offer somewhat higher shielding of low-frequency magnetic fields; however, it is difficult to weld because of toxic fumes released in the process. Of the three materials, stainless steel is the most expensive, followed by aluminum, with galvanized steel the least expensive. Since the material cost is small, it was not a deciding factor.

A lightweight nonconductive material was needed to separate the two walls in the double-wall enclosure. A rigid foam (Dow Chemical Company Styrofoam 1B) was chosen for that purpose. This material has a dielectric constant of approximately one, which is an additional advantage.

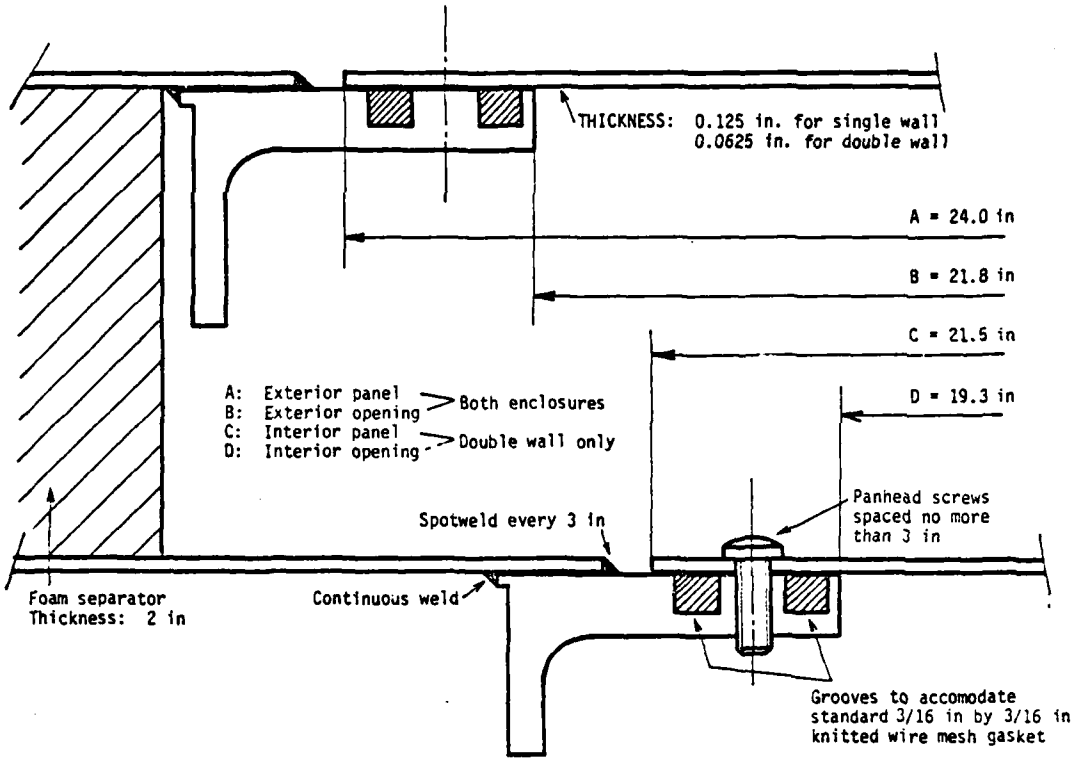

Figure 33. Construction detail of test panel closure.

c. Construction--The enclosures were continuously TIG*-welded at all 12 edges. The thickness of the material was chosen to be 0.125 in for the single-wall and 0.0625 in for the double-wall enclosure. For mechanical strength, thinner material might have sufficed, but would have been difficult to weld. Diffusion of electromagnetic energy through the walls of the enclosure is negligible, and the enclosures were expected to pass the MIL-STD-285 tests.

Particular attention was paid to the design of the openings to accommodate the various panels. The design detail of this is shown in Figure 33 for the double-wall enclosure. The design of the single-wall enclosure is identical, except that the material thickness of the sheet metal is twice the thickness

*Tungsten inert gas

shown in the figure. The L-shaped welded member serves both as a reinforcement and as a gasket holder. Dual gaskets were used to ensure that leakage at the panel edges was minimized. Knitted wire mesh (without a foam core) was chosen as a gasket. Tinned copper-clad steel is considered to be the optimum gasket material for this application. It combines high shielding effectiveness with good corrosion resistance and good resiliancy. Compatibility with aluminum in a normal atmosphere is good. Other materials are available; however, although they may excel in one particular parameter, none offers the optimum combination of characteristics that tinned copper-clad steel has for this application. It should be noted that the groove is a standard size, and rectangular gaskets are readily available in many different materials with and without foam core. If the enclosures are to be used temporarily in a high-humidity environment, a different material may be necessary because of corrosion problems. It might be desirable to use an elastomer as the outer gasket to achieve a complete environmental seal.

The panhead screws that fasten the panels are spaced less than 3 in apart. Screws with different heads may be used if desired, with the exception of countersunk heads. These require precision holes if interchangeability of the panels is to be maintained. Furthermore, the wall thickness of the double-wall enclosure is insufficient to accommodate a countersunk screw head. Steel rivet nuts were used in the frame instead of threading the frame directly. These rivet nuts are expected to last much longer than threads in aluminum; thread stripping is virtually eliminated. The possibility for a rivet nut to become loose is remote since each nut is pressed into the frame and expanded with a special tool.

The construction of the two enclosures is the same, except as already noted. The insides are, in general, plain. A few bolts are welded to the sides to attach soldering lugs and a flange is located opposite the connector panel (Fig. 32) to accommodate the pipe used in some of the experiments (Ref. 19).

3. PANEL CHARACTERISTICS

A major design goal was to keep the cost for the replaceable panels low. This has been achieved at the expense of a slightly more complicated design of the reinforcement of the panel opening. Each panel consists of a square piece

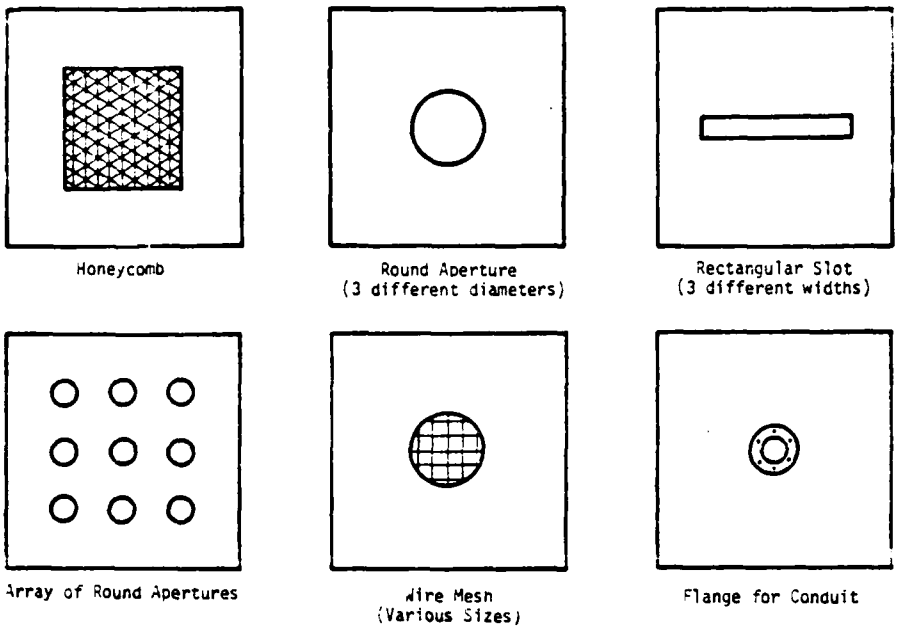

Figure 34. Examples of test panels.

of sheet metal with the holes around the perimeter to fasten the panel to the enclosure. All panels on the outside walls have the same width, but not the same thickness: panels for the single-wall enclosure are 0.125 in thick; those for the double-wall enclosure are 0.0625 in thick. The panels used for the inside wall in the double-wall enclosure are smaller than the other panels so that they can be attached from the outside (see Fig. 33).

Many different panels were constructed from sheet metal. Figure 34 illustrates some of these panels.

a. Honeycomb--Waveguides beyond cutoff are well known and widely used, either as a single waveguide for small apertures, or as a collection of waveguides for large apertures. This panel has a square opening, about 30 cm wide, filled with an array of waveguides beyond cutoff with 0.125 in hexagonal holes. The honeycomb material extends only on one side of the panel. Since the panels are reversible, tests can be made either with a flush surface or with the honeycomb protruding from the surface.

b. Circular aperture--Circular apertures are common in aircraft systems. Three circular-aperture panels were provided with each enclosure. These panels had aperture diameters of 5, 10, and 20 cm. A large body of

analysis exists concerning the electromagnetic properties of circular apertures in this application (Ref. 10). This analysis will aid in understanding measured data.

c. Rectangular slot--Rectangular slots (or slits) are also common in aircraft systems. Again, it is desirable to test three different sizes. Setting the length to a constant 40 cm, and the widths to 2, 4, and 8 cm, gives three different slot ratios of 20, 10, and 5. Testing the slots in the double wall would be very difficult, since it is not known at this time how to predict the performance of the slots in the two walls. Therefore, rectangular slot panels were provided for the single-wall enclosure only.

d. Array of holes--It is common practice to drill an array of many holes of the same size in an equipment enclosure for air circulation and ventilation. Therefore, a panel should be tested with an array of holes. One panel with nine holes of 5 cm diameter and spaced 15 cm apart in a 3 by 3 matrix form was constructed. Other patterns may be developed at a later stage. This panel was provided for the single-wall enclosure only.

e. Wire mesh--Apertures in shielded enclosures are frequently covered with wire mesh to regain some of the shielding while still permitting air circulation. Many different kinds of mesh are available that can be tested in a single panel with a round aperture of 20-cm diameter. This panel was made of brass, so that any mesh can be soldered to the panel.

f. Connector panel--Unlike the aperture panels, only one connector panel was prepared (in addition to the plain one). This connector panel was designed to accommodate a conduit specified for some of the experiments (Ref. 19), and to accommodate one to connect the two enclosures when it is desired to use the double-wall enclosure as an instrumentation box and the single-wall enclosure as the test object. Two 12-ft sections of conduit (2-in outside diameter) were provided.

g. Composite materials--Kevlar, graphite epoxy, and other composite materials not shown are widely used in the aircraft industry for doors, access hatches, and so forth. A Kevlar panel does not give much more insight into coupling problems than does removal of a panel (Kevlar is a dielectric). However, graphite epoxy has moderate conductivity (about 10 kS/m), and a standard panel of this material was fabricated and delivered.

h. Access panel--THe access panel is a plain panel with no holes other than those required for fastening. A few spare plain panels were also provided.

i. Panel to test seams--It has been proposed that a panel be fabricated to test a variety of seams with and without gaskets. While this is feasible, it should be noted that the enclosures were not designed to test seams, and any conclusions drawn from such tests would, therefore, have to be interpreted with caution. A special fixture to test seams in a well-defined environment was constructed by SRI International (SRI) several years ago. The design of the fixture and the testing of commonly used seam designs are discussed in Reference 20.

4. CONCLUSIONS

Two shielded enclosures were designed, fabricated, tested, and delivered ɔ AFWL in accordance with contractual requirements. The two enclosures are identical on the outside, but one has a single-layer topology, while the other has a double-layer topology. Several replaceable panels were made to test various aperture treatment techniques.

The qualification tests of the enclosures are described in Section IV.

IV. QUALIFICATION TESTS FOR SHIELDED ENCLOSURES

1. INTRODUCTION

This section discusses the qualification tests performed with the two shielded enclosures described in Section III. Two kinds of tests were performed to comply with the contractual requirements: (1) measurements according to MIL-STD-285 (Ref. 2) and (2) one additional test with transmission lines, which was selected from several possible alternatives.

The tests according to MIL-STD-285 were performed because this is the only military standard for testing shielded enclosures. The purpose of performing a test in addition to MIL-STD-285 was to investigate alternative methods of defining and measuring shielding effectiveness to circumvent the shortcomings of MIL-STD-285. The additional test affirmed some key ideas: (1) attempting to measure diffusion through a solid wall of metal is, in practice, impossible if the wall is tens of skin-depths thick and (2) as a corollary, the weak points of a shielded enclosure, such as seams, apertures, and penetrations, need to be tested.

Also considered was a test where the enclosures would be immersed in the near field of a commercial broadcast antenna. The field strengths inside and outside of the enclosure would then be compared. (This test was not performed.) A similar test could be performed after delivery to AFWL using the ALECS simulator facility.

2. MIL-STD-285 TESTS

The MIL-STD-285 tests were performed for the single-wall enclosure in accordance with the standard at 150 kHz, 1 MHz, 18 MHz, and 400 MHz. The results are shown in Table 1. The experimental setup was as shown in the standard (Ref. 2).

TABLE 1. MIL-STD-285 TEST RESULTS

Frequency	Antenna	Minimum Insertion Loss (dB)
150 kHz	Loop (12 in diameter)	87
200 kHz	Dipole (41 in long)	113
1 MHz	Dipole (41 in long)	(see text)
18 MHz	Dipole (41 in long)	100
400 MHz	Folded dipole (1/2 wavelength)	100

The enclosure thus passes the MIL-STD-285 requirements, which are 70 dB insertion loss for the loop antenna and 100 dB for all other antennas. At 1 MHz, the signal was buried in the noise, because the dynamic range in this case was limited to 90 dB (no receiver preamplifier was available at this frequency). The tests were not repeated with the double-wall enclosure since that enclosure is much better than the single-wall enclosure.

It should be noted that the test is not really suitable for a small enclosure. The standard was written to test large commercial RF-shielded rooms. However, there are shortcomings in the standard even for large enclosures. The system designer needs to know how a source on one side of the shield interacts with a circuit on the other side of the shield. Measurement of this insertion loss when the shield is placed between two loops or other antennas does not provide this information, except in the unique case where the source is the transmitting loop and the circuit is the receiving loop. In the more likely cases where the source is a lightning strike, a power transient, a broadcast radio wave, or the nuclear EMP and the circuit is some digital electronics or radio receiver inside the shielded enclosure, the circuit response cannot be evaluated from the insertion loss measured in accordance with MIL-STD-285.

It could be argued that MIL-STD-285 requires that the minimum insertion loss be measured and that the interaction can therefore be bounded by assuming that the minimum insertion loss applies throughout the space inside the shield. Unfortunately, this bound is not valid. The test excitation of the shield is not representative of the operational excitation. Below 100 MHz, the operational excitation of the shield is almost always dominated by the currents induced on long power, signal, and ground cables that then flow onto the shield wall. A proper simulation of this would be to inject current on these cables and then to measure some internal response to this current. Above 100 MHz, RF attenuation on cables is large, but aperture coupling is efficient. Hence, it is important that apertures (cracks, seams, vents, etc.) be properly excited in this frequency range. Unfortunately, this is difficult to do because the shield structure, aperture spacings, and interaction distances are electrically large. Consequently, phasing and directional effects tend to dominate the interaction process. Spot illumination, as prescribed by MIL-STD-285, does not reveal the importance of these phased-array effects.

3. TRANSMISSION LINE TEST

A 50-Ω transmission line was constructed over the top of the enclosure to excite the aperture test panel (Fig. 35). The line consisted of copper tape 0.75 in wide which was insulated from the enclosure by 0.25 in of polyethylene material. On the inside, a sensing line was constructed with RG 174 cable (using the shield only). Both lines were checked for reflections with a time-domain reflectometer, and the characteristic impedances of both lines were found to be within 5 percent of 50 Ω.

The results obtained with the single-wall enclosure are shown in Figure 36. Curve 1 shows the coupling when the gasket is removed from the panel mounting joint. Above about 10 MHz the coupling increases with frequency at a rate of 20 dB/decade, which is typical for apertures and riveted or bolted joints. Curve 2 shows the result with the RF-gasket in place. Below 1 MHz there is no systematic difference between curves 1 and 2. The effect of the gasket can be clearly seen at frequencies above 1 MHz.

Curve 3 shows measurements obtained with the transmission lines mounted on a side face without a panel. To some extent, this curve shows the limits of the measurement setup and the available dynamic range. This is because at 1 MHz the material is 30 skin-depths thick, which amounts to more than 260 dB of attenuation by diffusion alone. For practical purposes, this has to be considered infinite attenuation. That a signal was actually detected indicates the effect of coupling between the input and output lines along paths other than directly between the two transmission lines. In this particular measurement, one of these coupling paths was via instrumentation cables entering an opened access panel on one face of the box.

Additional tests were performed that were not required by the work statement: a test with a wide transmission line (but still 50 Ω) on the single-wall enclosure for comparison with the results from the narrow line used in the test described above, and another narrow-line test with the double-wall enclosure. The results of both tests are shown in Figure 37. Great care was taken in both cases to ensure that the topology of the shielded enclosure was not compromised, i.e., all panels were closed.

The wide transmission line for the single-wall enclosure was 50 cm wide and 10 cm high, tapered, and terminated at the end in 50 Ω. The results

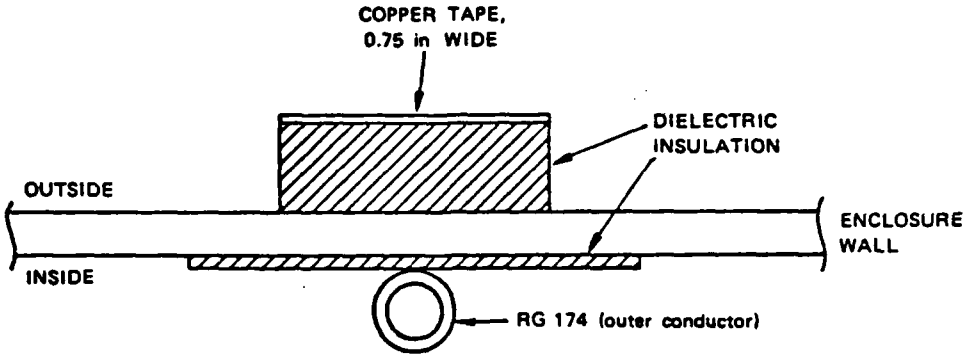

(a) Enlarged cross section of transmission lines (impedance: 50 Ω).

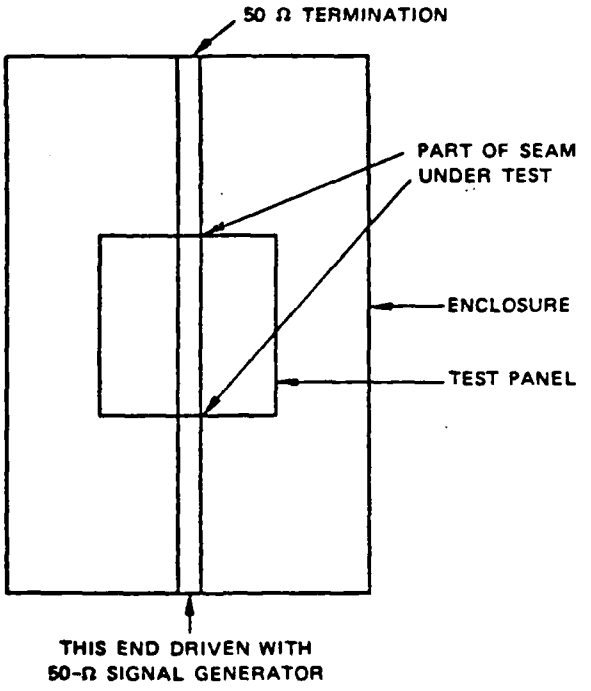

(b) Top view of transmission line.

Figure 35. Transmission line test setup.

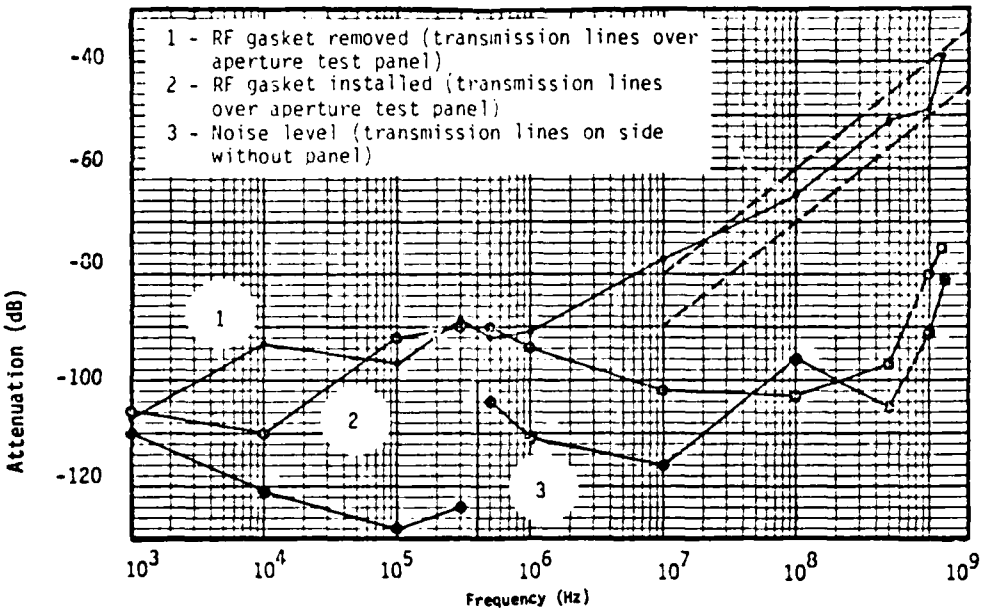

Figure 36. Attenuation of single-wall enclosure.

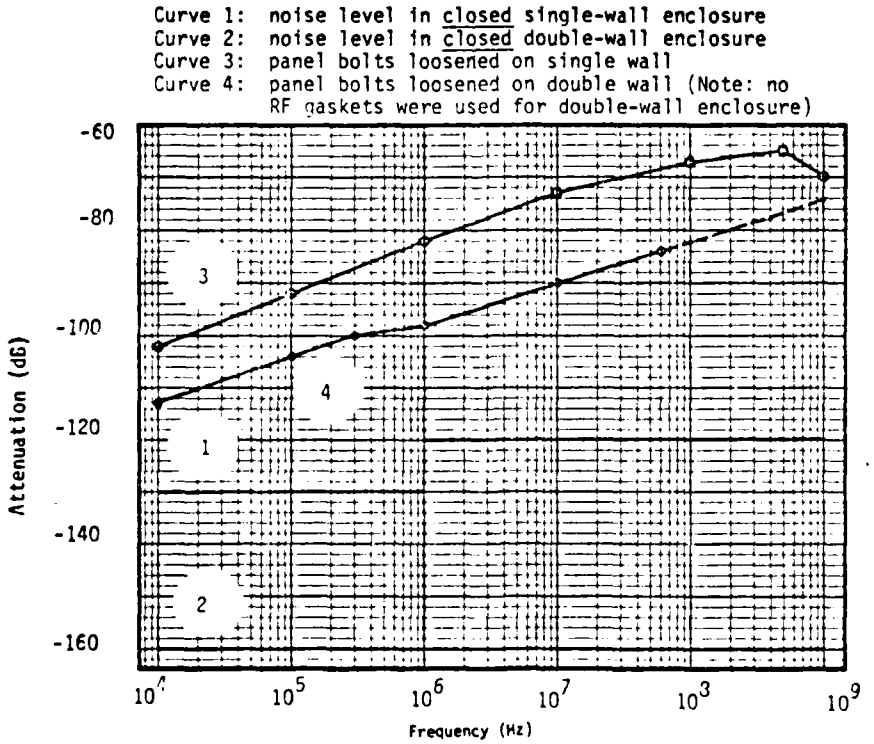

Figure 37. Attenuation of single- and double-wall enclosure.

indicate that the single-wall box has a much better performance than the curves in Figure 36 suggest. No attempt was made in those earlier tests to close apertures other than the panel under test, and hence a significant amount of direct cable-coupling was possible.

The double-wall enclosure tests (with the same narrow line used before) confirmed the expectation that the double-wall panels are better than the single-wall panel. All measurements were taken with the RF-gaskets removed from both panels under test, yet the performance of the double-wall panel was substantially better than the single wall with gasket (compare Figs. 36 and 37).

Some caution is necessary when comparing these figures because the setups were not the same. Note in Figure 37 when the enclosures were properly sealed (i.e., panel bolts were tightened), that no signal could be measured other than the noise inherent in the setup. However, the noise level is considerably lower than in the tests first performed with the single-wall enclosure. Also, when the panel under test was loose, the induced voltage appeared to be proportional to the square root of frequency.

The curves of Figure 37 refer to the following conditions: (1) noise level with closed single-wall enclosure, (2) noise level with closed double-wall enclosure, (3) panel bolts loosened on single-wall, and (4) panel bolt loosened on double-wall (no RF gaskets were used for double-wall panels).

4. CONCLUSIONS

Both enclosures pass the requirements of MIL-STD-285. In fact, the insertion loss of the enclosures meets the more stringent requirements stated in the contract of 120 dB from 10 kHz to 100 MHz, if insertion loss is measured with a parallel-plate transmission line (see Fig. 37). Further work is necessary to determine whether the transmission line test can be developed into a useful alternative to MIL-STD-285.

REFERENCES

1. Baum, C. E., "Electromagnetic Topology: A Formal Approach to the Analysis and Design of Complex Electronic Systems," Interaction Note 400, Air Force Weapons Laboratory, Kirtland AFB, NM, September 1980.

2. Military Standard Attenuation Measurements for Enclosures, Electromagnetic Shielding, for Electronic Test Purposes, Method of, MIL-STD-285 (25 June 1956).

3. Vance, E. F., W. Graf, J. E. Nanevicz, "Unification of Electromagnetic Specifications and Standards," Part I. Evaluation of Existing Practices," Interaction Note 420, Air Force Weapons Laboratory, Kirtland AFB, NM, July 1981.

4. Baum, C. E., T. K. Liu, and F. M. Tesche, "On the Analysis of General Multiconductor Transmission-Line Networks," Interaction Note 350, Air Force Weapons Laboratory, Kirtland AFB, NM, November 1979.

5. Baum, C. E., "Norms and Eigenvector Norms," Mathematics Note 63, Air Force Weapons Laboratory, Kirtland AFB, NM, November 1979.

6. P. Lancaster, Theory of Matrices, Academic Press, 1969.

7. Baum, C. E., "Sublayer Sets and Relative Shielding Order in Electromagnetic Topology," Interaction Note 416, Air Force Weapons Laboratory, Kirtland AFB, NM, April 1982.

8. Baum, C. E., "Black Box Bounds," to be published as an Interaction Note.

9. Agrawal, A. K., and C. E. Baum, "Bounding of Signal Levels at Terminations of a Multiconductor Transmission-Line Network," Interaction Note 419, Air Force Weapons Laboratory, Kirtland AFB, NM, April 1983.

10. Lee, K.S.H., editor, "EMP Interaction: Principles, Techniques, and Reference Data," AFWL-TR-80-402, Air Force Weapons Laboratory, Kirtland AFB, NM, December 1980.

11. Baum, C. E., "EMP Simulators for Various Types of Nuclear EMP Environments: An Interim Categorization," IEEE Transactions on Antennas and Propagation, Vol. AP-26, No. 1, January 1978. Also, Sensor and Simulation Note 240, Air Force Weapons Laboratory, Kirtland AFB, NM.

12. Davis, W. A., and M. K. Sistanizadeh, "Bounding Signal Levels at Terminations of a Multiconductor Transmission Line Behind an Aperture," Interaction Note 412, Air Force Weapons Laboratory, Kirtland AFB, NM, June 4, 1981. (See also IEEE Transactions on Antennas and Propagation, Vol. AP-30, No. 6, November 1982.)

13. Chen, K., et al., "ACHATES Design," AFWL ACHATES Memo No. 1, November 5, 1976 (revised).

14. Shen, H. M., and R.W.P. King, "Experimental Investigation of the Rhombic EMP Simulator: Comparison with Theory and Parallel Plate Simulator," IEEE Transactions on EMC, Vol. EMC-24, No. 3, August 1982.

15. Lee, K.S.H., F. C. Yang, and K. C. Chen, "Cavity Excitation via Apertures," Interaction Note 316, Air Force Weapons Laboratory, Kirtland AFB, NM, February 1977.

16. Davis., W., "Bounding EMP Interaction and Coupling," IEEE Transactions on Antennas and Propagation, Vol. AP-29, No. 6, November 1981.

17. Casey, K. F., "Low Frequency Electromagnetic Penetration of Loaded Apertures," IEEE Transactions on EMC, Vol. EMC-23, No. 4, November 1981.

18. Yang., F. C., and C. E. Baum, "Use of Matrix Norms of Interaction Supermatrix Blocks for Specifying Electromagnetic Performance of Subshields," Dikewood Report DC-TR-1026.610-1 (December 1982).

19. Kokorowski, S. A., K.S.H. Lee, J. Hamm, and W. Graf, "Experiments for Characterizing the Shielding of an Enclosure," Dikewood Report DC-TR-1026.610-2 (February 1983).

20. Vance, E. F., and W. C. Wadsworth, "Rectangular Coaxial Skin Tester," SRI Technical Memorandum 24, Contract F29601-69-C-0127, September 1973.

A-1. Ramo, S., J. R. Whinnery, and T. Van Suzer, Fields and Waves in Communication Electronics, John Wiley and Sons, Inc., New York, 1965.

APPENDIX A
DERIVATION OF SUPERMATRIX EQUATION

An aeronautic system can be described by a topological diagram which can, in turn, be used to construct a corresponding interaction sequence diagram (Fig. 1). An interaction sequence diagram consists of vertices and edges. The vertices represent surfaces and layers (volumes) in the topological diagram and the edges indicate how the electromagnetic signals transport. There are voltages and currents on the edges which satisfy the familiar transmission-line equations. The voltages and currents are coupled in the transmission-line equations. This complexity can be avoided by introducing the following combined voltages (Fig. A-1)

$$(\tilde{V}_n)_u = (\tilde{V}_n^{(+)})_u + (\tilde{Z}_{c_{n,m}})_u \cdot (\tilde{I}_n^{(+)})_u$$

$$(\tilde{V}_n)_v = (\tilde{V}_n^{(+)})_u - (\tilde{Z}_{c_{n,m}})_u \cdot (\tilde{I}^{(+)})_u \qquad \text{(A-1)}$$

With the combined voltages as the dependent variables, the transmission-line equations become uncoupled and are given as

$$\frac{d}{dz_u}(\tilde{V}_n)_u = -(\tilde{\gamma}_{c_{n,m}})_u \cdot (\tilde{V}_n)_u + (\tilde{V}'_{s_n})_u^{temp}$$

$$\frac{d}{dz_u}(\tilde{V}_n)_v = (\tilde{\gamma}_{c_{n,m}})_u \cdot (\tilde{V}_n)_v + (\tilde{V}'_{s_n})_v^{temp} \qquad \text{(A-2)}$$

where $(\tilde{\gamma}_{c_{n,m}})_u$ is the propagation matrix, $(\tilde{V}_{s_n}')_u^{temp}$ and $(\tilde{V}_{s_n}')_v^{temp}$ are distributed combined voltage source vectors given by (Fig. A-2)

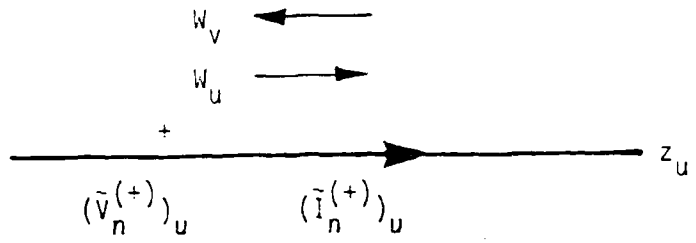

$$(\tilde{V}_n)_u = (\tilde{V}_n^{(+)})_u + (\tilde{Z}_{c_{n,m}})_u \cdot (\tilde{I}_n^{(+)})_u$$

$$(\tilde{V}_n)_v = (\tilde{V}_n^{(+)})_u - (\tilde{Z}_{c_{n,m}})_u \cdot (\tilde{I}_n^{(+)})_u$$

Figure A-1. Sign conventions for real voltages and currents used for the combined voltage definition.

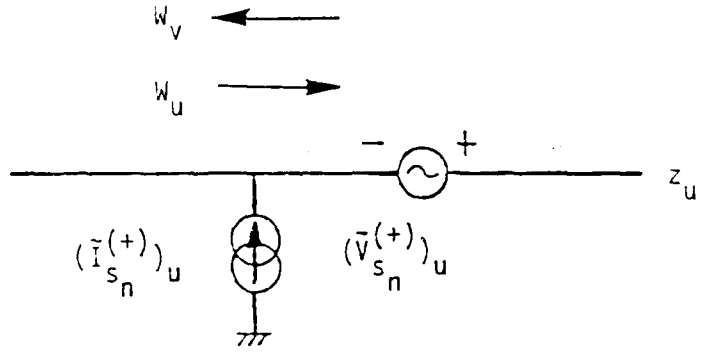

$$(\tilde{V}_{s_n})_u^{temp} = (\tilde{V}_{s_n}^{(+)})_u + (\tilde{Z}_{c_{n,m}})_u \cdot (\tilde{I}_{s_n}^{(+)})_u$$

$$(\tilde{V}_{s_n})_v^{temp} = (\tilde{V}_{s_n}^{(+)})_u - (\tilde{Z}_{c_{n,m}})_u \quad (\tilde{I}_{s_n}^{(+)})_u$$

$$(\tilde{Z}_{c_{n,m}})_u = (\tilde{Z}_{c_{n,m}})_v$$

Figure A-2. Sign conventions for the real voltages and currents used for a temporary combined source voltage definition.

$$(\tilde{V}'_{s_n})_u^{temp} = (\tilde{V}_{s_n}^{(+)'})_u + (\tilde{Z}_{c_{n,m}})_u \cdot (\tilde{I}_{s_n}^{(+)'})_u$$

$$(\tilde{V}'_{s_n})_v^{temp} = (\tilde{V}_{s_n}^{(+)'})_u - (\tilde{Z}_{c_{n,m}})_u \cdot (\tilde{I}_{s_n}^{(+)'})_u \qquad \text{(A-3)}$$

The superscript "temp" indicates that these are temporary definitions and that a different combined voltage source vector will be defined later. Equation A-2 clearly indicates that the combined voltages of the two oppositely propagating waves still satisfy different differential equations. To unify these two equations, another coordinate system, $z_v = \ell_u - z_u$, is introduced for the vectors involving z_v (Fig. A-3). With this new set of coordinate systems which has $z = 0$ and $z = \ell_u$ (z can be either z_u or z_v, and ℓ_u is the length of the edge) indicating, respectively, the initiating and terminating points of the wave, Equation A-2 becomes

$$\frac{d}{dz_u}(\tilde{V}_n)_u = -(\tilde{\gamma}_{c_{n,m}})_u \cdot (\tilde{V}_n)_u + (\tilde{V}'_{s_n})_u \qquad \text{(A-4)}$$

Here u represents eitner wave on the edge and

$$(\tilde{V}'_{s_n}) = (\tilde{V}_{s_n}^{(+)'})_u + (\tilde{Z}_{c_{n,m}})_u \cdot (\tilde{I}_{s_n}^{(+)'})_u \qquad \text{(A-5)}$$

with $(\tilde{\gamma}_{s_n}^{(+)'})_u$ being positive when it increases with the wave propagating direction and $(\tilde{I}_{s_n}^{(+)'})_u$ being positive when it flows into the edge (Fig. A-4).

Equation A-4 can be solved to relate the combined voltages at the wave terminating points (at $z_u = \ell_u$) to those at the wave initiating points (at $z_o = 0$). Under the assumption of short edge length (i.e., under the condition that $\|((\tilde{\gamma}_{c_{n,m}})_u)\| \|(\ell_u)\| \ll 1$), the relation is simply

$$((\tilde{V}_n)_u)\Big|_{(z_u) = (\ell_u)} = ((\tilde{V}_n)_u)\Big|_{(z_u) = (0)} + ((\tilde{V}_{s_n})_u) \qquad \text{(A-6)}$$

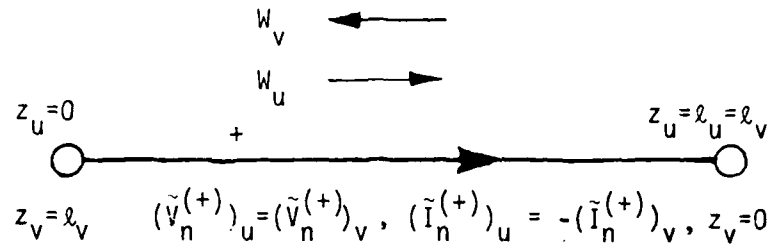

$$(\tilde{V}_n)_u = (\tilde{V}_n^{(+)})_u + (\tilde{Z}_{c_{n,m}})_u \cdot (\tilde{I}_n^{(+)})_u$$

$$(\tilde{V}_n)_v = (\tilde{V}_n^{(+)})_u - (\tilde{Z}_{c_{n,m}})_u \cdot (\tilde{I}_n^{(+)})_u$$

$$= (\tilde{V}_n^{(+)})_v + (\tilde{Z}_{c_{n,m}})_v \cdot (\tilde{I}_n^{(+)})_v$$

Figure A-3. Sign conventions for the coordinate systems, real voltages, and currents used in the combined voltage definition.

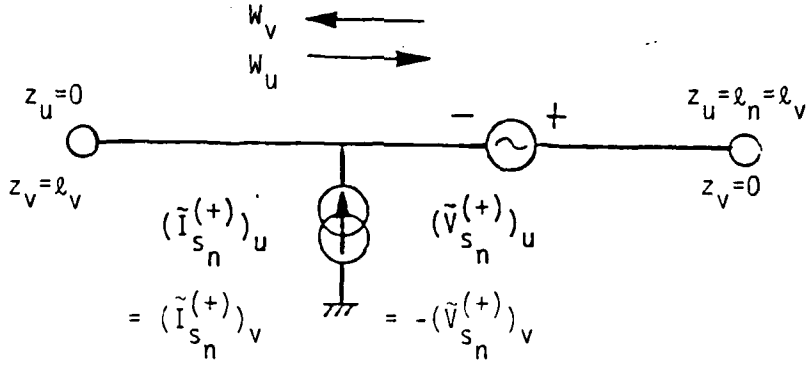

$$(\tilde{V}_{s_n})_u = (\tilde{V}_{s_n}^{(+)})_u + (\tilde{Z}_{c_{n,m}})_u \cdot (\tilde{I}_{s_n}^{(+)})_u$$

$$(\tilde{V}_{s_n})_v = -(\tilde{V}_{s_n}^{(+)})_u + (\tilde{Z}_{c_{n,m}})_u \cdot (\tilde{I}_{s_n}^{(+)})_u$$

$$= (\tilde{V}_{s_n}^{(+)})_v + (\tilde{Z}_{c_{n,m}})_v \cdot (\tilde{I}_{s_n}^{(+)})_v$$

Figure A-4. Sign conventions for the coordinate systems, real voltages, and currents used in the combined source voltage definition.

where $((\tilde{V}_{s_n})_u)$ is the combined voltage source supervector which is the integral of the corresponding distributed quantity along the edge.

Equation A-6 describes how the combined voltages vary along the edges. Another equation is still needed to describe how the combined voltages behave at the vertices. At a vertex, incident waves are scattered. The scattered waves are related to the incident waves through a scattering matrix (Ref. A-1). Since the incident and scattered waves at a vertex are, respectively, the terminating and initiating combined voltages on the edges connecting to the vertex, the relationship is given by

$$((\tilde{V}_n)_u)\Big|_{(z_u)=(0)} = ((\tilde{S}_{n,m})_{u,v}) \odot ((\tilde{V}_n)_u)\Big|_{(z_u)=(\ell_u)} \tag{A-7}$$

Equations A-6 and A-7 can then be combined to give

$$[((1_{n,m})_{u,v}) - ((\tilde{S}_{n,m})_{u,v})] \odot ((\tilde{V}_n)_u)\Big|_{(z_u)=(0)}$$

$$= ((\tilde{S}_{n,m})_{u,v}) \odot ((\tilde{V}_{s_n})_u) \tag{A-8}$$

With the abbreviated symbol $((\tilde{V}_n)_u$ for $((\tilde{V}_n)_u)\Big|_{(z_u)=(0)}$, this equation is Equation 1.

APPENDIX B

TRANSMISSION COEFFICIENTS (MATRIX) FOR APERTURE PENETRATION

The source quantities of voltage and current on the wire in the outer layer are needed to quantify the wire-to-wire interaction through an aperture. Appropriate source reference quantities constructed from this voltage and current must be used to define the transmission coefficients for such an interaction mechanism. The transmission coefficients were defined in Section I-2 using only the combined voltage

$$\tilde{V}^{(+)}_{\alpha;\lambda} + \tilde{Z}_{c_{\alpha;\lambda}} \tilde{I}^{(+)}_{\alpha;\lambda}$$

of the incoming wave (with respect to the point where the wire penetrates or is attached to the shield, see Fig. 4) on the wire in the outer layer as the reference quantity. Alternative reference quantities are used in this appendix for the definition.

Consider Figure B-1, where the internal wire is extended in both directions away from the aperture with arbitrary loads. This is a more general configuration than shown in Figure 4. The equivalent circuit for the internal wire of Figure B-1 is given in Figure B-2. An alternative transmission matrix using the combined voltages of both waves as reference quantities will now be defined. The transmission matrix is given via

$$\begin{pmatrix} \tilde{V}^{(+)}_{1;2} + \tilde{Z}_{c_2} \tilde{I}^{(+)}_{1;2} \\ \tilde{V}^{(+)}_{2;2} + \tilde{Z}_{c_2} \tilde{I}^{(+)}_{2;2} \end{pmatrix} = \begin{pmatrix} \tilde{T}_{1,1;2,1} & \tilde{T}_{1,2;2,1} \\ \tilde{T}_{2,1;2,1} & \tilde{T}_{2,2;2,1} \end{pmatrix} \cdot \begin{pmatrix} \tilde{V}^{(+)}_{1;1} + \tilde{Z}_{c_1} \tilde{I}^{(+)}_{1;1} \\ \tilde{V}^{(+)}_{1;1} - \tilde{Z}_{c_1} \tilde{I}^{(+)}_{1;1} \end{pmatrix}$$

$$+ \begin{pmatrix} \tilde{R}_{1,1;2,2} & 0 \\ 0 & \tilde{R}_{2,2;2,2} \end{pmatrix} \cdot \begin{pmatrix} \tilde{V}^{(+)}_{1;2} - \tilde{Z}_{c_2} \tilde{I}^{(+)}_{1;2} \\ \tilde{V}^{(+)}_{2;2} - \tilde{Z}_{c_2} \tilde{I}^{(+)}_{2;2} \end{pmatrix} \qquad \text{(B-1)}$$

$\tilde{T}$ and $\tilde{R}$ are used here instead of $\tilde{S}$ to distinguish them from the definition given in Section I-2, and to specifically indicate that the transmission and reflection quantities and $\lambda = 1$, $\alpha = 1$, and $\beta = 2$ are arbitrarily assigned. Additional artificial wires connecting to the aperture node must be introduced

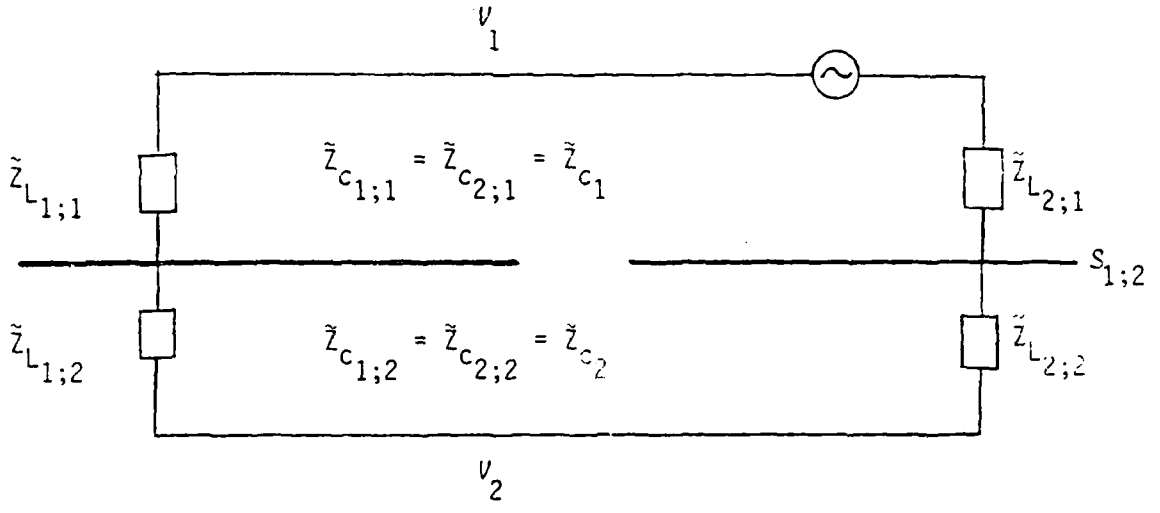

Figure B-1. Schematic of wires interacting through an aperture.

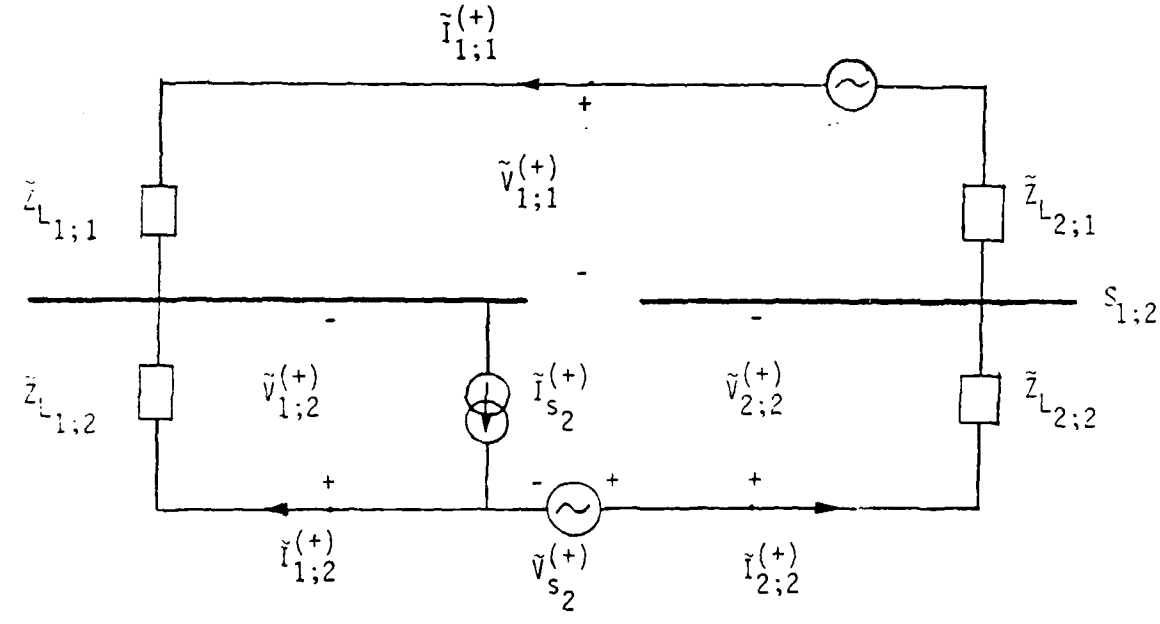

Figure B-2. Schematic of equivalent circuit for the inner wire of schematic shown in Figure B-1.

to fit this definition into the overall scattering matrix formulation. The transmission and reflection coefficients can be calculated using Equation B-1. For example, $\tilde{T}_{2,1;2,1}$ can be obtained by solving the circuit of Figure B-2 by taking

$$\tilde{Z}_{L_{2;2}} = \tilde{Z}_{c_2} \text{ and } \tilde{Z}_{L_{1;1}} = \tilde{Z}_{c_1}$$

That is,

$$(\tilde{T}) = \begin{pmatrix} \tilde{T}_{1,1;2,1} & \tilde{T}_{1,2;2,1} \\ \tilde{T}_{2,1;2,1} & \tilde{T}_{2,2;2,1} \end{pmatrix}$$

$$= \begin{pmatrix} \dfrac{-\tilde{Z}_{c_2}\,\tilde{v}_{s_{2,1}} + \tilde{Z}_{L_{2;2}}\,\tilde{i}_{s_{2,1}}}{\tilde{Z}_{L_{2;2}} + \tilde{Z}_{c_2}} & \dfrac{\tilde{Z}_{c_2}\,\tilde{v}_{s_{2,1}} + \tilde{Z}_{L_{2;2}}\,\tilde{i}_{s_{2,1}}}{\tilde{Z}_{L_{2;2}} + \tilde{Z}_{c_2}} \\ \dfrac{\tilde{Z}_{c_2}\,\tilde{v}_{s_{2,1}} + \tilde{Z}_{L_{1;2}}\,\tilde{i}_{s_{2,1}}}{\tilde{Z}_{L_{1;2}} + \tilde{Z}_{c_2}} & \dfrac{-\tilde{Z}_{c_2}\,\tilde{v}_{s_{2,1}} + \tilde{Z}_{L_{1;2}}\,\tilde{i}_{s_{2,1}}}{\tilde{Z}_{L_{1;2}} + \tilde{Z}_{c_2}} \end{pmatrix} \qquad \text{(B-2)}$$

and

$$\tilde{R}_{1,1;2,2} = \frac{\tilde{Z}_{L_{2;2}} - \tilde{Z}_{c_2}}{\tilde{Z}_{L_{2;2}} + \tilde{Z}_{c_2}}\,; \quad \tilde{R}_{2,2;2,2} = \frac{\tilde{Z}_{L_{1;2}} - \tilde{Z}_{c_2}}{\tilde{Z}_{L_{1;2}} + \tilde{Z}_{c_2}} \qquad \text{(B-3)}$$

Various natural matrix norms can be calculated for the transmission matrix $(\tilde{T})$. For example,

$$\|(\tilde{T})\|_\infty = \max\left\{ \frac{\left|-\tilde{Z}_{C_2}\,\tilde{v}_{s_{2,1}} + \tilde{Z}_{L_{j;2}}\,\tilde{i}_{s_{2,1}}\right| + \left|\tilde{Z}_{C_2}\,\tilde{v}_{s_{2,1}} + \tilde{Z}_{L_{j;2}}\,\tilde{i}_{s_{2,1}}\right|}{\left|\tilde{Z}_{L_{j;2}} + \tilde{Z}_{C_2}\right|};\ j = 1,2 \right\}$$

$$= \begin{cases} 2\left|\tilde{i}_{s_{2,1}}\right| \text{ , for } \tilde{Z}_{L_{j;2}} = \infty,\ j=1,2 \\ 2\left|\tilde{v}_{s_{2,1}}\right| \text{ , for } \tilde{Z}_{L_{j;2}} = 0,\ j = 1,2 \\ \max\left\{ 2\left|\tilde{v}_{s_{2,1}}\right| ;\ 2\left|\tilde{i}_{s_{2,1}}\right| \right\}, \text{ for } \tilde{Z}_{L_{1;2}} = 0,\ \tilde{Z}_{L_{2;2}} = \infty \\ \tfrac{1}{2}\left|\tilde{v}_{s_{2,1}} + \tilde{i}_{s_{2,1}}\right| + \tfrac{1}{2}\left|-\tilde{v}_{s_{2,1}} + \tilde{i}_{s_{2,1}}\right| \leq \left|\tilde{v}_{s_{2,1}}\right| + \left|\tilde{i}_{s_{2,1}}\right| \\ \quad \text{(equal when } \tilde{v}_{s_{2,1}}/\tilde{i}_{s_{2,1}} \text{ is real), for } \tilde{Z}_{L_{j;2}} = \tilde{Z}_{C_2},\ j = 1,2 \end{cases} \tag{B-4}$$

and,

$$\|(\tilde{T})\|_2 = \max\left\{ \left| \frac{2\tilde{Z}_{C_2}\,\tilde{v}_{s_{2,1}}}{\tilde{Z}_{L_{1;2}} + \tilde{Z}_{C_2}} \right| ;\ \left| \frac{2\tilde{Z}_{L_{1;2}}\,\tilde{i}_{s_{2,1}}}{\tilde{Z}_{L_{1;2}} + \tilde{Z}_{C_2}} \right| \right\}, \text{ for } \tilde{Z}_{L_{1;2}} = \tilde{Z}_{L_{2;2}}$$

$$= \begin{cases} 2\left|\tilde{i}_{s_{2,1}}\right| \text{ , for } \tilde{Z}_{L_{j;2}} = \infty \text{ , } j = 1,\ 2 \\ 2\left|\tilde{v}_{s_{2,1}}\right| \text{ , for } \tilde{Z}_{L_{j;2}} = 0,\ j = 1,\ 2 \\ \max\left\{ \left|\tilde{v}_{s_{2,1}}\right| ;\ \left|\tilde{i}_{s_{2,1}}\right| \right\}, \text{ for } \tilde{Z}_{L_{j;2}} = \tilde{Z}_{C_2} \text{ , } j = 1,\ 2 \end{cases} \tag{B-5}$$

The above consideration, of course, can be used for the wire-to-wire aperture penetration configuration discussed in Subsection I-2c(1), i.e., Figure 3. For that configuration (taking $\lambda = 1$, $\beta = 2$, $\alpha = 1$), Equation B-1 reduces to

$$\tilde{V}^{(+)}_{2;2} + \tilde{Z}_{c_2} \tilde{I}^{(+)}_{2;2} = \tilde{T}_{2,1;2,1} \left[\tilde{V}^{(+)}_{1,1} + \tilde{Z}_{c_1} \tilde{I}^{(+)}_{1;1}\right] + \tilde{T}_{2,2;2,1} \left[\tilde{V}^{(+)}_{1;1} - \tilde{Z}_{c_1} \tilde{I}^{(+)}_{1;1}\right] \tag{B-6}$$

Then, in the norm (magnitude, for a scalar) sense,

$$\begin{aligned}
\left|\tilde{V}^{(+)}_{2;2} + \tilde{Z}_{c_2} \tilde{I}^{(+)}_{2;2}\right| &\le \left|\tilde{T}_{2,1;2,1}\right| \left|\tilde{V}^{(+)}_{1;1} + \tilde{Z}_{c_1} \tilde{I}^{(+)}_{1;1}\right| \\
&\quad + \left|\tilde{T}_{2,2;2,1}\right| \left|\tilde{V}^{(+)}_{1;1} - \tilde{Z}_{c_1} \tilde{I}^{(+)}_{1;1}\right| \\
&\le \left\{\left|\tilde{T}_{2,1;2,1}\right| + \left|\tilde{T}_{2,2;2,1}\right|\right\} \left|\tilde{V}^{(+)}_{1;1} + \tilde{Z}_{c_1} \tilde{I}^{(+)}_{1;1}\right| \\
&\qquad \text{if } \left|\tilde{V}^{(+)}_{1;1} + \tilde{Z}_{c_1} \tilde{I}^{(+)}_{1;1}\right| \ge \left|\tilde{V}^{(+)}_{1;1} - \tilde{Z}_{c_1} \tilde{I}^{(+)}_{1;1}\right| \\
&\le \max\left\{2 \left|\tilde{v}_{s_{2,1}}\right| ; 2 \left|\tilde{i}_{s_{2,1}}\right|\right\} \left|\tilde{V}_{1;1} + \tilde{Z}_{c_1} \tilde{I}^{(+)}_{1;1}\right|
\end{aligned} \tag{B-7}$$

which agrees with Equation 10 where a transmission coefficient was defined using only

$$\tilde{V}^{(+)}_{1;1} + \tilde{Z}_{c_1} \tilde{I}_{1;1}$$

as the reference source quantity.

So far, the discussion in this appendix deals with the wire-to-wire aperture penetration problem. The same procedure can be used for the field-to-wire aperture penetration problem so that, instead of just $a[\tilde{E}_{sc} + Z_o \tilde{H}_{sc}]$, both $a[\tilde{E}_{sc} \pm Z_o \tilde{H}_{sc}]$ can be used for the transmission matrix definition. That is, Equation B-8 is similar to Equation B-1.

$$\begin{pmatrix} \tilde{V}^{(+)}_{1;2} + \tilde{Z}_{c_2} \tilde{I}^{(+)}_{1;2} \\ \tilde{V}^{(+)}_{2;2} + \tilde{Z}_{c_2} \tilde{I}^{(+)}_{2;2} \end{pmatrix} = \begin{pmatrix} \tilde{T}_{1,1;2,1} & \tilde{T}_{1,2;2,1} \\ \tilde{T}_{2,1;2,1} & \tilde{T}_{2,2;2,1} \end{pmatrix} \cdot \begin{pmatrix} a\left[\tilde{E}_{sc} + Z_o \tilde{H}_{sc}\right] \\ a\left[\tilde{E}_{sc} - Z_o \tilde{H}_{sc}\right] \end{pmatrix}$$

$$+ \begin{pmatrix} \tilde{R}_{1,1;2,2} & 0 \\ 0 & \tilde{R}_{2,2;2,2} \end{pmatrix} \cdot \begin{pmatrix} \tilde{V}^{(+)}_{1;2} - \tilde{Z}_{c_2} \tilde{I}^{(+)}_{1;2} \\ \tilde{V}^{(+)}_{2;2} - \tilde{Z}_{c_2} \tilde{I}^{(+)}_{2;2} \end{pmatrix} \qquad \text{(B-8)}$$

Equation B-8 can then be used to obtain relations the same as Equations B-2 through B-7, except that $\tilde{v}_{s_{2,1}}$ and $\tilde{i}_{s_{2,1}}$ must be changed to $\tilde{v}^{(f)}_{s_{2,1}}$ and $\tilde{i}^{(f)}_{s_{2,1}}$.

GLOSSARY

Indices (appeared as subscripts)

u or v	wave index
λ or η	layer (volume) index
ℓ or ℓ'	sublayer index
τ or τ'	elementary layer index
μ or μ'	layer-part index (= 1, 2, 3)
σ or σ'	dual-wave index (= 1, 2)
n or m	wire (POE) index
$\mu \sim (\alpha;\lambda) \sim (\sigma;\tau;\ell;\mu;\lambda)$	

Superscripts

(+)	for true quantities (to be in contrast with combined quantities)
(L)	for line penetrations
(f)	for field aperture penetrations
(i)	aperture index

General matrix/vector symbols

$(\ )$	matrix/vector symbol
$\odot$	generalized dot product
$\cdot$	dot product
$((\tilde{A}_{n,m})_{u,v})$	supermatrix whose element $\tilde{A}_{n,m;u,v}$ is associated with n-wire of u-wave and m-wire of v-wave
$((\tilde{B}_{n})_{u})$	supervector whose element $\tilde{B}_{n;u}$ is associated with n-wire of u-wave
$((1_{n,m})_{u,v})$	identity supermatrix
$((0_{n,m})_{u,v})$	zero supermatrix
$(\ )^{-1}$	inverse of a matrix

$( )^{\dagger}$ conjugate transpose of a matrix

$\rho\{ \}$ spectral radius of a matrix

$\|( )\|$ natural matrix/vector norm

$\|( )\|_p$ p-norm, p=1,2,...., ∞

Symbols associated with EM topology and interaction

$V_{\lambda,\ell}$ ℓ-sublayer in λ-layer

$S_{\lambda,\ell;\lambda+1,\ell'}$ surface separating ℓ-sublayer in λ-layer from ℓ'-sublayer in $(\lambda+1)$ - layer

W_u u-wave

$\tilde{V}_{n;u}$ combined voltage on n-wire of u-wave

$\tilde{V}^{(+)}_{n;u}$, $\tilde{I}^{(+)}_{n;u}$ true voltage, current on n-wire of u-wave

$\tilde{V}^{(-)}_{n;u}$ combined source voltage on n-wire of u-wave

$\tilde{V}^{(-)}_{s_{n;u}}$, $\tilde{I}^{(+)}_{s_{n;u}}$ true source voltage, source current on n-wire of u-wave

$\tilde{S}_{n,m;u,v}$ scattering coefficient which scatters combined voltage on m-wire of v-wave into n-wire of u-wave

$\tilde{I}_{n,m;u,v}$ interaction supermatrix element = $1 - \tilde{S}_{n,m;u,v}$

$\tilde{E}_{n;u}$ excitation supervector element, with $((\tilde{E})_n)_u = ((\tilde{S}_{n,m})_{u,v}) \odot ((\tilde{V}_{s_n})_u)$

$\tilde{Z}_{c_{n,m;u,v}} = 1_{u,v}(\tilde{Z}_{c_{n,m}})_u$ normalization impedance matrix for wires on an edge containing u- and v-wave: $1_{u,v}$ = Kronecker delta function, =1 for u=v, =0 for u≠v.

a normalization length used in field-to-wire aperture interaction

$\left\{\begin{matrix} \tilde{I}^{(+)}_{s_{\lambda+1}}, \tilde{V}^{(+)}_{s_{\lambda+1}} \\ [\tilde{I}^{(f)}_{s_{\lambda+1}}, \tilde{V}^{(f)}_{s_{\lambda+1}}] \end{matrix}\right.$ true equivalent current source, voltage source on a wire in $(\lambda+1)$ - layer due to wire-to-wire [field-to-wire] aperture interaction, superscripts "+" have been neglected for simplicity for the field-to-wire interaction

$\left\{ \tilde{i}_{s_{\lambda+1,\lambda}}, \tilde{v}_{s_{\lambda+1,\lambda}} \right.$ $\left. [\tilde{i}^{(f)}_{s_{\lambda+1,\lambda}}, \tilde{v}^{(f)}_{s_{\lambda+1,\lambda}}] \right\}$	normalized equivalent current source, voltage source on a wire in $(\lambda+1)$ - layer due to interaction through an aperture from wire [field] in λ-layer, see Figures 2.3, 2.4 for definition
$\left\{ \tilde{\Phi}_m, \tilde{\Phi}_e \right.$ $\left. [\tilde{\Phi}^{(f)}_m, \tilde{\Phi}^{(f)}_e] \right\}$	magnetic flux linkage, electric charge deposited on wire due to wire-to-wire [field-to-wire] aperture interaction
α_m, α_e	magnetic, electric polarizability
$\tilde{E}_{sc}$, $\tilde{H}_{sc}$, $\tilde{\sigma}_{sc}$, $\tilde{J}_{sc}$	short-circuited electric field, magnetic field, surface charge density, surface current density
$\tilde{V}_{oc}$, $\tilde{I}_{sc}$	open-circuited voltage, short-circuited current
$\tilde{Z}_{in}$, $\tilde{Z}_L$	input impedance, loading impedance
ρ	radius of exclusion region or volume
r_o	wire radius
A	effective aperture area
ζ_m	magnetic flux penetration factor = $\tilde{\Phi}_m/(\mu_o \tilde{H}_{sc})$